Award Number: W81XWH-13-1-0160

TITLE: FRET Imaging Trackable Long-Circulating Biodegradable Nanomedicines for Ovarian Cancer Therapy

PRINCIPAL INVESTIGATOR: Jindřich Kopeček

CONTRACTING ORGANIZATION: University of Utah
Salt Lake City, UT 84112

REPORT DATE: November 2015

TYPE OF REPORT: Final

PREPARED FOR: U.S. Army Medical Research and Materiel Command
Fort Detrick, Maryland 21702-5012

REPORT DOCUMENTATION PAGE

Form Approved
OMB No. 0704-0188

1. REPORT DATE	2. REPORT TYPE	3. DATES COVERED
November 2015	Final	1 Sept 2013 – 31 Aug 2015

4. TITLE AND SUBTITLE
FRET Imaging Trackable Long-Circulating Biodegradable Nanomedicines for Ovarian Cancer Therapy

5a. CONTRACT NUMBER

5b. GRANT NUMBER
W81XWH-13-1-0160

5c. PROGRAM ELEMENT NUMBER

6. AUTHOR(S)
Jindřich Kopeček

E-Mail: Jindirch.Kopecek@utah.edu

5d. PROJECT NUMBER

5e. TASK NUMBER

5f. WORK UNIT NUMBER

7. PERFORMING ORGANIZATION NAME(S) AND ADDRESS(ES)
University of Utah
201. S. President Circle, Room 408
Salt Lake City, UT 84112-9023

8. PERFORMING ORGANIZATION REPORT NUMBER

9. SPONSORING / MONITORING AGENCY NAME(S) AND ADDRESS(ES)
U.S. Army Medical Research and Materiel Command
Fort Detrick, Maryland 21702-5012

10. SPONSOR/MONITOR'S ACRONYM(S)

11. SPONSOR/MONITOR'S REPORT NUMBER(S)

12. DISTRIBUTION / AVAILABILITY STATEMENT
Approved for Public Release; Distribution Unlimited

13. SUPPLEMENTARY NOTES

14. ABSTRACT Enter a brief (approximately 200 words) unclassified summary of the most significant finding during the research period
The major goal of the proposed project is to develop a novel FRET imaging strategy, which permits visualizing the biodegradation of copolymer-drug conjugates at the body, tissue and cell levels in real time. The information will initiate the understanding of *in vivo* behavior of biodegradable polymers and support the design of highly efficient drug delivery systems. In the first year of the project we have synthesized numerous FRET trackable biodegradable *N*-(2-hydroxypropyl)methacrylamide (HPMA) copolymer conjugates that were labeled with Cy3 and/or Cy5, conjugates that contained epirubicin and performed click reactions for chain extension to manipulate their molecular weight. The conjugates were characterized by physicochemical methods and in vitro using human ovarian carcinoma cells. FRET technique was used to investigate the conjugates at cellular level. We achieved correlation of the FRET signal on one hand with the level of cathepsin B expression and with the intracellular degradation of the conjugates on the other hand. In fluorescence spectrophotometry experiments we have demonstrated a quantitative correlation between the FRET signal and the degradation of the HPMA copolymer conjugates. Thus our hypothesis that FRET imaging is suitable for the determination of the degradation and fate of backbone degradable HPMA copolymer conjugates has been validated at the cellular level.

15. SUBJECT TERMS: Key words or phrases identifying major concepts in the report
FRET imaging; biodegradable HPMA copolymer carriers; epirubicin; ovarian cancer; long-circulating nanomedicines; cathepsin B.

16. SECURITY CLASSIFICATION OF:			17. LIMITATION OF ABSTRACT	18. NUMBER OF PAGES	19a. NAME OF RESPONSIBLE PERSON
a. REPORT	b. ABSTRACT	c. THIS PAGE			USAMRMC
U	U	U	UU	67	19b. TELEPHONE NUMBER *(include area code)*

FINAL REPORT

Project: **FRET Imaging Trackable Long-Circulating Biodegradable Nanomedicines for Ovarian Carcinoma Therapy**

Award No.: **W81XWH-13-1-0160**

Budget period: **09/01/2013 – 08/31/2015**

Principal Investigator: **Jindřich Kopeček, Ph.D., D.Sc.**

TABLE OF CONTENTS

1. Introduction

Ovarian cancer is the seventh most common cancer in women worldwide. Approximately 239, 000 cases were recorded in 2012, accounting for nearly 4 per cent of all new cases of cancer in women (2 per cent overall) [1]. This cancer is fatal, as the disease is usually diagnosed in advanced stages. In the United States, ovarian cancer remains the deadliest gynecologic malignancy, with estimated 15,500 deaths in the United States in 2012 [2]. The treatment of ovarian cancer comprises a surgical cytoreductive procedure followed by postoperative combination chemotherapy. While surgery is an important component of initial therapy, most patients cannot be cured by surgery alone due to residual microscopic and macroscopic peritoneal lesions. Ovarian cancer is a chemosensitive disease and numerous chemotherapeutic agents have been shown to produce objective responses following surgery. Current treatment with combination chemotherapy results in a clinical complete remission rate in approximately 75% of all patients with advanced ovarian cancer. The 5-year survival remains 44% for all stages and 27% for advanced stages [2]. Despite aggressive primary therapy and high initial response rates, relapse and development of drug-resistance have led to a dismal 5-year survival rate, which highlights the crucial need to develop better therapeutic agents and strategies. The purpose of this project is to draw on the recent advances in polymer science, chemotherapy and molecular imaging to develop a new therapeutic modality, which will be potentially more effective than existing therapeutic agents for the treatment of ovarian cancer. This project proposes to develop a new biodegradable polymeric drug delivery system capable of non-invasive assessment of therapeutic efficacy by using Fluorescence (Förster) Resonance Energy Transfer (FRET) imaging. This strategy can provide information on biodistribution of the polymer-drug conjugate, biodegradation of polymer carrier, and drug release at the cellular, tissue and whole-body levels. Thus, the outcome of this project is to provide a powerful tool for tracking and screening biodegradable nanomedicines in preclinical evaluation. Moreover, this real-time monitoring technique will permit to gain a deep insight into the structure-efficacy relationship and identify factors impacting effectiveness. Ultimately, optimized polymer-drug conjugates with significant efficacy toward ovarian cancer will be produced. More importantly, the results from the current research project may be broadly applicable not only to the treatment of other cancer types, but also to other drug delivery systems.

2. Keywords

FRET imaging; biodegradable HPMA copolymer carriers; epirubicin; ovarian cancer; long-circulating nanomedicines; cathepsin B.

3. Overall Project Summary

In general, small molecule anticancer drugs quickly distribute throughout the body after intravenous injection, with no selectivity towards the tumor, which to a great extent confines their therapeutic efficacy and increase non-specific toxicity. To address this issue, the concept of polymer-based drug delivery systems is advocated and has been introduced into clinical trials [3-6]. Our group has been working on *N*-(2-hydroxypropyl)methacrylamide (HPMA) copolymer conjugates for years since the first HPMA copolymers were developed in our laboratory. The HPMA copolymer-based drug formulations have superior properties over small molecule drugs, such as a) enhanced drug bioavailability; b) improved pharmacokinetics [7]; c) increased drug accumulation in the tumors by passive or active targeting effect [8-10]; d) decreased non-specific toxicity [5]; e) potential to overcome multidrug resistance [11]; and f) decreased immunogenicity of the targeting moiety [12]. The “1st generation” (HPMA) copolymer conjugate containing doxorubicin (DOX) was the first synthetic polymer-based anticancer conjugate to enter a clinical trial [13, 14]. In humans, this DOX conjugate showed a 4 to 5-fold increase in the maximum tolerated dose (MTD) over free DOX (320 mg/m^2 vs. 60-80 mg/^{m2} DOX equivalent). This remarkable improvement in clinical toxicity is mainly due to less effective accumulation and endocytosis of polymer conjugates in heart tissue [13]. Subsequently, other “1st generation” HPMA copolymer-drug conjugates were also investigated in clinical trials [15-19].

However, the therapeutic performance of the 1st generation HPMA copolymer-drug conjugates in human did not match the results obtained from animal studies. The most likely reason is that the molecular weight (Mw) of the conjugates used in the trials was about 25 kDa - not large enough to ensure sufficient circulation time in human body and sufficient extravasation of the conjugates at the tumor by the EPR (enhanced permeability and retention) effect [20]. Consequently, tumors were not exposed to effective drug concentrations. Molecular weight and molecular weight distribution are important factors in the design of effective macromolecular therapeutics. The higher the molecular weight of the polymer carrier, the higher the accumulation of the polymer-drug conjugates in the tumor tissue with concomitant increase in

therapeutic efficacy. For prolonged plasma circulation and enhanced tumor accumulation, it is imperative to employ polymeric carriers with increased molecular weight. Therefore, high-molecular weight degradable polymer conjugates are considered as the most attractive candidates for next clinical applications [21].

Our design employs a cathepsin B-sensitive linker GFLG, which is not only inserted into the polymer backbone for degradation, but also incorporated into the side chain as drug attachment/release site. This GFLG linker is stable during transport but able to be released by cathepasin B in the lysosomal compartment of the target cells at a predetermined rate. The cysteine proteinase, cathepsin B, normally locates in the cellular lysosomes, and contributes to degradation and regulation of proteins [22]. However, in malignant tumors, such as melanoma [23], breast [24], ovarian [25, 26], lung [27], stomach [28], and colon [29] tumors, cathepsin B is secreted extracellularly and acts as an important proteinase of matrix materials to degrade surrounding proteins and other tissue components so that cancer cells can invade and metastasize. It has been reported that cathepsin B level is much higher in malignant ovarian tumor than in normal ovary tissues [25] and its expression is regarded as a marker for ovarian cancer prognosis [30]. In our design, the 2nd generation enzyme-responsive carriers can release drug in the same organ, tissue, or cells with a high level of cathepsin B, like ovarian tumors, so as to enhance the uptake ratio of tumor-to-nontumor.

Epirubicin (Pharmorubicin®), the 4'-epimer of the anthracycline DOX, is an antineoplastic agent that inhibits DNA replication, transcription and repair by binding to nucleic acids [31]. Epirubicin has been regarded as one of the most active drugs for the patients with cancer, particularly with metastatic disease. It has shown equivalent cytotoxic effects to DOX in human ovarian cancer cells, but decreased cardiotoxicity and myelotoxicity than DOX at equimolar doses [31]. Thus, epirubicin is thought to have a better therapeutic index than DOX. In this project, we propose to use HPMA copolymer-epirubicin conjugates as a "proof-of-concept" model for the development of new imaging strategy. It should be noted that other chemo agents could be easily used to substitute for epirubicin.

In order to investigate the in vitro and in vivo performance of the new drug delivery system, FRET imaging has been applied in this study. FRET is a process in which energy is transferred

non-radiatively from a fluorophore in an electronic excited state serving as a donor, to another chromophore or acceptor by long-range dipole-dipole coupling [32]. It is unique in generating fluorescence signals sensitive to molecular conformation, association, and separation in less than 10 nm distance. Over the past decade, FRET imaging has been proven to be an extremely useful tool to visualize protein-protein interactions and protein conformational changes with high spatial resolution in microscopy. To date, the advances in optical imaging technology, coupled with the development of new fluorescent probes and the increasing capability of computer software for image acquisition and analysis, have enabled FRET to elucidate molecular interactions inside living animals with improved sensitivity and spatial/temporal resolution. In particular, the development of near-infrared fluorescence (NIRF) probes plays a vital role in real-time imaging of dynamic molecular events *in vivo* [33]. Thus, FRET imaging has a great potential for gaining insight into the function-mechanism relationship.

In summary, the major goal of the proposed project is to develop a novel FRET imaging strategy, which permits visualizing the backbone degradation and drug release of copolymer-drug conjugates at the body, tissue and cell levels. The information will enhance the understanding of in vivo behavior of biodegradable polymer carrier and help to shape the design of highly efficient delivery systems with decreased adverse effects. We anticipate that the success of this project will accelerate the translation of this new drug delivery system from bench to clinic and ultimately spark a breakthrough for the treatment of ovarian cancer and other diseases.

4. Key Research Accomplishments

The major goal of the project is to develop a novel FRET imaging strategy, which permits visualizing the drug release and backbone degradation of copolymer-drug conjugates at the body, tissue and cell levels in real time. To reach this goal, the following studies were accomplished.

4.1 Design and Synthesis of FRET-trackable HPMA Copolymer Conjugates

To visualize the payload release and backbone degradation process of HPMA copolymer carrier by FRET imaging, two chromophores need be included in our delivery system, one donor and one acceptor, and their relative position is crucial. As shown In Figure 1, we present two designs for investigation of backbone degradation and drug release from FRET-trackable polymers.

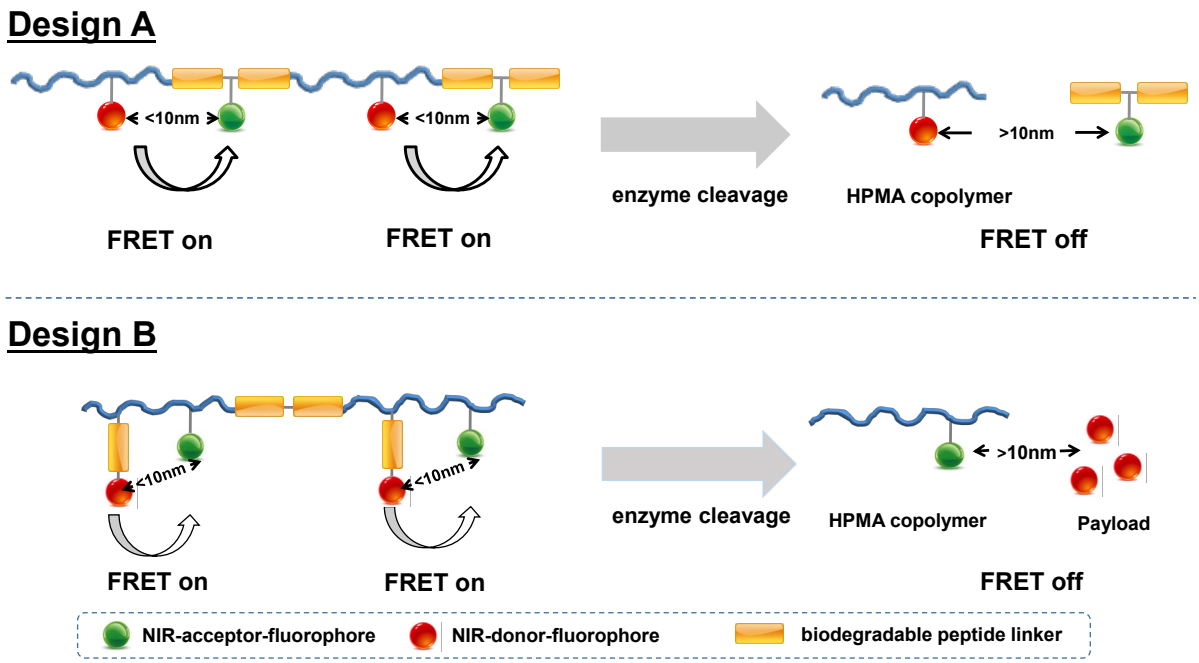

Figure 1. Design of FRET-trackable HPMA copolymer conjugates for monitoring backbone degradation (Design A) and drug release (Design B).

In both designs, one chromophore will be conjugated to the main chain polymer segment, and the other will be incorporated into an enzyme-sensitive peptide linker. Upon exposure to lysosomal cathepsin B or a similar protease, the peptide will be cleaved, thereby leading to the separation of the fluorophore pair. It has been reported that the hydrodynamic radius of polyHPMA is 2~4 nm when molecular weight is 20-45 kDa [34]. Therefore, in both designs (Fig. 1), FRET occurs when the polymer is in its native state, prior to enzymatic degradation, because of intimate distance between the donor and the acceptor ("FRET ON"). However, subsequent detachment of one chromophore from the backbone by enzymatic cleavage will result in a loss of energy transfer ("FRET OFF"). The two designs differ in regards to the placement of the fluorophores within the polymer. In both cases, one fluorophore is conjugated directly to the polymer backbone via a non-degradable bond for constitutive tracking. In Design A, the second fluorophore is conjugated to a degradable sequence within the polymer backbone, linking energy transfer to backbone integrity. In Design B, the second fluorophore in the FRET pair is

anchored to the polymer via a degradable sequence incorporated as a side chain, simulating a stimuli-sensitive drug release system. Each design enables us to ascertain complementary knowledge for polymer optimization along the lines of backbone degradation (Design A) and drug release (Design B). Here, we will present the data of design A and B separately, as follows.

4.1.1 Synthesis of FRET Pair-labeled HPMA Copolymer Conjugates for Tracking Backbone Degradation (Design A)

In order to synthesize the polymer presented in Figure 1, Design A, a two-step approach was utilized (Fig. 2) [35]. First, alkyne telechelic polymers containing the FRET donor fluorophore were synthesized using RAFT polymerization. Then, click chemistry and a diazido "chain extender" containing the FRET acceptor fluorophore was used to linearly conjoin the polymers. Cy3 and Cy5 were selected for the donor and acceptor, respectively, due to their high degree of spectral overlap (encouraging significant energy transfer) and extensive use as a FRET pair in literature [36].

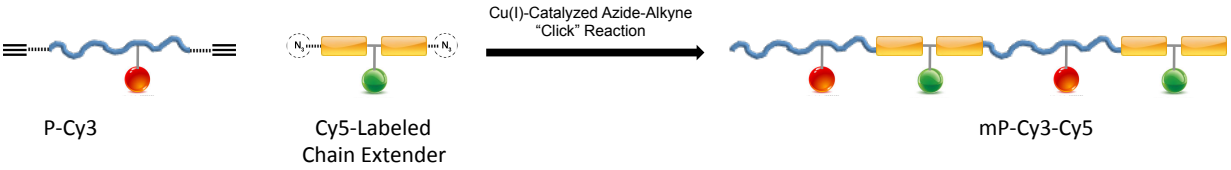

Figure 2. Illustration demonstrating the process of chain extension to generate dual-labeled, backbone-degradable HPMA copolymers for tracking backbone degradation.

Synthesis of Alkyne-Terminated HPMA Copolymer-Cy3 Conjugates. An α,ω-dialkyne chain transfer agent for RAFT polymerization was synthesized as described previously [37]. As the CTA forms the active radical during the RAFT polymerization reaction, the termini of the polymer product is defined by the CTA end functional groups, enabling telechelic polymers to be produced in a single reaction step. As described in Figure 3, this CTA was used to copolymerize HPMA with *N*-(3-Aminopropyl)methacrylamide (APMA) as a comonomer (3 mole percent), using 4,4'-Azobis(4-cyanovaleric acid) (V-501) as the initiator. The comonomer provided reactive amine sidechains for subsequent dye attachment to the polymer. After removal of the unreacted monomer via dialysis against acidified deionized water, the side chain amino content of the polymer was analyzed via ninhydrin assay. Cy3-NHS was then used to attach the dye to the polymer backbone via the amine sidechains. Unreacted dye was removed via column chromatography (LH20 resin stationary phase, methanol mobile phase). The

content of Cy3 in the polymer chain was determined via UV-Vis spectroscopy (Varian Cary 400 Bio UV–visible spectrophotometer).

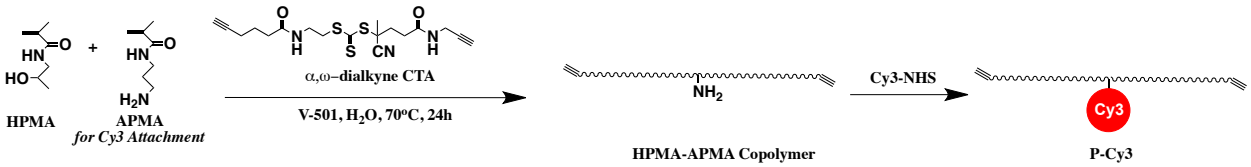

Figure 3. Synthesis of HPMA copolymer conjugate containing Cy3 fluorophore (P-Cy3).

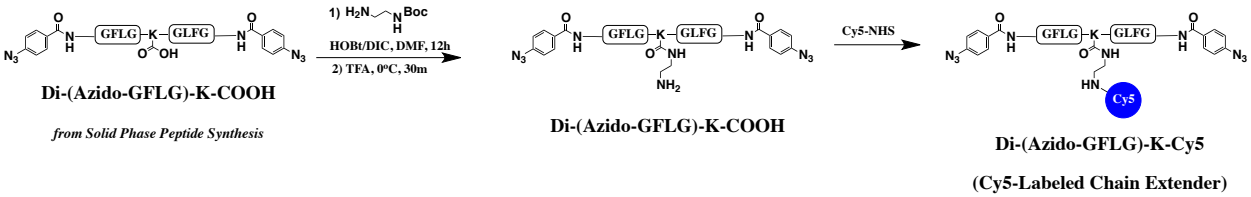

Figure 4. Synthesis of enzymatically degradable chain extender containing Cy5 fluorophore (Di-(Azido-GFLG)-K-Cy5).

Synthesis of Azide-Terminated, Cy5-Labeled, Degradable Chain Extender (Di-(Azido-GFLG)-K-Cy5). The Cy5-labeled, α,ω-azido chain extender was synthesized in three steps (Fig. 4). First, solid phase peptide synthesis (Fmoc protection chemistry, HBTU/HOBt coupling agents, 2-chlorotrityl chloride resin) was used to synthesize $N^{\alpha},N^{\varepsilon}$-*di*-((4-azidobutanoyl)glycylphenylalanylleucylglycyl)lysine (Di-(Azido-GFLG)-K-COOH, diazido chain extender). Fmoc-Lys(Fmoc)-OH was loaded onto the resin as the first residue. The two amine functional groups were then used to synthesize two symmetric Gly-Leu-Phe-Gly (GLFG) oligopeptide arms via stepwise coupling of the amino acid residues. The terminal amines were then capped with 4-azidobenzoic acid to generate two azide termini. Following cleavage from the resin by a solution of 30% trifluoroethanol in dichloromethane, the peptide was isolated by precipitation in precooled diethyl ether, followed by drying under vacuum. The C-terminus of the peptide was then modified using an excess of *N*-Boc-ethylenediamine using HOBt and DIPEA as coupling agents. Unreacted *N*-Boc-ethylenediamine was removed via precipitation and washing in diethyl ether. The peptide was then dissolved in chilled trifluoroacetic acid to remove the protecting group. The reaction was allowed to proceed for 30 minutes on ice, followed by precipitation in precooled diethyl ether and drying under vacuum. The crude product was then purified via RP-HPLC (Agilent 1100 series, Zorbax C18 column 9.4 x 250 mm). The newly deprotected primary amine was then used attach the Cy5-NHS acceptor dye. Unreacted dye was removed via column chromatography (LH20 resin stationary phase, methanol mobile phase). Identity of the final product was confirmed via ESI MS (Q-ToF-II, Micromass/ Waters)

([M^{2+} 846.7]) and purity was validated via RP-HPLC (Agilent 1100 series, Zorbax C18 column 4.6 x 250 mm) (Fig. 5).

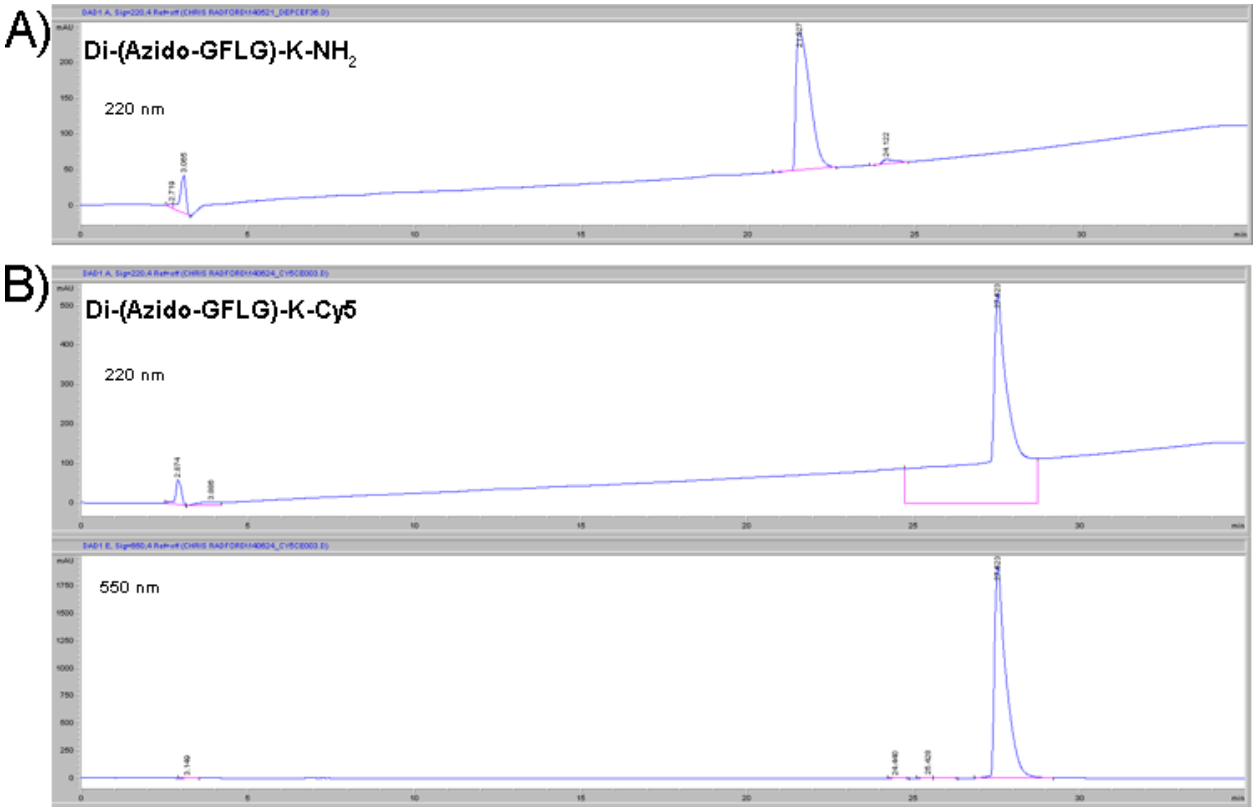

Figure 5. RP-HPLC profiles of (A) Di-(Azido-GFLG)-K-NH_2 and (B) Di-(Azido-GFLG)-K-Cy5

Chain Extension of P-Cy3 with Cy5-lableled Chain Extender. After synthesis of the Cy3-labeled polymer (P-Cy3), and the Cy5-labeled chain extender, click chemistry was used to conjugate the two sets of molecules together in an alternating block fashion to generate high molecular weight backbone degradable polymer incorporating both dyes (mP-Cy3-Cy5). The Cy3-labeled polymer and the Cy5-labeled chain extender were dissolved in an equimolar ratio in a Cu(I)-rich aqueous solution and allowed to react for 24 hours under nitrogen atmosphere. The Cu(I) ion catalyzed a azide-alkyne Huisgen cycloaddition, forming a covalent bond between polymer and chain extender, positioning the degradable peptide sequence between each polymer unit ("unimer") in the chain to form multimeric linear polymers. Unreacted peptide was removed via column chromatography (LH20 resin stationary phase, methanol mobile phase) and complete removal was confirmed via HPLC. Chain extension was confirmed by comparing the product's size exclusion chromatograph against the profile of the consistent unimer. The SEC data was obtained on an ÄKTA FPLC system (GE Healthcare) equipped with miniDAWN and OptilabEX

detectors (Wyatt) with acetate/30% acetonitrile (pH 6.5) as mobile phase and Superose 6 HR10/30 column. The shift in the profile indicated a higher molecular weight product characteristic of successful multimerization. Incorporation of Cy5 dye into the polymer was confirmed via the emergence of a second absorbance peak at 646 nm (corresponding to the λ_{max} of Cy5) that was not present in the unimer spectra (Fig. 6B).

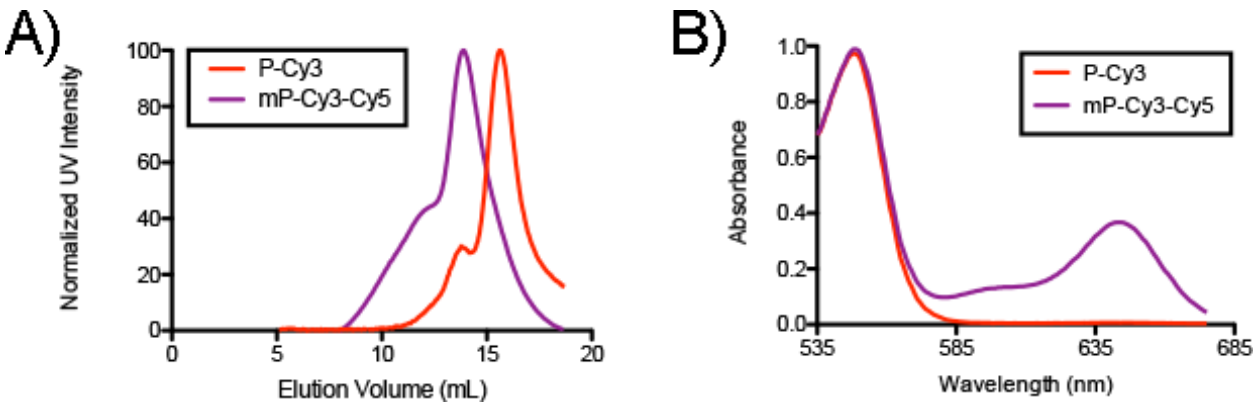

Figure 6. Analysis of the products of the click reaction via (A) size exclusion chromatography and (B) absorbance to confirm macromolecular chain extension and incorporation of both dyes into the backbone.

4.1.2 FRET ON/OFF of Conjugates in the Presence of Enzyme

Here, we establish that the co-localization of Cy3 and Cy5 in the polymer backbone gives rise to a distinct shift in the fluorescence profile as a result of fluorescence resonance energy transfer (FRET) between the dye pair (Fig. 7). Furthermore, this link between fluorescence and backbone integrity enables fluorescence to serve as a surrogate measure to obtain real-time information on the biodegradation of the polymer [35].

Characterization of FRET in mP-Cy3-Cy5. The fluorescence profile of the dual-labeled multimer was analyzed using a Teacan Infinite M1000 PRO Microplate Spectrophotometer and compared against the fluorescence profile of its two components (the Cy3-labeled unimer and the Cy5-labeled chain extender) (Fig. 8). When controlling for the intensity in the Cy3 channel, the emission in the FRET channel was significantly greater than could be accounted for by the simple sum of the two components. Furthermore, mixing the two components in a copper-free solution at similar concentration (as determined by absorbance at 546 and 646 nm) did not give rise to an equivalent FRET channel intensity. Therefore, this phenomenon is an emergent property of successful chain extension and the resulting proximity of the dye pair.

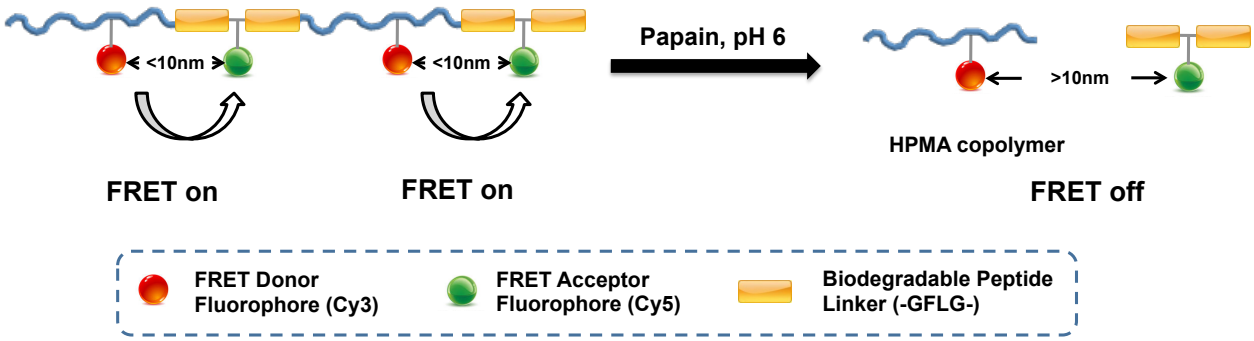

Figure 7. Illustration of FRET ON/OFF tracking of polymer degradation, with multimers (mP-Cy3-Cy5) enabling energy transfer between the dyes, which is subsequently terminated upon enzymatic degradation.

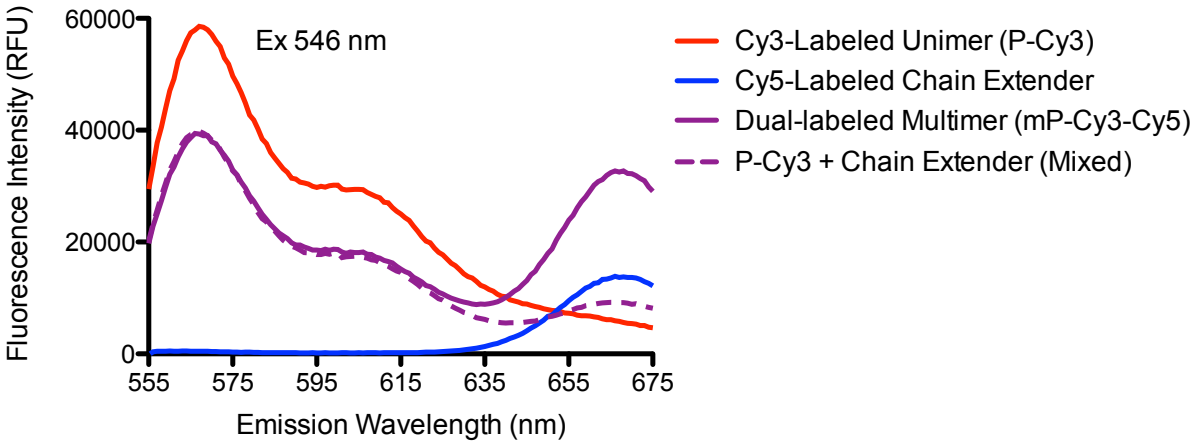

Figure 8. Comparison of fluorescence emission profile for the mono-labeled components, a simple mixture of the two, and their clicked multimer product. All samples were excited at 546 nm to obtain the above profile.

The multimer was then exposed to papain (a thiol protease with similar specificity to lysosomal cathepsin B) which acts on the oligopeptide substrate Gly-Phe-Leu-Gly (GFLG). After 2 h of incubation with 8 μM papain, the size exclusion chromatograph of the polymer matched the profile of the unimer product, indicating complete degradation of the oligopeptide links (Fig. 9A). Furthermore, after exposure to papain, the emission in the FRET channel is significantly reduced and the fluorescence profile also converges back to that of the constituent Cy3-labeled unimers (Fig. 9B). This result indicates that the energy transfer between the Cy3 and Cy5 dye is severed upon enzymatic cleavage of the backbone.

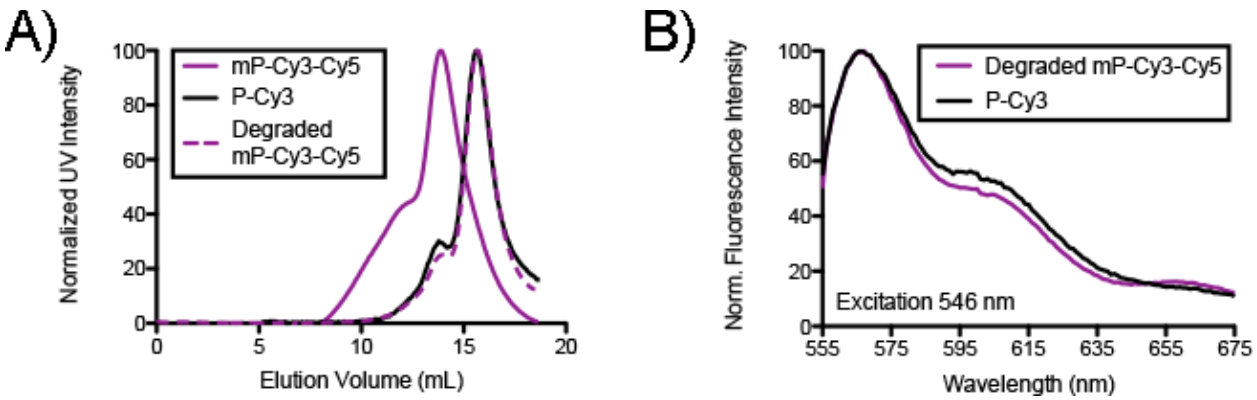

Figure 9: A) SEC profiles of Cy3-labeled unimers (black), click-extended multimers containing both Cy3 and Cy5 dyes in their backbone (purple), and multimers after exposure to 8 μM model lysosomal enzyme papain for 2 h (purple dashed). B) Comparison of fluorescence emission profiles for dual-labeled multimer after exposure to 8 μM papain for 2 h (purple dashed) with the constituent Cy3-labeled unimer (red solid). All samples were excited at 546 nm.

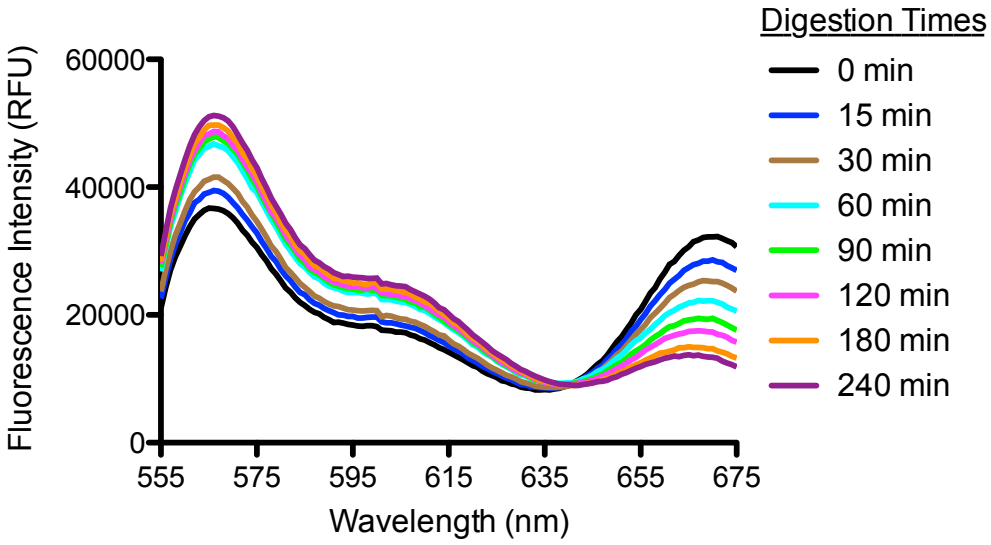

Figure 10. Evolution of fluorescence emission profile over the course of degradation. Times correspond to length of incubation with 0.08μM of papain before inhibition. All profiles are the result of excitation at 546 nm and measurement of the emission from 555 to 675 nm.

Table 1: Summary of Fluorescence Channels Analyzed

Channel	Excitation (nm)	Emission (nm)	Interpretation
Cy3	546	567	Emission from the Cy3 dye resulting from its direct excitation
Cy5	646	669	Emission from the Cy5 dye resulting from its direct excitation
FRET	546	669	Emission from the Cy5 dye arising from direct excitation of Cy3 followed by nonradiative energy transfer to Cy5

Correlation between Fluorescence Signal and Extent of Polymer Degradation. Now that we have validated the FRET ON/OFF property of this dual-labeled polymer design, we exploit this change in the fluorescence profile to extract information on the extent of degradation. The dual-labeled multimer (concentration 3 mg/mL) was incubated in a 0.08 μM papain solution. At predetermined time points, a sample was withdrawn from the reaction, added to an inhibitor solution (methanol solution of iodoacetic acid sodium salt (100 μM) acidified with 0.02% v/v acetic acid) to inactivate the enzyme, and stored at -20 ^{o}C until analysis. At each time point, the fluorescence emission profile of the sample was analyzed in addition to its size exclusion chromatograph. As shown in Figure 10, the fluorescence profile is observed to gradually transition from the bimodal spectra of the initial mP-Cy3-Cy5 to the single peak of the constituent P-Cy3. In order to quantify this transition, we define three fluorescence channels in Table 1, each consisting of an excitation and emission wavelength pair. The trends in each channel as a function of digestion time are presented in Figure 11.

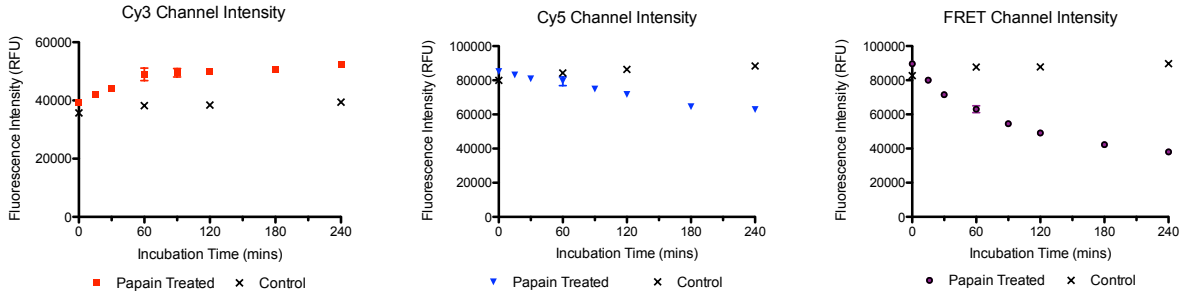

Figure 11. Fluorescence intensity in each channel as a function of incubation time with papain. Controls were incubated in identical buffer conditions without enzyme present. Each point corresponds to the mean of three samples, each taken from a different stock. Error bars indicate standard error of the mean. Each channel was measured independently.

As expected, the intensity in the Cy3 channel gradually increases and the intensity in the FRET channel gradually decreases as energy transfer between additional donor-acceptor pairs is terminated. The decrease in the Cy5 Channel over time is likely the result of a difference in quantum yield of the Cy5 dye when incorporated into the polymer backbone versus free peptide. This is also supported by the observed shift in the Cy5 emission maxima from 669 to 664 nm upon cleavage and release of the free peptide. In addition, the size exclusion chromatograph of a sample at each time point was obtained on an ÄKTA FPLC system (GE Healthcare) equipped with miniDAWN and OptilabEX detectors (Wyatt) with acetate/30% acetonitrile (pH 6.5) as mobile phase and Superose 6 HR10/30 column. As seen in the chromtographs (Fig. 12), longer digestion times resulted in an increase in lower molecular weight polymers, represented by a shift in signal intensity to higher elution volumes. These spectra were then used to calculate

average molecular weight of the sample at each time point as a standard measure of extent of degradation. These molecular weights were mapped against their corresponding FRET channel intensity. Both number-average (Mn) and weight-average (Mw) molecular weights showed strong linear correlation with the fluorescence intensity (r^2 = 0.969 and 0.989, respectively). The weight-average has higher correlation due to the Cy3-labeling process for the polymers, in which the dye content (and therefore number of fluorophores contributing to FRET) is proportional to the mass of polymer. As a result of this strong linearity between these values, the degree of FRET provides significant insight into the extent of degradation of mP-Cy3-Cy5, enabling us to monitor the process of enzymatic degradation in real time using only fluorescence data.

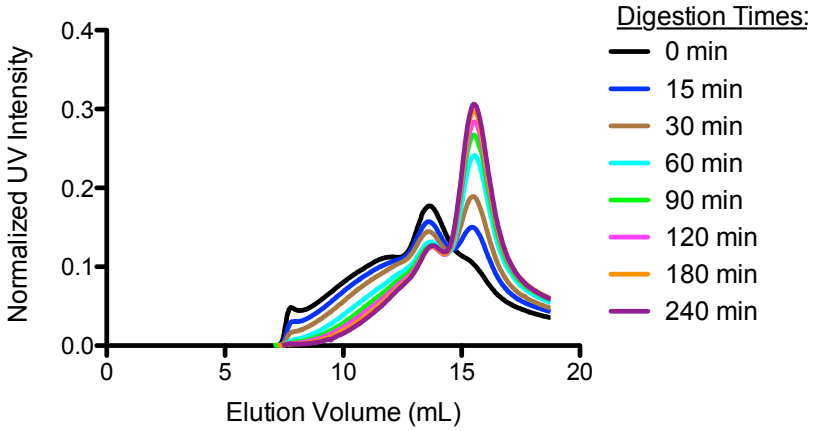

Figure 12. SEC chromatographs as a function of incubation time with papain. Profiles were obtained by measuring absorbance of elution at 280 nm

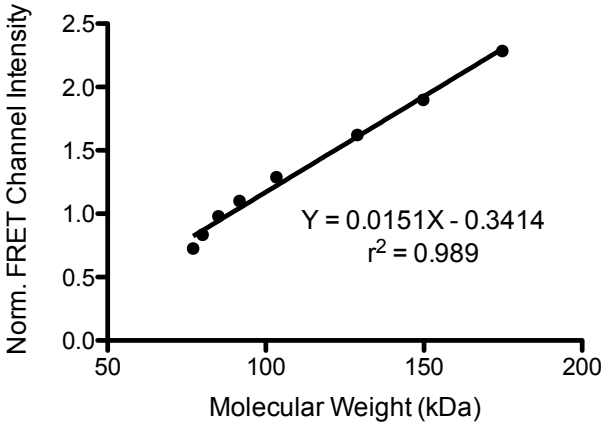

Figure 13. FRET Channel intensity (normalized to Cy3 channel intensity to account for small variations in concentration) plotted against weight-average molecular weight values calculated from the SEC profiles. Normalized FRET channel intensity is represented as the mean of three samples, each taken from a different stock. Error bars indicate standard error of the mean. Molecular weights were calculated from size exclusion chromatographs.

4.1.3 Synthesis of FRET Pair-labeled HPMA Copolymer Conjugates for Tracking Drug Release (Design B)

In order to visualize the process of drug release at the cell, tissue, and whole-body levels, a series of FRET-trackable HPMA copolymer-conjugates bearing different FRET pairs were first designed (Figure 1, Design B), including 1) P-Cy3-Cy5 conjugate with the commonly used FRET pair Cy3/Cy5, which was mainly employed for in vitro evaluation [38]; 2) P-Cy5-Cy7 conjugate with near-infrared FRET pair Cy5/Cy7, which was suitable for in vivo and ex vivo studies [39]; 3) P-EPI-Cy5 conjugate with new FRET pair EPI/Cy5, as a new concept, which allowed to specifically investigate the relationship between the drug EPI and HPMA-copolymer backbone [38].

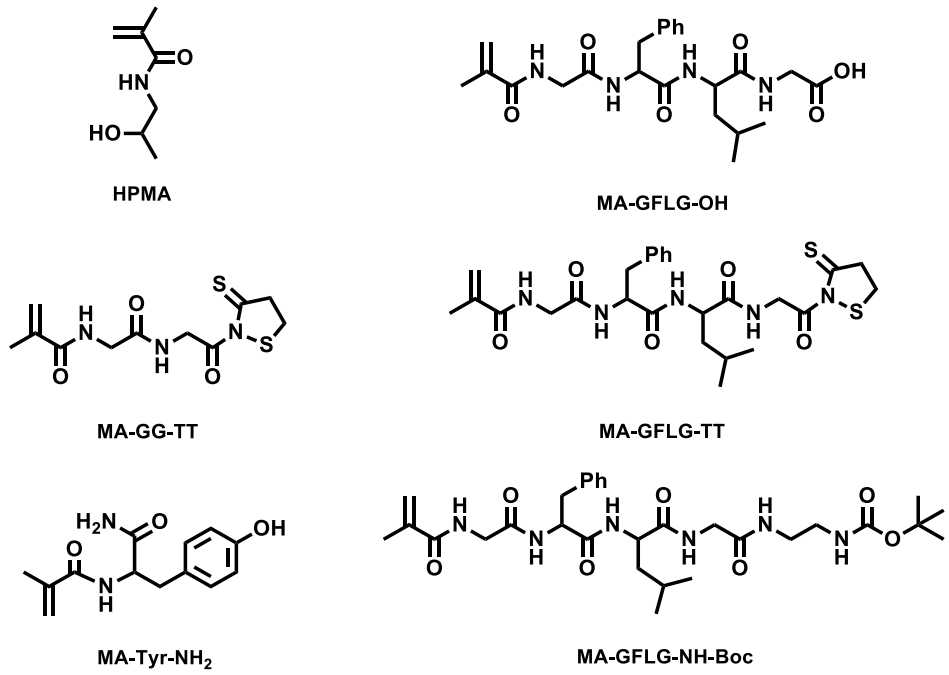

Figure 14. List and structure of the monomers synthesized in this study.

Synthesis of Monomers. Prior to polymerization, a series of the monomers were synthesized first. Figure 14 shows the list and structure of monomers. *N*-(2-Hydroxypropyl)methacrylamide (HPMA) was synthesized by acylating 1-aminopropan-2-ol with methacryloyl chloride in acetonitrile as previously described [40]. M.p. 69-71 °C; *N*-methacryloylglycylphenylalanylleucylglycine (MA-GFLG-OH) [41], *N*-methacryloyltyrosinamide (MA-Tyr-NH_2) [42], *N*-methacryloylglycylglycine thiazolidine-2-thione (MA-GG-TT) [43], 3-(*N*-methacryloylglycylphenylalanylleucylglycyl)thiazolidine-2-thione (MA-GFLG-TT) [43], 2-(*N*-methacryloylglycylphenylalanylleucylglycine)-*N*′-Boc-ethylenediamine (MA-GFLG-NH-Boc) [44],

and RAFT agents, 4-cyanopentanoic acid dithiobenzoate (CPA) [45] and Peptide2CTA (N^{α},N^{ε}-bis(4-cyano-4-(phenylcarbonothioylthio)pentanoylglycylphenylalanylleucylglycyl)lysine) [46], were synthesized as previously described.

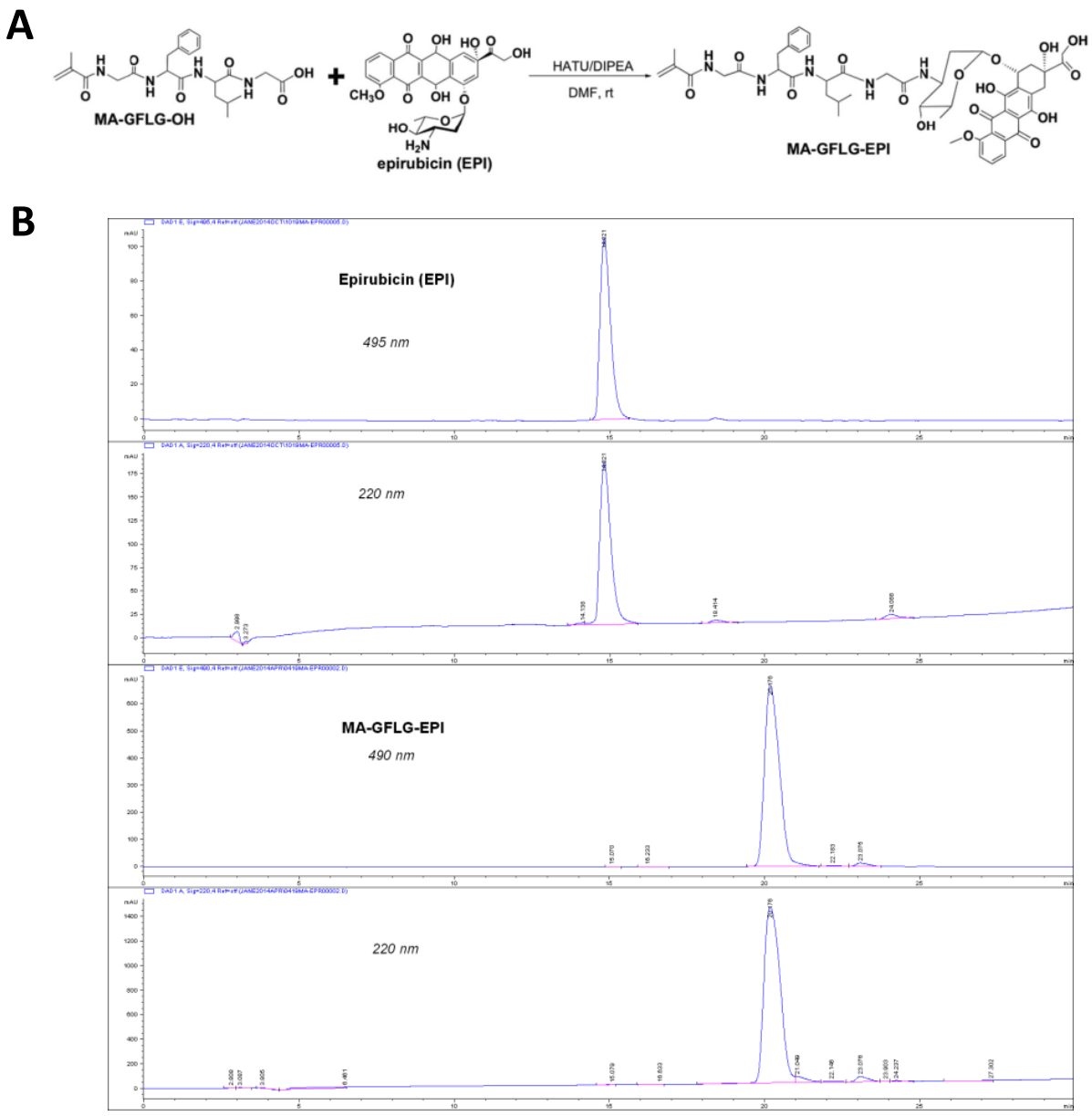

Figure 15. (A) Synthesis of the epirubicin monomer MA-GFLG-EPI. (B) RP-HPLC profile of free drug EPI and monomer MA-GFLG-EPI.

Synthesis of polymerizable derivative of epirubicin (MA-GFLG-EPI). Beside the aforementioned monomers, polymerizable derivative of drug epirubicin (EPI) was also prepared in this study [38]. In brief, *N*-(methacryloylglycylphenylalanylleucylglycyl) epirubicin (MA-GFLG-EPI) was

synthesized by the reaction of MA-GFLG-OH with EPI in DMF using HATU/DIPEA as coupling agent (Fig. 15). In brief, EPI (54 mg, 0.1 mmol) was first dissolved in 0.2 mL DMF. MA-GFLG-OH (50 mg, 0.11 mmol) was dissolved in 0.5 mL DMF, followed by addition of HATU (38 mg, 0.1 mmol) and DIPEA (45 µL, 0.25mmol). After activation at room temperature for 2 min, MA-GFLG-OH/HATU/DIPEA solution was added to the vial containing EPI solution. The system was kept stirring in dark overnight. The reaction solution (10 µL, diluted with methanol) was then loaded onto an analytical column (Zorbax C18, 4.6 × 250 mm) and checked by HPLC. The peak of free EPI (15.34 min) disappeared, whereas a new peak showed up (20.14 min) indicating the reaction had finished. The solvent was removed by rotary evaporator under vacuum. The crude product was purified by column chromatography (silica gel 60 Å, 200-400 mesh) with elution 6:1 dichloromethane/methanol. A dark red powder was obtained after removal of the solvents with a yield of 70 mg (70%). The structure of the monomer (MA-GFLG-EPI) was confirmed by MALDI ToF MS (LTQ-FT, ThermoElectron) ($[M + Na]^+$ 1024.43), and the purity was verified by HPLC (Agilent 1100 series).

4.1.4 Synthesis of FRET Pair-labeled HPMA Copolymer Conjugates for Imaging

Synthesis of HPMA copolymer conjugates containing fluorophore Cy3 and/or Cy5. To synthesize polymer conjugates suitable for FRET evaluation, P-Cy3-Cy5/2P-Cy3-Cy5, the polymer precursor containing side chain thiazolidine-2-thione (TT) and GFLG linker terminated with protected amino group was first synthesized by RAFT copolymerization of the amino-protected monomer (MA-GFLG-NH-Boc) [45], HPMA and MA-GG-TT (Fig. 16A). After chain end-modification, the content of TT groups in the copolymer was determined by UV (ε_{305} = 10,900 M^{-1} cm^{-1} in methanol). Cy5-NH_2 was dissolved in DMSO and reacted with polymer precursor. Unbound dye was removed using PD10 column. To incorporate the second dye, Cy3, the polymer was dissolved in water followed by addition of trifluoroacetic acid. The sample was kept stirring in ice-bath for 30 min, then condensed under reduced pressure and precipitated in precooled ether/acetone. The side-chain amino content in the deprotected polymer was analyzed by ninhydrin assay. Cy3-NHS was used to attach Cy3 to the polymer backbone via GFLG enzyme-cleavable linker. The content of Cy3 and Cy5 in the polymer chain was determined via UV–vis spectroscopy. As control, HPMA copolymers containing fluorophore Cy3 or Cy5 (P-Cy3 or P-Cy5) were synthesized by polymer analogous reaction of HPMA polymer precursor containing pendant amino groups with Cy3-/Cy5-NHS ester (Fig. 16B). Free dye was removed using PD10 column (Amersham Biosciences). The content of Cy3/Cy5 in

polymer conjugates was determined via UV–vis spectroscopy (Varian Cary 400 Bio UV–visible spectrophotometer).

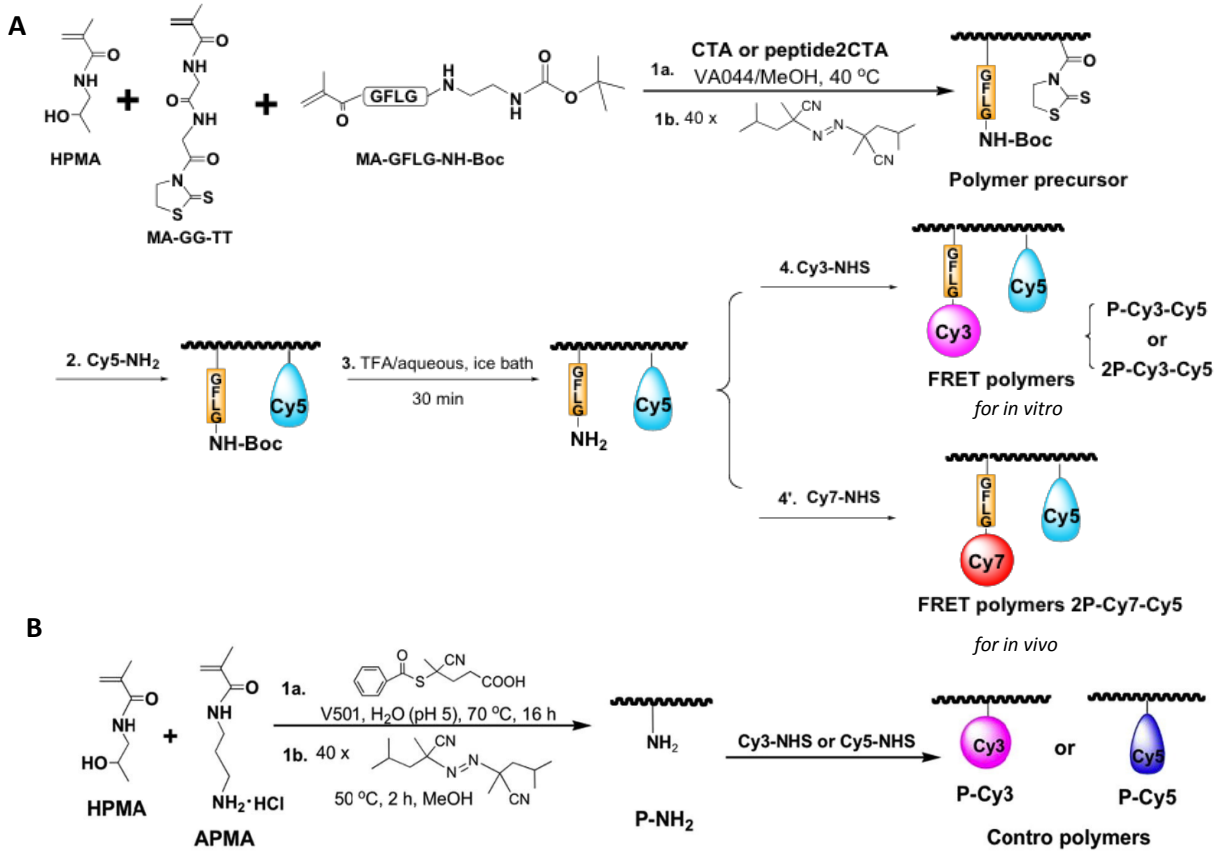

C

	Mw (kDa)	Mw/Mn	Cy3 (nmol/mg)	Cy5 (nmol/mg)	Ex (nm)	Em (nm)
P-Cy3	41	1.10	294		548	562
P-Cy5	41	1.10		284	646	664
P-Cy3-Cy5	61	1.09	332	268	520	500-750
2P-Cy3-Cy5	86	1.27	112	143	520	500-750

Figure 16. Synthesis and characterization of HPMA copolymer conjugates containing fluorophores Cy3/Cy5 or Cy5/Cy7.

Synthesis of HPMA copolymer conjugate containing fluorophore Cy5 and Cy7. Similarly as 2P-Cy3-Cy5, 2P-Cy5-Cy7 conjugate was also synthesized for in vivo study (Fig. 16A) [39]. In brief, the polymer precursor containing side chain thiazolidine-2-thione (TT) and GFLG linker terminated with protected amino group was first synthesized by RAFT copolymerization of the monomers HPMA, MA-GG-TT and MA-GFLG-NH-Boc (Fig. 16A). The polymer precursor 2P-

GG-TT-GLFG(NH-BOC) characterization: Mw = 115,500; Mn = 87,800; PDI (Mw/Mn) = 1.31; content of side-chain functional groups in nmol/mg – TT = 143 and NH_2 = 195.

After end-modification, Cy5-NH_2 was dissolved in DMSO and reacted with polymer precursor. Free Cy5 dye was removed using PD10 column. To incorporate the Cy7 dye, the polymer was dissolved in water followed by addition of trifluoroacetic acid. The sample was kept stirring in ice-bath for 30 min, then condensed under reduced pressure and precipitated in precooled ether/acetone. Cy7-NHS was added to attach Cy7 to the polymer backbone via GFLG enzyme-cleavable linker.

Synthesis of HPMA copolymer-EPI conjugate containing fluorophore Cy5. FRET polymer P-EPI-Cy5 was synthesized in two steps (Fig. 17) [38]: First, RAFT copolymerization of HPMA (134 mg, 0.94 mmol), MA-GFLG-EPI (33 mg, 0.035 mmol) and MA-GG-TT (7.5 mg, 0.025 mmol) was conducted in methanol at 40 °C as described above. The dithiobenzoate end group was removed by addition of 40× V65 to the polymer solution at 55 °C for 2 h. The TT group was then aminolyzed by Cy5-NH_2. The free dye was removed using PD10 column. The final contents of EPI and Cy5 were determined by UV–vis spectroscopy.

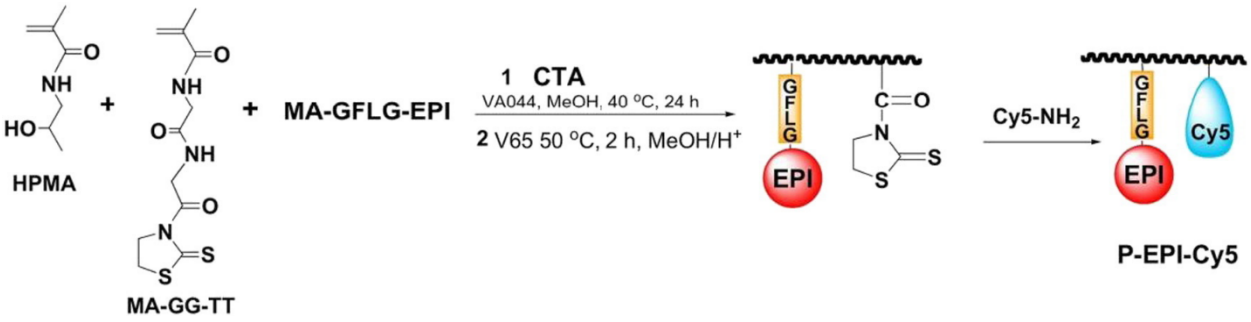

Figure 17. Synthesis of HPMA copolymer conjugate containing drug EPI and fluorophore Cy5 (P-EPI-Cy5).

4.1.5 Synthesis of HPMA Copolymer-Epirubicin Conjugates (P-EPI/2P-EPI and P-Tyr-EPI/2P-Tyr-EPI) for Pharmacokinetics, Biodistribution and Therapeutic Efficacy

HPMA copolymer-epirubicin conjugates (P-EPI and 2P-EPI) were synthesized by the copolymerization of HPMA with MA-GFLG-EPI using VA044 as initiator and 4-cyanopentanoic acid dithiobenzoate (CTA) or Peptide2CTA as chain transfer agent [38]. As an example, HPMA (138 mg, 0.965 mmol) and MA-GFLG-EPI (35 mg, 0.035mmol) were dissolved in 0.3 mL methanol under N_2 atmosphere. Peptide2CTA (60 µL with conc. 8.5 mg/mL in methanol, [M] / [CTA] = 1400) and VA044 at a molar ratio of 3:1 were added using a syringe. The ampoule was

bubbled with N_2 in ice bath for 5 min then sealed and polymerization was carried out at 40 °C for 24 h. The copolymer was precipitated in acetone. The resultant orange-color copolymer was re-dissolved in methanol and re-precipitated in acetone to remove unreacted monomers. The dithiobenzoate end group was replaced by radical-induced end-modification using excess of V-65 in methanol at 55 °C for 2 h. The final product (2P-EPI) was isolated by precipitation and dried under vacuum at room temperature with yield of 80 mg (50%). Similarly, P-EPI was obtained when CTA was used as RAFT agent with [M] / [CTA] = 550 (Fig. 18A). The molecular weight and molecular weight distribution of the conjugates were determined by size-exclusion chromatography (SEC) on an ÄKTA FPLC system (GE Healthcare) equipped with miniDAWN and OptilabEX detectors (Wyatt) with acetate/30% acetonitrile (pH 6.5) as mobile phase (Fig. 18B & 18C). Superose 6 HR10/30 column was used. The drug content in conjugates was determined by enzyme cleavage of free drug from polymer side chain GFLG linker using papain according to the procedure described previously (Fig. 18C) [46].

A

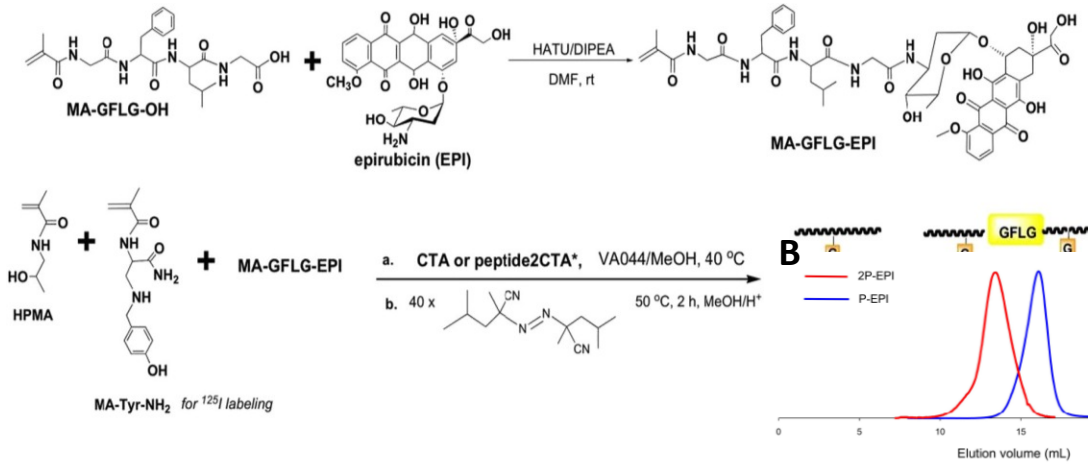

B

C

	Mn (kDa)	Mw (kDa)	Mw/Mn	EPI % (wt)
P-EPI	39	43	1.10	7.4
P-Tyr-EPI	26	28	1.08	6.5
2P-EPI	76	106	1.39	5.9
2P-Tyr-EPI	61	84	1.38	6.4

Figure 18. Synthesis and characterization of HPMA copolymer-EPI conjugates (P-EPI and 2P-EPI, P-Tyr-EPI and 2P-Tyr-EPI). (A) Synthesis scheme of conjugates. (B) Normalized SEC profile of 2P-EPI and P-EPI. Superose 6 HR10/30 column with mobile phase 0.1 M sodium/30% acetonitrile (pH 6.5), flow rate 0.4 mL/min. (C) Molecular weight and drug content of the conjugates.

To synthesize a ^{125}I-labeled conjugate, comonomer MA-Tyr-NH_2 (1.5% molar ratio in feed) was added and the same procedure shown above was used to produce P-Tyr-EPI/2P-Tyr-EPI (Fig.18).

4.1.6 FRET ON/OFF of the Conjugates in the Presence of Enzyme

Here, we used FRET ON/OFF strategy to monitor drug release from HPMA copolymer conjugates [38]. As mentioned above, we designed and prepared HPMA copolymer conjugates containing a popular FRET pair Cy3/Cy5 or a new FRET pair EPI/Cy5 - the donor fluorophore Cy3 or EPI was attached to HPMA polymer backbone as a payload via a cleavable (by lysosomal proteases) tetrapeptide linker Gly-Phe-Leu-Gly (GFLG), while the acceptor Cy5 was directly labeled on the HPMA backbone as a tag (Fig. 19A). After polymerization, the FRET property of the conjugates was determined using fluorescence spectrometry before and after exposure to papain, a thiol proteinase with specificity similar to lysosomal cathepsin B. For P-Cy3-Cy5 conjugate, excitation wavelength 520 nm was selected to minimize direct emission of Cy5. As shown in Figure 19B, detectable FRET occurred in the original non-treated conjugate (Red), but not in the same conjugate incubated with papain (Blue). Loss of FRET was due to the

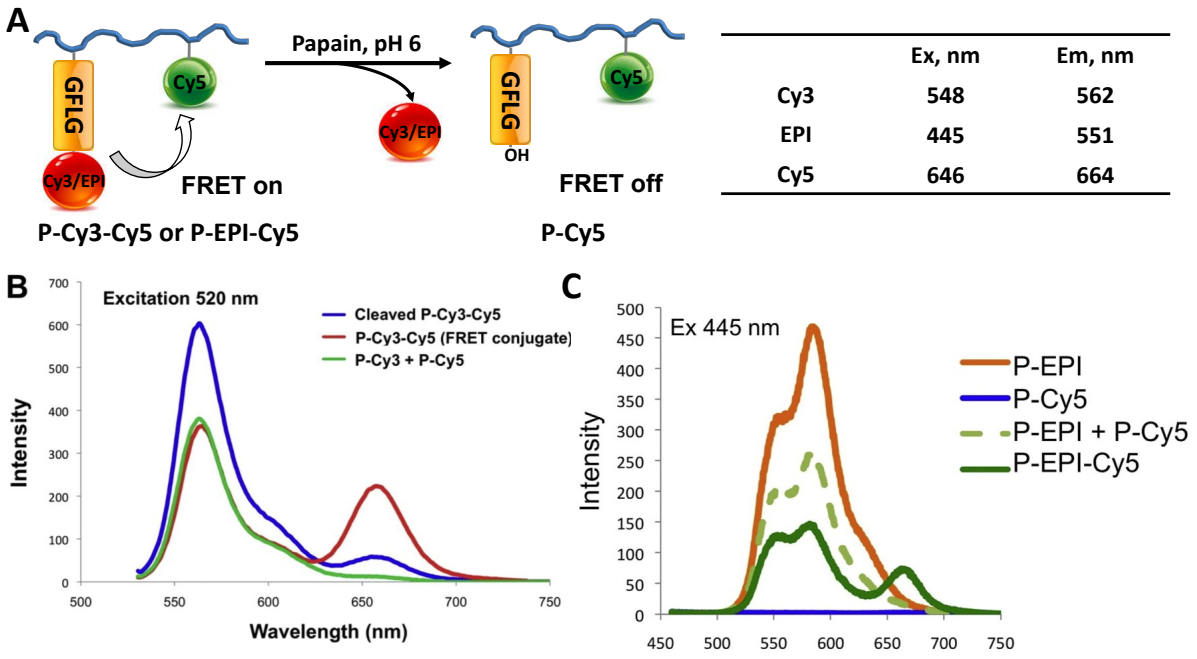

Figure 19. Illustration of FRET principle of dual-labeled enzyme-cleavable polymer conjugates containing Cy3/EPI (donor) and Cy5 (acceptor). (B) Fluorescence spectra of conjugate P-Cy3-Cy5 before and after cleavage by papain. The mixture of conjugates P-Cy5/P-Cy3 was measured as control (excitation 520 nm using methanol as solvent). Fluorescence spectra of FRET conjugate P-EPI-Cy5 compared with P-EPI, P-Cy5 and their mixture P-Cy5 + P-EPI.

cleavage of the linker GFLG by enzyme, and consequently, the release of Cy3 from backbone. Similarly, due to the cleavage of papain, P-EPI-Cy5 conjugate lost FRET signal (Fig. 19C), indicating the release of EPI from the backbone. In sum, both conjugates showed the FRET ON/OFF effect in the presence of enzyme.

4.2. Evaluation of FRET Pair-labeled HPMA Copolymer Conjugates (FRET ON/OFF) in Cultured Cells

In vitro FRET measurement. After evaluation under the enzyme condition, the FRET property of conjugates (P-Cy3-Cy5 and 2P-Cy3-Cy5) was further elucidated in living cells [38, 39]. Human ovarian cancer A2780 cells that overexpress cathepsin B were incubated with the FRET conjugates, and NIH3T3 mouse fibroblast cells (low cathepsin B expression) were used as a control. The release of model drug Cy3 will result in decrease of FRET intensity that can be investigated via cell lysis using fluorescence spectrometry. According to the previous reports [47-49], the ratio, I_{Cy3}/I_{FRET}, was calculated to quantify the FRET change, where I_{Cy3} and I_{FRET} are the fluorescence intensity at 562 nm and 664 nm, respectively (excitation 520 nm). For the conjugate P-Cy3-Cy5, the ratio in medium alone was 2.35, and in initial stock was 1.97. When the conjugate was incubated with A2780 cancer cells, the ratio increased to 2.71 at 4 h, then gradually increased to 3.99 at 12 h and 5.25 at 24 h, whereas in NIH3T3 cells, the ratio only increased to 2.73 at 24 h (Fig. 20A). A similar FRET change in the 2nd generation conjugate (2P-Cy3-Cy5) was also observed (Fig. 20B). There was significant difference in the release efficacy between cancer and normal cells. This observation suggests an effective release of Cy3 from the conjugate, which is highly dependent on the cathepsin B level. Following the same principle, we synthesized the conjugates P-Cy5-Cy7 and P-EPI-Cy5. The conjugates were characterized using FRET spectra. The payload Cy7/EPI release were determined by FRET intensity changes (Fig. 20C,D). For 2P-Cy5-Cy7 conjugate, three different cell lines were used, including cathepsin B-negative NIH/3T3 normal cells, and cathepasin B-positive human ovarian cancer cells (A2780 and OVCAR-3). Obviously, conjugate had faster Cy7 release in cancer cells, as compared to that in normal cells (Fig. 20C). For P-Cy5-EPI conjugate, the FRET ratio in A2780 cancer cells increased from 0.12 (initial stock) to 0.19 at 4 h and gradually to 0.28 at 24 h (Fig. 20D). The increase of FRET ratio indicated that drug EPI molecules could be released from the conjugate inside A2780 cancer cells over the time. Taken together, the aforementioned results from those three conjugates showed potential to use FRET as a tool for future in vivo real-time monitoring drug delivery, tracking chain scission of HPMA copolymer-

drug conjugates, and for improved cancer diagnostics and therapy. Compared to normal cells, cathepsin B level is much higher in malignant tumors, such as ovarian cancer, breast cancer, and melanoma. It acts as an important proteinase of matrix materials to degrade surrounding proteins and other tissue components so that cancer cells can invade and metastasize [26]. Therefore, high expression of cathepsin B in tumor cells can induce a fast release of drugs from conjugates and thereby mediates a relatively high concentration of active free drug inside the tumor cells.

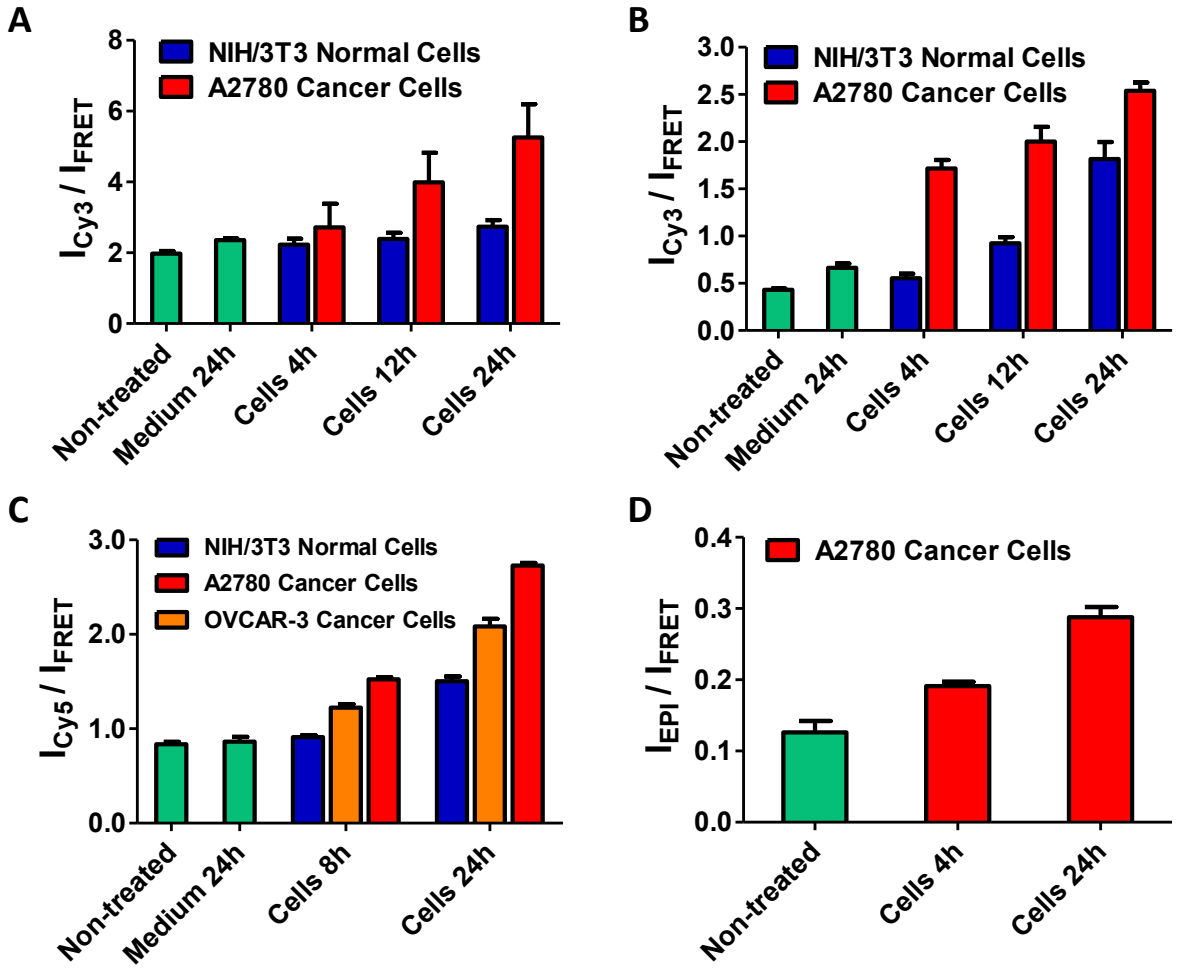

Figure 20. FRET changes of different FRET-trackable conjugates in normal and cancer cells at different time intervals. (A) FRET ratio of P-Cy3-Cy5 conjugate in normal NIH3T3 mouse fibroblast cells (low cathepsin B expression) and A2780 ovarian cancer cells (high cathepsin B expression). (B) FRET ratio of 2P-Cy3-Cy5 conjugate in normal NIH3T3 and A2780 ovarian cancer cells. (C) FRET ratio of 2P-Cy5-Cy7 conjugate in NIH3T3, A2780, and OVCAR-3 cells. (D) FRET ratio of P-EPI-Cy5 conjugate in A2780 cancer cells. The cells were incubated with conjugates at 37 °C first for 4 or 8 h and then cultured in fresh medium for additional time. Then cell lysate was measured by fluorescence spectroscopy. FRET ratio = I_{donor}/I_{FRET}, was calculated to quantify the FRET change, where I_{donor} and I_{FRET} are the fluorescence intensity, respectively (using donor excitation wavelength). Increase of the ratio revealed effective payload release following enzyme exposure.

In vitro FRET imaging. The conjugate P-Cy3-Cy5 was further evaluated using FRET confocal microscopy [38], which is a more straightforward approach for performing FRET. In this experiment, pre-bleach and post-bleach images were collected. To do the photo-bleaching, the cells were exposed to high excitation intensity at an excitation wavelength of 646 nm (Ex of Cy5) for a 20 min period. After high-energy laser treatment, there was a dramatic reduction of Cy5 intensity in the bleached regions (Fig. 21). It was found that bleaching the acceptor Cy5, in the cells immediately following 4 h incubation, resulted in FRET intensity significantly decreased, and donor Cy3 fluorescence substantial increase, because the acceptor can no longer accept energy from the donor. However, those intensity changes did not occur in the same batch of cells after additional 20 h culture (Fig. 21).

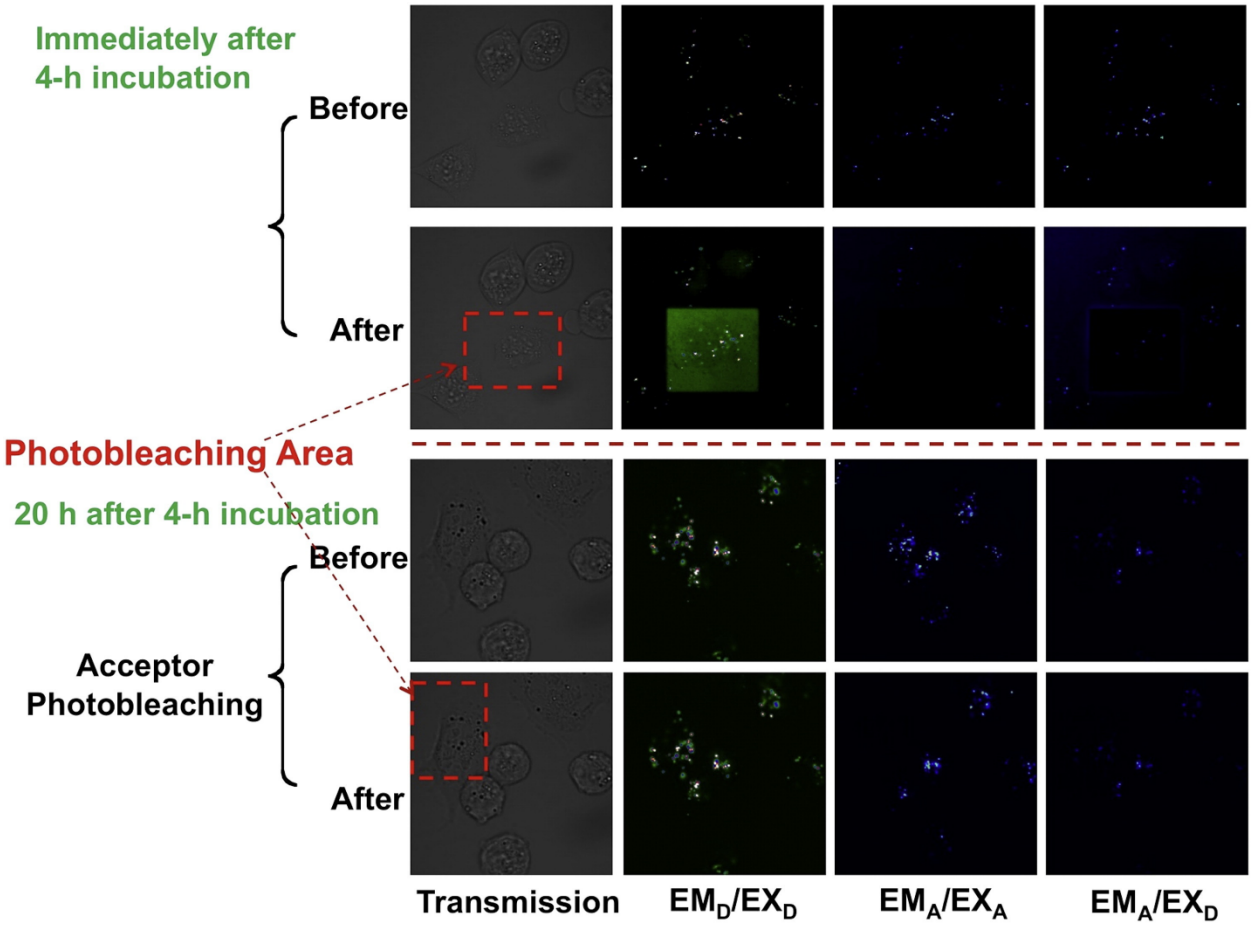

Figure 21. Visualization of payload Cy3 release from conjugate P-Cy3-Cy5 in cathepsin B over-expressing A2780 human ovarian cancer cells by comparison of FRET images of pre- and post-bleaching. The cells were first incubated with P-Cy3-Cy5 at 37 °C for 4 h and then were washed. Half of the cells were fixed immediately, while the other half were incubated with fresh medium at 37 °C for another 20 h and fixed. The fixed cells were observed under confocal microscope using the standard acceptor Cy5 photobleaching method. Bleached areas are indicated by red boxes.

These results indicated that the model drug Cy3 had been released from the backbone after cellular internalization and lysosomal cleavage. The microscopic result confirmed the previous findings from FRET measurement.

4.3 FRET ON/OFF of the Conjugates in Mice Tumor Model

To obtain better in vivo imaging, 2P-Cy5-Cy7 conjugate was used. The far-red fluorescent donor Cy5 and near-infrared acceptor Cy7 have relatively large gap between the excitation and emission maxima, which can significantly reduce the background. In addition, both of them have enhanced penetration ability, which are suitable for animal studies. The Cy5 is absorbed by Cy7 and reemitted until enzymatic cleavage of the peptide sequence GFLG by cathepsin B. As we mentioned above, increased cathepsin B level has been shown to be associated with many different types of cancer, particularly in ovarian carcinoma. Upon cleavage by cathepsin B, tissue retention of the Cy5 containing fragment occurs, while uncleaved conjugates continue to emit fluorescence signal at Cy7 wavelength. In order to compare the drug release speed in different tissues, FRET ratio I_{cy5}/I_{FRET} was measured, where I_{cy5} and I_{FRET} are the fluorescence intensity at 680 nm and 760 nm, respectively (excitation 640 nm). Here, the ratiometric approach is relatively independent of interindividual difference in pharmacokinetics such as total probe uptake and washout, as well as thresholding. In this study, female nude mice bearing subcutaneous A2780 human ovarian carcinoma xenografts were used. 2P-Cy5-Cy7 conjugate was intravenously injected into the tumor-bearing mice via tail vein. The mice were imaged using IVIS (in vivo imaging system) at 12 h, 24 h, 48 h, and 144 h after administration. Figure 22 showed the fluorescence images of the mice. Following intravenous injection of the conjugate, mice showed greater Cy5/Cy7 ratio in tumor. In addition, the tumor and major tissues were harvested at different time intervals, and their fluorescence images were immediately taken by IVIS camera (Fig. 22A). We found higher Cy5/Cy7 ratiometric fluorescence in A2780 tumor as compared to normal tissues (Fig. 22B&22C). The rapidity of ratiometric change in tumors is likely due to their high cathepsin B level. In parallel, we also measured the fluorescence signal intensity of Cy7 at the same time. As shown in Figure 22D, there was high accumulation of Cy7 in tumor. At 48 h after administration, the Cy7 uptake in the tumor reach the highest value, due to the EPR effect. In contrast, the Cy7 in the kidney and liver, was cleared significantly from 24 h to 72 h.

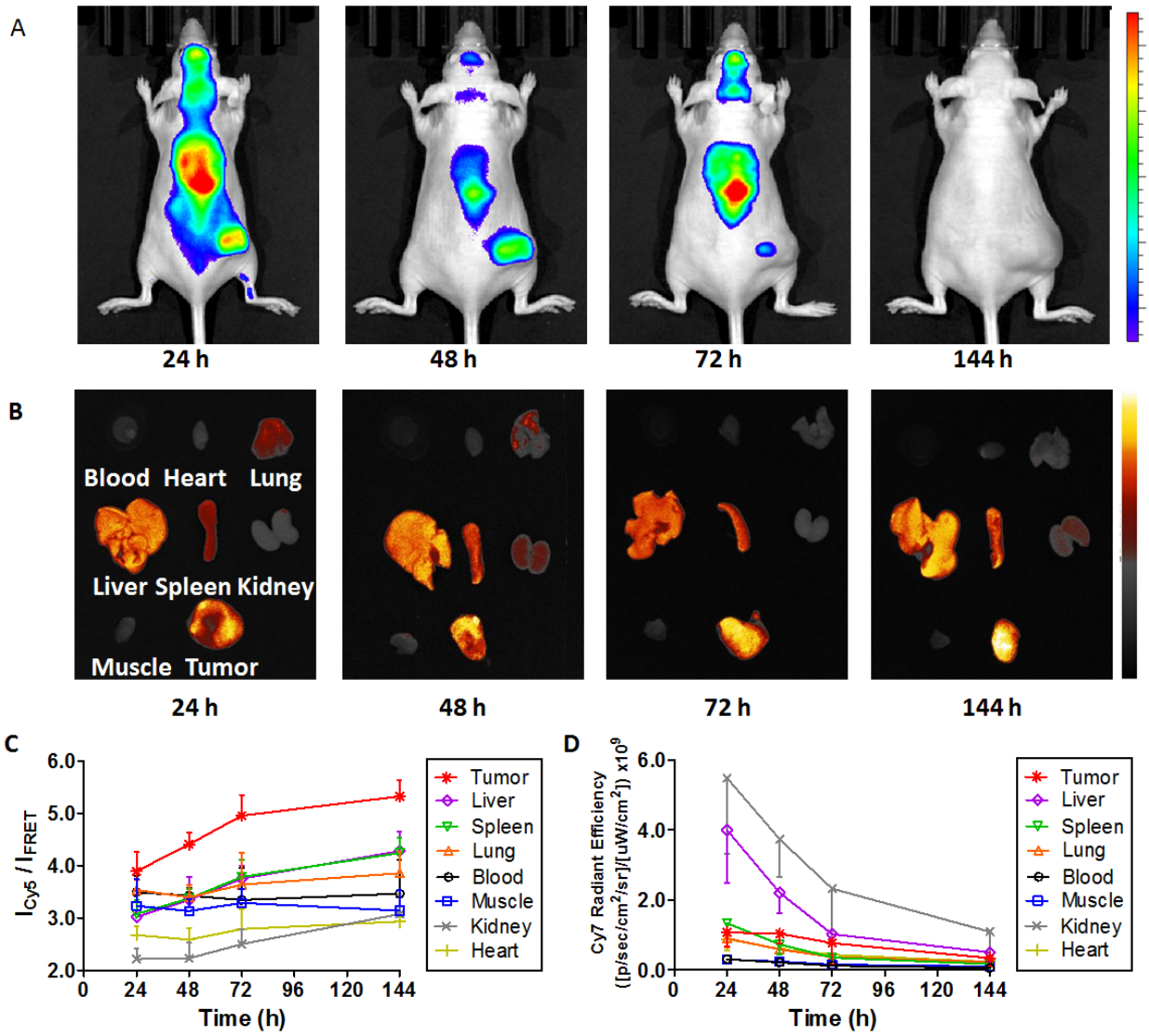

Figure 22. FRET Change in the mice bearing A2780 human ovarian tumor. (A) Whole-body FRET images of mice at different time intervals (24, 48, 72, and 144 h p.i.) after i.v. administration of 2P-Cy5-Cy7 conjugate. (B) Ratiometric images of ex vivo tissues at different time intervals. Ratiometric images were derived from the division of the Cy5 image by the FRET image in the same mouse. (C) FRET ratio of 2P-Cy5-Cy7 conjugate in the tumor and major tissues over the time. FRET ratio = ICy5/IFRET, was calculated to quantify the FRET change, where ICy5 and IFRET are the fluorescence intensity at 680 nm and 760nm, respectively (using Cy5 excitation wavelength 640 nm). (D) Cy7 fluorescence signal of 2P-Cy5-Cy7 conjugate in the tumor and major tissues over the time (excitation 740 nm/ emission 800 nm). The tumor-bearing mice were intravenously injected with the 2P-Cy5-Cy7 conjugate. At 24, 48, 72, and 144 h after administration, the tissues and tumor were harvested and imaged using IVIS. The fluorescent images were taken using different filter settings. The data are presented as mean ± standard deviation (n = 4-5).

4.4 Cell Uptake and In Vitro Cytotoxicity of the Conjugates P-EPI and 2P-EPI

The cell uptake of the conjugates (P-EPI and 2P-EPI) was analyzed using flow cytometry with EPI fluorescence signal (Fig. 23A) [38]. The free drug EPI was used as a control. A2780 human ovarian cancer cells were incubated with different EPI formulations, respectively. Free EPI showed a higher cell uptake than the two conjugates (P-EPI and 2P-EPI). This difference is likely due to their distinct entry pathways - diffusion (free drugs) vs. endocytosis (conjugates). In addition, the cytotoxicity of free EPI and its HPMA copolymer conjugates (P-EPI and 2P-EPI) against A2780 human ovarian cancer cells was determined. Figure 23B shows the representative cell growth inhibition curves. Overall, free drug EPI and its conjugates (P-EPI, 2P-EPI) showed a dose-dependent cytotoxicity against A2780 cells. On the basis of the IC50 values (Fig. 23B), both HPMA copolymer-EPI conjugates possessed lower in vitro cytotoxicity than free EPI, due to the different mechanisms of cell uptake.

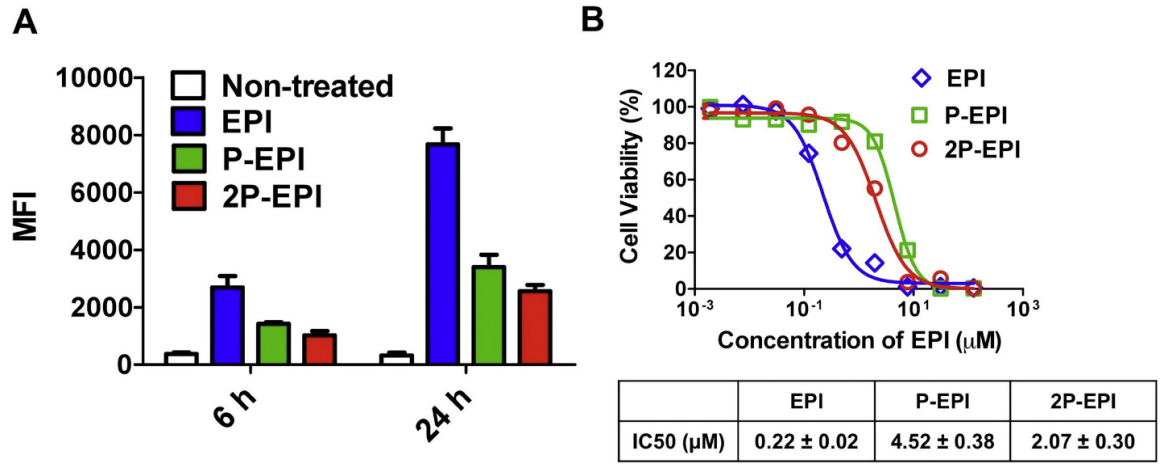

	EPI	P-EPI	2P-EPI
IC50 (μM)	0.22 ± 0.02	4.52 ± 0.38	2.07 ± 0.30

Figure 23. Cell uptake and cytotoxicity of free drug EPI and its conjugates (P-EPI, 2P-EPI) in A2780 human ovarian cancer cells. (A) Flow cytometry analysis of cell uptake in the A2780 cells incubated with medium alone (non-treated), free EPI, or its conjugates (P-EPI, 2P-EPI) at 37 °C for 6 and 24 h. MFI, mean fluorescence intensity. (B) In vitro cytotoxicity of free drug EPI and its HPMA conjugates (P-EPI, 2P-EPI) toward A2780 human ovarian carcinoma cells. The data are presented as mean ± standard deviation (n = 3-4).

4.5 Pharmacokinetic Study of ^{125}I-labeled HPMA Copolymer-EPI Conjugates

It has been reported that conjugation of free drug to HPMA polymer carrier markedly slows its blood clearance [50]. For example, the fast initial clearance of DOX ($t_{1/2}$) is 4 min, however, there was still 55% polymer-bound drug in circulation 1 h after injection of P-DOX (Mw 25 kDa) [50]. In this study, we compared pharmacokinetic profiles of 1st generation conjugate (P-(Tyr)-EPI, Mw 28 kDa) and 2nd generation conjugate (2P-(Tyr)-EPI, Mw 84 kDa) to highlight the

effect of molecular weight on plasma concentration and circulation time [38]. Tyrosine moiety was inserted into the conjugates for radiolabeling (^{125}I) in order to enhance accuracy and sensitivity of the analysis. The blood radioactivity-time profiles were determined and illustrated in Figure 24. The pharmacokinetic parameters of the two conjugates in mice are listed in Figure 24, and the previously reported half-lives of 2P-PTX/P-PTX and 2P-GEM/P-GEM are cited here for comparison [44].

.

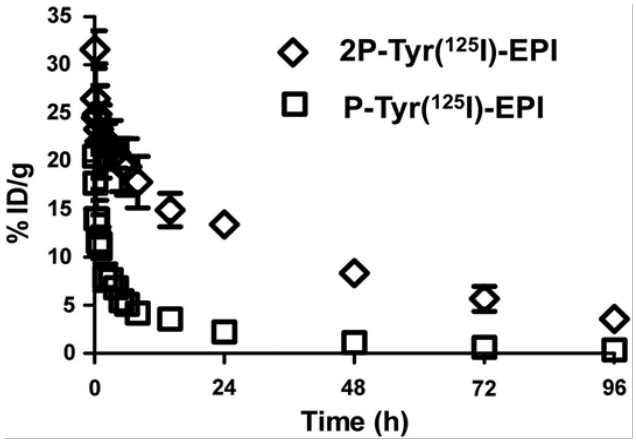

	P-EPI	P-PTX	P-GEM	2P-EPI	2P-PTX	2P-GEM
$T_{1/2,\alpha}$ (h)	0.33±0.07	*0.88±0.11*	*0.26±0.02*	0.18±0.06	*1.13±0.13*	*1.45±0.36*
$T_{1/2,\beta}$ (h)	7.55±1.55	*13.30±1.28*	*6.36±0.66*	33.22±3.18	*37.90±3.55*	*32.07±2.50*
AUC (%ID h/mL blood)	110.10±14.06	*420.95±26.05*	*108.66±6.74*	1060.48±88.83	*1206.42±85.97*	*1481.23±83.06*
CL (mL/h)	0.91±0.12	*0.24±0.01*	*0.92±0.06*	0.09±0.01	*0.08±0.01*	*0.07±0.004*
MRT (h)	10.34±2.09	*18.25±1.71*	*8.49±0.88*	47.79±4.57	*52.86±4.95*	*45.39±3.43*
Vss (mL)	9.39±0.82	*4.34±0.16*	*7.82±0.38*	4.51±0.11	*4.38±0.16*	*3.06±0.10*

Figure 24. Pharmacokinetic profiles of ^{125}I-labeled conjugates P-EPI and 2P-EPI in mice, and the summary of PK parameters of 1st generation and 2nd generation of HPMA copolymer-drug conjugates. $T_{1/2,\alpha}$ = initial half-life; $T_{1/2,\beta}$ = terminal half-life; AUC = total area under the blood concentration versus time curve; %ID = percentage of injected dose; CL = total body clearance; MRT = mean residence time; Vss = steady-state volume of distribution. The data represent the mean radioactivity expressed as a percentage of the injected dose per gram of blood (n=5)

Higher Mw 2P-EPI conjugate showed a longer terminal half-life (33.22 h) than low Mw conjugate P-EPI (7.55 h). 2P-EPI (AUC = 1060.48%ID/mL) had a 10-fold higher systemic exposure than P-EPI (110.10%ID/mL) ($p < 0.001$). The increased exposure of 2P-EPI is mainly attributed to its significantly slower systemic clearance (CL) (2P-EPI: 0.09 mL/h vs. P-EPI: 0.91 mL/h) ($p < 0.001$). Taken all together, the 2nd generation conjugate 2P-EPI with increased Mw possesses an improved pharmacokinetic profile. Although individual drugs (EPI, PTX, and GEM) have

different metabolism and clearance time, the new generation conjugate 2P-EPI showed significant improved pharmacokinetics with parameters similar to 2P-PTX and 2P-GEM, such as terminal half-life, total body clearance, and steady-state volume of distribution [44], which indicates that conjugation of drug to polymer carrier can improve its stability in plasma, and the elimination rate of the conjugates is primarily determined by the polymer carrier.

In summary, the in vitro results demonstrated that our designed FRET-trackable conjugates possessed FRET ON/OFF effect when applied on cells in the presence of enzyme. Next, we evaluated the in vivo performance of the conjugate.

4.6 In Vivo Anti-tumor Activity

The therapeutic potential of the backbone degradable long circulating HPMA copolymer-EPI conjugate (2P-EPI) was evaluated in female nude mice bearing A2780 human ovarian carcinoma xenografts [38]. Briefly, subcutaneous injection of $5x10^6$ A2780 human ovarian cancer cells into the right flank led to the development of tumors with a diameter of 3-4 mm after 3 to 4 weeks. Then, the mice were intravenously injected with three doses of 5 mg/kg EPI equivalent on days 0, 4, and 8. Free drug EPI and the 1st generation conjugate P-EPI were also administered for comparison. Tumor growth was closely monitored during and after treatment. On day 20, complete tumor regression was achieved in the five mice treated with conjugate 2P-EPI (Fig. 25); the tumors treated with P-EPI shrank to 80 ± 37% of the initial size. In contrast, free drug EPI at equivalent doses only slightly delayed tumor growth when compared with saline (control), and mice had to be sacrificed on day 20 as the tumor had reached 1772±840% of the baseline. However, there was no significant difference between treatment with 2P-EPI and P-EPI until day 35 when tumor started regrowth in P-EPI group, and four of the tumors grew back to ~1200% at day 80 ($p < 0.01$) (Fig. 25B,C). On the contrary, no observable tumor was detected in the mice treated with 2P-EPI at day 100. These results demonstrate the importance of long-term experiments for evaluation of tumor growth inhibitory effect. The results also indicated that 2P-EPI is highly superior to both P-EPI and free EPI. The complete tumor regression and long-term inhibition of tumorigenesis by 2P-EPI treatment are attributed to long circulation time and sufficient extravasation of the conjugates at the tumor site by the enhanced permeability and retention (EPR) effect. In addition, this result also suggests that 2P-EPI conjugate may be able to arrest both tumor progenitor cells and differentiated cells as we

observed in another scenarios. For safety concern, body weight of the mice was closely recorded during and after treatment (Fig. 25D). The body weights of the mice temporarily decreased (less than 10%) when P-EPI and 2P-EPI were administered as multiple dosages but recovered gradually and remained stable after withdrawal, which suggests the doses used were tolerable.

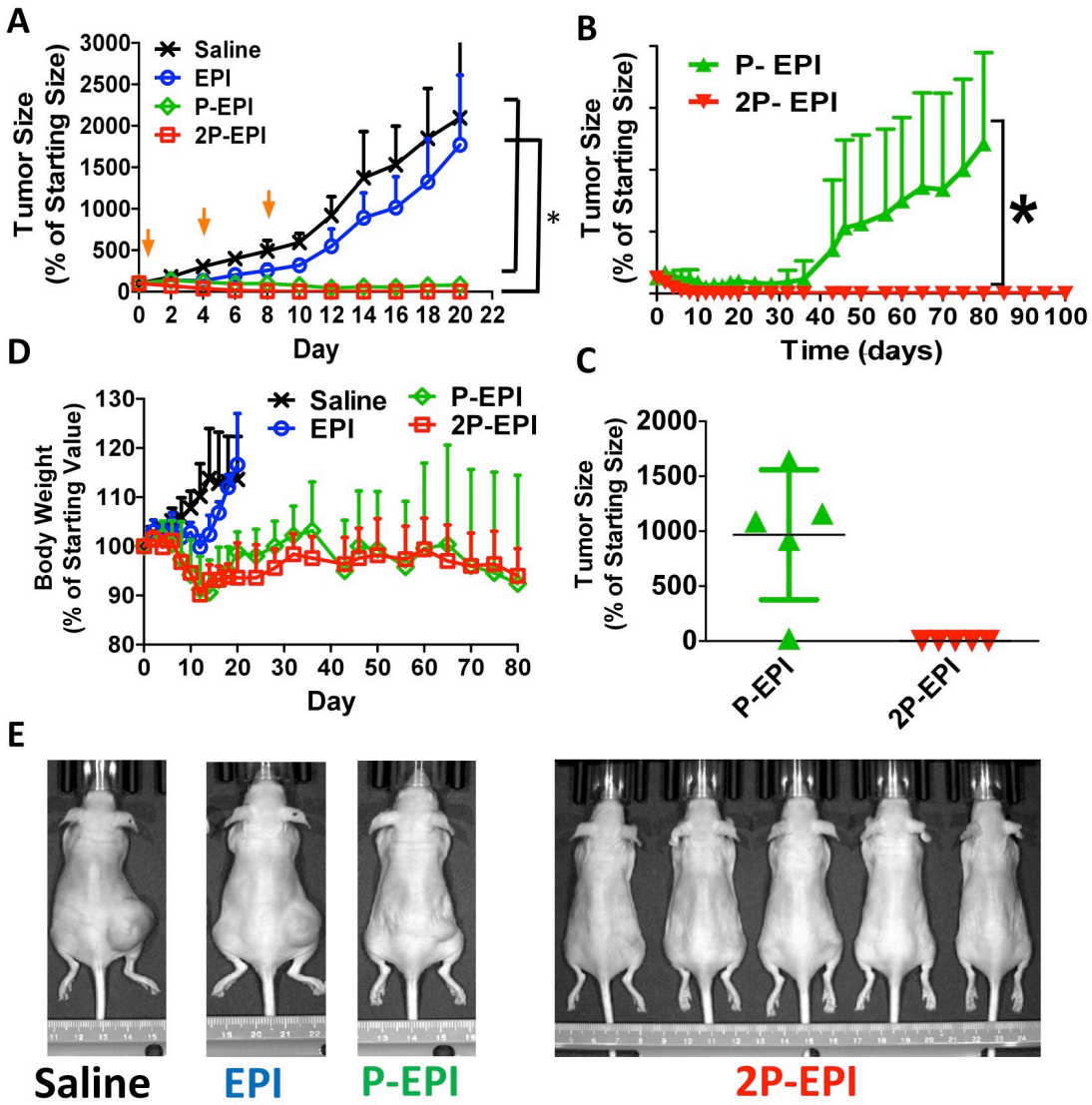

Figure 25. Comparison of in vivo anti-tumor activity on female nude mice bearing A2780 human ovarian carcinoma xenografts. (A) The mice were intravenously injected with 3 doses of EPI or HPMA copolymer-EPI conjugates (P-EPI and 2P-EPI). Free drug and untreated groups were stopped on day 20 due to large size of tumors. (B) Long-term monitoring of tumor growth in conjugate treatments. (C) The tumor size in the mice treated with conjugate on day 80. (D) Body weight changes of mice during the treatment, and (E) End point photographs of tumor-bearing mice from various treatments.

5. Conclusion

We have developed a biodegradable polymeric drug delivery system with the capacity for non-invasive fate monitoring using FRET-based methodology. In this project, Epirubicin (EPI) served as antineoplastic agent. In vitro cell studies determined via FRET intensity changes clearly demonstrated cathepsin B levels are decisive and responsible for drug anti-tumor activity. In vivo FRET imaging showed that the drug can be relatively rapidly released in the tumor cells to cause high concentration of free drugs inside tumors. In addition, PK data provided strong evidence that 2nd generation backbone degradable HPMA copolymer-drug conjugates remarkably enhanced circulation time. As a result, the degradable diblock HPMA copolymer-EPI conjugate (2P-EPI) produced complete tumor remission and long-term inhibition of tumorigenesis (100 days) after intravenous injection into the mice bearing human ovarian carcinoma A2780 xenografts. In contrast, the free drug EPI and 1st generation low-Mw conjugate P-EPI could not achieve such progress in the trial.

6. Publications, Abstracts, and Presentations

Publications

1. J. Yang, J. Kopeček, Macromolecular Therapeutics. J. Controlled Release 190, 288-303 (2014). PMCID: PMC4142088

2. J. Yang, R. Zhang D.C. Radford, J. Kopeček, FRET-Trackable Biodegradable HPMA Copolymer-Epirubicin Conjugates for Ovarian Carcinoma Therapy. J. Controlled Release 218, 36-44 (2015). NIHMSID 729442

3. J. Yang, J. Kopeček, Polymeric Biomaterials and Nanomedicines. J. Drug Deliv. Sci. Technol. (2015) http://dx.doi.org/10.1016/j.jddst.2015.05.012 NIHMSID 693394

4. J. Yang, J. Kopeček, Design of Smart HPMA Copolymer-Based Nanomedicines. J. Controlled Release (2015) http://dx.doi.org/10.1016/j.jconrel.2015.10.003 NIHMSID 729622

5. D.C. Radford, R. Zhang, J. Yang, J. Kopeček, A FRET-Based Strategy to Monitor and Quantitate Biodegradation of Backbone Degradable HPMA Copolymers. In preparation.

6. R. Zhang, J. Yang, D.C. Radford, J. Kopeček, FRET-Trackable HPMA Copolymer Conjugate for the Treatment of Ovarian Cancer. In preparation.

Abstracts/Presentations

7. J. Yang, J. Kopeček, Progress in HPMA-based Macromolecular Therapeutics. 2014 International Advanced Drug Delivery Symposium, National Tsing Hua University, Taiwan, April 29-30, 2014.

*8. J. Yang, R. Zhang, D.C. Radford, J. Kopeček, Design and Synthesis of FRET-Trackable HPMA-Based Biodegradable Conjugates for Drug/Gene Delivery. 3rd Symposium on Innovative Polymers for Controlled Delivery (SIPCD 2014), Suzhou, China, September 16-19, 2014.

*9. J. Kopeček, J. Yang, Rational Design of Macromolecular Therapeutics. Chinese Pharmaceutics Conference, Changsha, Hunan Province, China, September 19-22, 2014.

10. D.C. Radford, J. Yang, R. Zhang, J. Kopeček, Quantification of Polymer Backbone Degradation Using Fluorescence Resonance Energy Transfer. NanoUtah 2014 Conference, Grand America Hotel, Salt Lake City, Utah, October 12-15, 2014.

11. J. Yang, R. Zhang, D.C. Radford, J. Kopeček, FRET-Trackable Biodegradable HPMA Copolymer-Epirubicin Conjugates for Ovarian Carcinoma Therapy – In Vitro and In Vivo Evaluation. 17th International Symposium on Recent Advances in Drug Delivery Systems, Salt Lake City, Utah, June 14-17, 2015.

12. D.C. Radford, J. Yang, R. Zhang, J. Kopeček, A FRET-Based Strategy to Monitor and Quantitate Biodegradation of Backbone Degradable HPMA Copolymers.17th International Symposium on Recent Advances in Drug Delivery Systems, Salt Lake City, Utah, June 14-17, 2015.

13. L. Zhang, R. Zhang, J. Yang, J. Kopeček, Dual-Radioisotope HPMA Copolymer-Drug Conjugate for In Vivo Imaging Studies. 17th International Symposium on Recent Advances in Drug Delivery Systems, Salt Lake City, Utah, June 14-17, 2015.

*14. D.C. Radford, J. Yang, R. Zhang, J. Kopeček, A FRET-Based Imaging Strategy to Rapidly Quantify Biodegradation of Degradable Nanomedicines. Biomedical Engineering Society 2015 Annual Meeting, Tampa, Florida, October 7-10, 2015.

15. D.C. Radford, J. Yang, R. Zhang, J. Kopeček, A FRET-Based Imaging Strategy to Rapidly Quantify Biodegradation of Degradable Nanomedicines. Conference NanoUtah 2015, University of Utah, Salt Lake City, Utah, October 13, 2015.

16. J. Yang, R. Zhang, D.C. Radford, J. Kopeček, FRET-Trackable Biodegradable HPMA Copolymer-Epirubicin Conjugates for Ovarian Carcinoma Therapy. 11th International Symposium on Stimuli-Responsive Materials, Santa Rosa, California, October 25-27, 2015.

7. Inventions, Patents, and Licenses

- The results of therapeutic activity of HPMA copolymer-EPI conjugates contributed to the approval of our patent application (US Non-Provisional Patent Application “Polymeric Drug

Delivery Conjugates and Methods of Making and Using Thereof; Serial No. 13/583,270) that was a result of another grant. We just received a Notice of Allowance.

8. Reportable Outcomes

- We developed a technique for independent monitoring of the in vivo fate of polymer carrier and drug.
- FRET technique is suitable for monitoring of the degradation of both the backbone and of side-chains terminated in drug.
- Second-generation backbone degradable HPMA copolymer–EPI conjugates possess high efficacy to treat experimental ovarian cancer - complete tumor remission and long-term inhibition of tumorigenesis (100 days).

9. Other Achievements

- Graduate student D. Christopher Radford submitted a F31 grant proposal to NIH for a pre-doctoral fellowship (A Multimodal Imaging Strategy for Preclinical Optimization of Anticancer Nanomedicines). It was reviewed by the "Surgical Sciences, Biomedical Imaging and Bioengineering" review panel and received a 23 percentile; this is below the last year's payline and most probably he will be awarded the fellowship early next year.

List of Personnel

Jindřich Kopeček, Ph.D., D. Sc.	Principle Investigator Dates: September 2013 – August 2015
Jiyuan Yang, Ph.D.	Co-Investigator Dates: September 2013 – August 2015
Rui Zhang, Ph.D.	Postdoctoral Fellow Dates: September 2013 – June 2015
Libin Zhang, Ph.D.	Postdoctoral Fellow Dates: July 2015 – August 2015
Stewart Low	Graduate Student Dates: September 2013 – November 2013
David Christopher Radford	Graduate Student Dates: November 2013 – August 2015

Jiawei Wang | Graduate Student
Dates: June 2015 – August 2015

10. References

[1] J. Ferlay, I. Soerjomataram, R. Dikshit, S. Eser, C. Mathers, M. Rebelo, et al. Cancer Incidence and Mortality Worldwide: Sources, Methods and Major Patterns in GLOBOCAN 2012. Intern. J. Cancer 136, E359-386 (2015).

[2] R. Siegel, J. Ma, Z. Zou, A. Jemal, Cancer Statistics, 2014. CA: Cancer J. for Clinicians 64, 9-29 (2014).

[3] J. Kopeček, Biomaterials and Drug Delivery: Past, Present, and Future. Mol. Pharmaceutics 7, 922-925 (2010). PMCID: PMC3124011

[4] J. Kopeček, P. Kopečková, HPMA Copolymers: Origins, Early Developments, Present, and Future. Adv. Drug Deliv. Rev. 62, 122-149 (2010). PMCID: PMC2836498

[5] J. Kopeček, Polymer-Drug Conjugates: Origins, Progress to Date and Future Directions. Adv. Drug Deliv. Rev. 65, 49-59 (2013). PMCID: PMC3565043

[6] Y. Zhou, J. Kopeček, Biological Rationale for the Design of Polymeric Anti-Cancer Nanomedicines. J. Drug Targeting 21, 1-26 (2013). PMCID: PMC4605218

[7] S.Q. Gao, Y. Sun, P. Kopečková, C.M. Peterson, J. Kopeček, Pharmacokinetic Modeling of Absorption Behavior of 9-Aminocamptothecin (9-AC) Released from Colon-Specific HPMA Copolymer-9-AC Conjugate in Rats. Pharmaceutical Res. 25, 218-226 (2008).

[8] K.D. Fowers, J. Kopeček, Targeting of Multidrug-Resistant Human Ovarian Carcinoma Cells with Anti-P-glycoprotein Antibody Conjugates. Macromol. Biosci. 12, 502-514 (2012). PMCID: PMC4613759

[9] Z.R. Lu, P. Kopečková, J. Kopeček, Polymerizable Fab' Antibody Fragments for Targeting of Anticancer Drugs. Nature Biotechnol. 1917, 1101-1104 (1999).

[10] J.G. Shiah, M. Dvořák, P. Kopečková, Y. Sun, C.M. Peterson, J. Kopeček, Biodistribution and Antitumour Efficacy of Long-Circulating N-(2-Hydroxypropyl)methacrylamide Copolymer-Doxorubicin Conjugates in Nude Mice. Europ. J. Cancer 37, 131-139 (2001).

[11] T. Minko, P. Kopečková, V. Pozharov, J. Kopeček, HPMA Copolymer Bound Adriamycin Overcomes MDR1 Gene Encoded Resistance in a Human Ovarian Carcinoma Cell Line. J. Controlled Release 54, 223-233 (1998).

[12] B. Říhová, L. Kovář, M. Kovář, O. Hovorka, Cytotoxicity and Immunostimulation: Double Attack on Cancer Cells with Polymeric Therapeutics. Trends Biotechnol. 27, 11-17 (2009).

[13] P.A. Vasey, S.B. Kaye, R. Morrison, C. Twelves, P. Wilson, R. Duncan, et al. Phase I Clinical and Pharmacokinetic Study of PK1 [N-(2-Hydroxypropyl)methacrylamide Copolymer Doxorubicin]: First Member of a New Class of Chemotherapeutic Agents-Drug-Polymer Conjugates. Cancer Research Campaign Phase I/II Committee. Clin. Cancer Res. 5, 83-94 (1999).

[14] L.W. Seymour, D.R. Ferry, D.J. Kerr, D. Rea, M. Whitlock, R. Poyner, et al. Phase II Studies of Polymer-Doxorubicin (PK1, FCE28068) in the Treatment of Breast, Lung and Colorectal Cancer. Intern. J. Oncol. 34, 1629-1636 (2009).

[15] L.W. Seymour, D.R. Ferry, D. Anderson, S. Hesslewood, P.J. Julyan, R. Poyner, et al. Hepatic Drug Targeting: Phase I Evaluation of Polymer-Bound Doxorubicin. J. Clin. Oncol. 20, 1668-1676 (2002).

[16] N.E. Schoemaker, C. van Kesteren, H. Rosing, S. Jansen, M. Swart, J. Lieverst, et al. A Phase I and Pharmacokinetic Study of MAG-CPT, a Water-Soluble Polymer Conjugate of Camptothecin. Brit. J. Cancer 87, 608-614 (2002).

[17] D. Bissett, J. Cassidy, J.S. de Bono, F. Muirhead, M. Main, L. Robson, et al. Phase I and Pharmacokinetic (PK) Study of MAG-CPT (PNU 166148): A Polymeric Derivative of Camptothecin (CPT). Brit. J. Cancer 91, 50-55 (2004).

[18] F.M. Wachters, H.J. Groen, J.G. Maring, J.A. Gietema, M. Porro, H. Dumez, et al. A Phase I Study with MAG-Camptothecin Intravenously Administered Weekly for 3 Weeks in a 4-Week Cycle in Adult Patients with Solid Tumours. Brit. J. Cancer 90, 2261-2267 (2004).

[19] J.M. Rademaker-Lakhai, C. Terret, S.B. Howell, C.M. Baud, R.F. De Boer, D. Pluim, et al. A Phase I and pharmacological study of the platinum polymer AP5280 given as an intravenous infusion once every 3 weeks in patients with solid tumors. Clin. Cancer Res. 10, 3386-3395 (2004).

[20] H. Maeda, Tumor-Selective Delivery of Macromolecular Drugs via the EPR Effect: Background and Future Prospects. Bioconjugate Chem. 21, 797-802 (2010).

[21] L.W. Seymour, R. Duncan, J. Strohalm, J. Kopeček, Effect of Molecular Weight (Mw) of *N*-(2-Hydroxypropyl)methacrylamide Copolymers on Body Distribution and Rate of Excretion after Subcutaneous, Intraperitoneal, and Intravenous Administration to Rats. J. Biomed. Mater. Res. 21, 1341-1358 (1987).

[22] B.F. Sloane, Cathepsin B and Cystatins: Evidence for a Role in Cancer Progression. Sem. Cancer Biol. 1, 137-152 (1990).

[23] B.F. Sloane, J.R. Dunn, K.V. Honn, Lysosomal Cathepsin B: Correlation with Metastatic Potential. Science 212, 1151-1153 (1981).

[24] T.T. Lah, G. Calaf, E. Kalman, B.G. Shinde, J. Russo, D. Jarosz, et al. Cathepsins D, B and L in Breast Carcinoma and in Transformed Human Breast Epithelial Cells (HBEC). Biol. Chem. Hoppe-Seyler 376, 357-363 (1995).

[25] L.S. Downs, Jr., P.H. Lima, R.L. Bliss, C.H. Blomquist, Cathepsins B and D Activity and Activity Ratios in Normal Ovaries, Benign Ovarian Neoplasms, and Epithelial Ovarian Cancer. J. Soc. Gynecol. Invest. 12, 539-544 (2005).

[26] H. Nishikawa, Y. Ozaki, T. Nakanishi, K. Blomgren, T. Tada, A. Arakawa, et al. The Role of Cathepsin B and cystatin C in the Mechanisms of Invasion by Ovarian Cancer. Gynecol. Oncol. 92, 881-886 (2004).

[27] W. Ebert, H. Knoch, B. Werle, G. Trefz, T. Muley, E. Spiess, Prognostic Value of Increased Lung Tumor Tissue Cathepsin B. Anticancer Res. 14, 895-899 (1994).

[28] S.M. Chung, K. Kawai, Protease Activities in Gastric Ccancer Tissues. Clin. Chim. Acta 189, 205-210 (1990).

[29] A. Adenis, G. Hue, F. Zerimech, B. Hecquet, M. Balduyck, J.P. Peyrat, Cathepsin B, L, and D Activities in Colorectal Carcinomas: Relationship with Clinico-Pathological Parameters. Cancer Lett. 96, 267-275 (1995).

[30] A. Scorilas, S. Fotiou, E. Tsiambas, J. Yotis, F. Kotsiandri, M. Sameni, et al. Determination of Cathepsin B Expression May Offer Additional Prognostic Information for Ovarian Cancer Patients. Biol. Chem. 383, 1297-1303 (2002).

[31] G.L. Plosker, D. Faulds, Epirubicin. A Review of its Pharmacodynamic and Pharmacokinetic Properties, and Therapeutic Use in Cancer Chemotherapy. Drugs 45, 788-856 (1993).

[32] E.A. Jares-Erijman, T.M. Jovin, FRET Imaging. Nature Biotechnol. 21, 1387-1395 (2003).

[33] V. Ntziachristos, J. Ripoll, L.V. Wang, R. Weissleder, Looking and Listening to Light: The Evolution of Whole-Body Photonic Imaging. Nature Biotechnol. 23, 313-320 (2005).

[34] S. Sadekar, A. Ray, M. Janát-Amsbury, C.M. Peterson, H. Ghandehari, Comparative Biodistribution of PAMAM Dendrimers and HPMA Copolymers in Ovarian-Tumor-Bearing Mice. Biomacromolecules 12, 88-96 (2011).

[35] D.C. Radford, R. Zhang, J. Yang, J. Kopeček, A FRET-Based Strategy to Monitor and Quantitate Biodegradation of Backbone-Degradable HPMA Copolymers. In preparation.

[36] R. Roy, S. Hohng, T. Ha, A Practical Guide to Single-Molecule FRET. Nature Meth. 5, 50-116 (2008).

[37] K. Luo, J. Yang, P. Kopečková, J. Kopeček, Biodegradable Multiblock Poly[*N*-(2-hydroxypropyl)methacrylamide] via Reversible Addition-Fragmentation Chain Transfer Polymerization and Click Chemistry. Macromolecules 44, 2481-2488 (2011). PMCID: PMC3025662

[38] J. Yang, R. Zhang, D.C. Radford, J. Kopeček, FRET-Trackable Biodegradable HPMA Copolymer-Epirubicin Conjugates for Ovarian Carcinoma Therapy. J. Controlled Release 218, 36-44 (2015). NIHMSID 729442

[39] R. Zhang, J. Yang, D.C. Radford, J. Kopeček, FRET-Trackable HPMA Copolymer Conjugate for the Treatment of Ovarian Cancer. In preparation.

[40] J. Kopeček, H. Bažilová, Poly[*N*-(2-Hydroxypropyl)methacrylamide]. 1. Radical Polymerization and Copolymerization. Europ. Polym. J. 9, 7-14 (1973).

[41] J. Kopeček, P. Rejmanová, J. Strohalm, K. Ulbrich, B. Říhová, V. Chytrý, J.B. Lloyd, R. Duncan, Synthetic polymeric drugs. US Pat 5,037,883 (1991).

[42] R. Duncan, H.C. Cable, P. Rejmanová, J. Kopeček, J.B. Lloyd, Tyrosinamide residues enhance pinocytic capture of N-(2-hydroxypropyl)methacrylamide copolymers. Biochim. Biophys. Acta 799, 1-8 (1984).

[43] V. Šubr, K. Ulbrich, Synthesis and Properties of New *N*-(2-Hydroxypropyl)methacrylamide Copolymers Containing Thiazolidine-2-thione Reactive Groups. React. Funct. Polym. 66, 1525-1538 (2006).

[44] R. Zhang, J. Yang, M. Sima, Y. Zhou, J. Kopeček, Sequential Combination Therapy of Ovarian Cancer with Degradable *N*-(2-Hydroxypropyl)methacrylamide Copolymer Paclitaxel and Gemcitabine Conjugates. Proc. Natl. Acad. Sci. USA 111, 12181-12186 (2014). PMCID: PMC4143033

[45] Y. Mitsukami, M.S. Donovan, A. Lowe, C.L. McCormick, Water-Soluble Polymers. 81. Direct Synthesis of Hydrophilic Styrenic-Based Homopolymers and Block Copolymers in Aqueous Solution via RAFT. Macromolecules 34, 2248-2256 (2001).

[46] H. Pan, J. Yang, P. Kopečková, J. Kopeček, Backbone Degradable Multiblock *N*-(2-hydroxypropyl)methacrylamide Copolymer Conjugates via Reversible Addition-Fragmentation Chain Transfer Polymerization and Thiol-ene Coupling Reaction. Biomacromolecules 12, 247-252 (2011). PMCID: PMC3025662

[47] S.J. Hauff, S.C. Raju, R.K. Orosco, A.M. Gross, J.A. Diaz-Perez, E. Savariar, et al. Matrix-Metalloproteinases in Head and Neck Carcinoma-Cancer Genome Atlas Analysis and Fluorescence Imaging in Mice. Otolaryngology--head and neck surgery 151, 612-618 (2014).

[48] T. Hussain, E.N. Savariar, J.A. Diaz-Perez, K. Messer, M. Pu, R.Y. Tsien, Q.T. Nguyen, Surgical Molecular Navigation with Ratiometric Activatable Cell Penetrating Peptide for Intraoperative Identification and Resection of Small Salivary Gland Cancers. Head Neck (2014) doi: 10.1002/hed.23946.

[49] E.N. Savariar, C.N. Felsen, N. Nashi, T. Jiang, L.G. Ellies, P. Steinbach, et al. Real-Time In Vivo Molecular Detection of Primary Tumors and Metastases with Ratiometric Activatable Cell-Penetrating Peptides. Cancer Res. 73, 855-864 (2013).

[50] L.W. Seymour, K. Ulbrich, J. Strohalm, J. Kopeček, R. Duncan, The Pharmacokinetics of Polymer-Bound Adriamycin. Biochem. Pharmacol. 39, 1125-1131 (1990).

11. Appendices

Appendix 1: J. Controlled Release 190, 288-303 (2014). PMCID: PMC4142088

Appendix 2: J. Controlled Release 218, 36-44 (2015). NIHMSID 729442

Appendix 3: J. Yang, R. Zhang, D.C. Radford, J. Kopeček, Design and Synthesis of FRET-Trackable HPMA-Based Biodegradable Conjugates for Drug/Gene Delivery. 3rd Symposium on Innovative Polymers for Controlled Delivery (SIPCD 2014), Suzhou, China, September 16-19, 2014.

Appendix 4: J. Yang, R. Zhang, D.C. Radford, J. Kopeček, FRET-Trackable Biodegradable HPMA Copolymer-Epirubicin Conjugates for Ovarian Carcinoma Therapy – In Vitro and In Vivo Evaluation. 17th International Symposium on Recent Advances in Drug Delivery Systems, Salt Lake City, Utah, June 14-17, 2015.

Journal of Controlled Release 190 (2014) 288–303

Contents lists available at ScienceDirect

Journal of Controlled Release

journal homepage: www.elsevier.com/locate/jconrel

Review

Macromolecular therapeutics

Jiyuan Yang [a], Jindřich Kopeček [a,b,*]

[a] Department of Pharmaceutics and Pharmaceutical Chemistry, University of Utah, Salt Lake City 84112, USA
[b] Department of Bioengineering, University of Utah, Salt Lake City 84112, USA

ARTICLE INFO

Article history:
Received 18 February 2014
Accepted 7 April 2014
Available online 18 April 2014

Keywords:
Water-soluble polymers
Macromolecular therapeutics
Degradable polymeric carriers
Drug-free macromolecular therapeutics
Cancer
N-(2-hydroxypropyl)methacrylamide

ABSTRACT

This review covers water-soluble polymer–drug conjugates and macromolecules that possess biological activity without attached low molecular weight drugs. The main design principles of traditional and backbone degradable polymer–drug conjugates as well as the development of a new paradigm in nanomedicines — (low molecular weight) drug-free macromolecular therapeutics are discussed. To address the biological features of cancer, macromolecular therapeutics directed to stem/progenitor cells and the tumor microenvironment are deliberated. Finally, the future perspectives of the field are briefly debated.

Contents

* Corresponding author at: Center for Controlled Chemical Delivery, 20 S 2030 E, BPRB 205B, University of Utah, Salt Lake City 84112-9452, USA. Tel.: +1 801 581 7211; fax: +1 801 581 7848.
E-mail address: jindrich.kopecek@utah.edu (J. Kopeček).

http://dx.doi.org/10.1016/j.jconrel.2014.04.013
0168-3659/

1. Introduction

Macromolecular therapeutics (polymeric nanomedicines, polymer–drug conjugates) are a group of compounds that are characterized by their large molecular weight. There is no clear definition of the term in the literature; some authors use it in the broadest sense, including any macromolecular system with biological activity. In this review, we shall restrict our discussion to water-soluble polymer–drug conjugates and macromolecules that possess biological activity without attached low molecular weight drugs. We shall discuss the main design principles, and the novel approaches that aim to speed up the translation into clinical practice. Finally, we will provide an outlook into the future of this important scientific field.

2. Water-soluble polymers with biological activity

Water-soluble polymers may possess intrinsic biological activity that relates to their structure, molecular weight, charge density, charge distribution, conformation, and stability [1]. Macromolecules such as dextran, poly(*N*-vinylpyrrolidone), and hydroxyethylstarch have been used as blood plasma expanders to restore the blood volume following trauma or shock [2]. Poly(2-vinylpyridine-*N*-oxide) has demonstrated activity against silicosis; its effect has been explained by adsorption of the weakly basic polymer on the weakly acidic surface of silica [1]. Polyelectrolytes stimulate interferon production in cells and living organisms [3,4]. Stereochemistry may have an impact on activity: isotactic poly(acrylic acid) possesses antiviral properties whereas atactic poly(acrylic acid) does not [5].

Water-soluble polymers, PEG [6–13], poly[*N*-(2-hydroxypropyl) methacrylamide] (polyHPMA) [14–18], polyoxazolines [19,20], poly(*N*-vinylpyrrolidone) [21], polyacryloylmorpholine [21], and poly(*N*,*N*-dimethylacrylamide) [21] have been used to modify proteins and increase their resistance to proteolysis, reduce their antigenicity, and prolong their intravascular half-life [22]. In addition, modification of liposomes, and nanoparticles with semitelechelic (ST) polymers is a widely used method to avoid recognition by the reticuloendothelial system [21,23–26]. These topics are covered in a recent review [27].

3. Water-soluble polymer–drug conjugates

3.1. Historical perspective

The conjugation of drugs to synthetic and natural macromolecules was initiated about sixty years ago — for reviews of the early work see refs. [1,28]. Jatzkewitz used a dipeptide (GL) spacer to attach a drug (mescaline) to polyvinylpyrrolidone in the early fifties [29] and Ushakov's group in Leningrad (now St. Petersburg) synthesized conjugates of poly(*N*-vinylpyrrolidone) with various antibiotics in the sixties and seventies [30–32]. Mathé et al. pioneered conjugation of drugs to immunoglobulins, setting the stage for targeted delivery [33]. DeDuve discovered (Nobel Prize 1974) that many enzymes are localized in the lysosomal compartment of the cell and the lysosomotropism of macromolecules [34], important phenomena for the design of polymer–drug conjugates. Finally, Ringsdorf analyzed the research results of the field and presented a clear concept of the use of polymers as targetable drug carriers [35].

The research on the use of HPMA copolymers as drug carriers commenced in the early 70s in the Kopeček laboratory in Prague. The choice of HPMA for development as a drug carrier was not random. Based on the detailed studies of the relationship between the structure of hydrophilic polymers and their biocompatibility [28,36–45], *N*-substituted methacrylamides were chosen as the target because the α-carbon substitution and the *N*-substituted amide bond ensured hydrolytic stability of the side-chains. We synthesized a series of compounds trying to identify a crystalline monomer for easy purification and reproducible synthesis. The first crystalline *N*-substituted methacrylamide we succeeded in synthesizing was HPMA, and it was chosen for future development [46,47]. In April of 1974, we filed two patent applications [48,49] which covered the synthesis of *N*-substituted (meth)acrylamides containing oligopeptide sequences and their application as drug (and other biologically active compounds) carriers. The amazing development of this polymer in the scientific community is summarized in Table 1 and Fig. 1. We designed oligopeptide spacers stable in the bloodstream [50] and susceptible to enzymatically catalyzed hydrolysis in the lysosomal compartment [51], demonstrated the targetability of the HPMA copolymer system [52,53], and revealed numerous advantages of polymer–drug conjugates over free drugs as will be described below.

3.2. Design principles

3.2.1. Water-soluble polymer carriers

There are numerous reviews that describe the design of macromolecular therapeutics [1,35,54–60]; thus we shall briefly review the important design principles. The *water-soluble polymer carrier* has to be biocompatible; hence it needs to be either degradable or have a molecular weight below the renal threshold (about 50 kDa for a random coil) to permit elimination from the organism by glomerular filtration. To prevent nonspecific reuptake of the macromolecule after being released into the bloodstream following cell death, its structure should warrant that internalization occurs by fluid-phase pinocytosis. The absence of nonspecific interactions with plasma membranes will minimize the accumulation of the carrier in non-targeted cells thus increasing the biocompatibility of the carrier. In addition, its structure should provide drug attachment/release sites for the incorporation of drugs. Different structures have been used and conjugates based on dextran [61], carboxymethyldextran [62], poly(glutamic acid) [63–65], poly(malic acid) [66,67], polyacetals [68,69], poly(vinyl alcohol) [70,71], PEG [72–74], poly(L-γ-glutamyl-glutamine) [75], and polyHPMA [76–78] have been successfully evaluated.

3.2.2. Spacers

The drug is bound to the carrier via a spacer that is stable in the bloodstream [50] and interstitial space but enzymatically or chemically cleavable in the lysosomal compartment of the cell. The lysosomal membrane is not permeable to macromolecules [79]. Consequently, the drug needs to be released from the carriers inside lysosomes. One option is to use the pH difference between blood and lysosomes and bind the drug via pH-sensitive bonds [80,81], using hydrazo [82], cis-aconityl [83], or maleic [84] spacers.

The other option is to design spacers that match the specificity of lysosomal enzymes. Based on detailed degradation studies of oligopeptide sequences attached to HPMA copolymers [85,86] with model enzymes [87–91] and lysosomal enzymes [92,93], the sequence GFLG, specific for cathepsin B, was identified [51]; it has been widely used in preclinical [94–96] and clinical settings [76,77]. Another widely used lysosomally degradable sequence is valine–citruline [97,98].

3.2.3. Self-immolative spacers

Elongated spacers, where the enzymatically cleavable bond is separated from the drug by a self-eliminating group, have been designed by several groups [99–101]. Such an approach was used for the design of oral drug delivery systems based on HPMA copolymer–9-aminocamptothecin conjugates [102] and for binding prostaglandin to HPMA copolymer via a cathepsin K sensitive terapeptide (GGPNle) and a self-eliminating 4-aminobenzylalcohol structure [103] (Fig. 2).

3.2.4. Targeting

Optionally, a *targeting moiety* is used that enhances the accumulation of the conjugate in target cells [52,53]. Active targeting of polymer–drug conjugates can be achieved by the incorporation of target cell specific ligands, such as peptides, carbohydrates, lectins,

Table 1
Milestones in HPMA (co)polymer research.

Year	Study	Publication
1973	First synthesis	J. Kopeček, H. Bažilová, Poly[*N*-(2-Hydroxypropyl)methacrylamide]. 1. Radical polymerization and copolymerization. Europ. Polym. J. 9 (1973) 7–14.
1974	Characterization of PHPMA solution properties	M. Bohdanecký, H. Bažilová, J. Kopeček, Poly[*N*-(2-hydroxypropyl) methacrylamide]. II. Hydrodynamic properties of diluted polymer solutions. Europ. Polym. J. 10 (1974) 405–410.
1974	First hydrogels	J. Kopeček, H. Bažilová, Poly[*N*-(2-Hydroxypropyl)methacrylamide]. III. Crosslinking copolymerization. Europ. Polym. J. 10 (1974) 465–470.
1976	First enzymatic release of ligand from a polymer conjugate *in vitro*	J. Drobník, J. Kopeček, J. Labský, P. Rejmanová, J. Exner, V. Saudek, J. Kálal, Enzymatic cleavage of side-chains of synthetic water-soluble polymers. Makromol. Chem. 177 (1976) 2833–2848.
1978	First HPMA modified protein	V. Chytrý, A. Vrána, J. Kopeček, Synthesis and activity of a polymer which contains insulin covalently bound on a copolymer of *N*-(2-hydroxypropyl)methacrylamide and *N*-methacryloylglycylglycine 4-nitrophenyl ester. Makromol. Chem. 179 (1978) 329–336.
1979	First HPMA–drug conjugate	B. Obereigner, M. Burešová, A. Vrána, J. Kopeček, Preparation of polymerizable derivatives of *N*-(4-aminobenzenesulfonyl)-*N′*-butylurea. J. Polym. Sci. Polym. Symp. 66 (1979) 41–52.
1981	First enzymatic release of ligand from a polymeric substrate by a polymer-modified enzyme	J. Kopeček, P. Rejmanová, V. Chytrý, Polymers containing enzymatically degradable bonds 1. Chymotrypsin catalyzed hydrolysis of p-nitroanilides of phenylalanine and tyrosine attached to side-chains of copolymers of *N*-(2-hydroxypropyl)methacrylamide. Makromol. Chem. 182 (1981) 799–809.
1981	First enzymatic release of ligand from a polymer conjugate *in vivo*	J. Kopeček, I. Cífková, P. Rejmanová, J. Strohalm, B. Obereigner, K. Ulbrich, Polymers containing enzymatically degradable bonds. 4. Preliminary experiments *in vivo*. Makromol. Chem. 182 (1981) 2941–2949.
1982	First degradable hydrogels	K. Ulbrich, J. Strohalm, J. Kopeček, Polymers containing enzymatically degradable bonds. VI. Hydrophilic gels cleavable by chymotrypsin. Biomaterials 3 (1982) 150–154.
1985	First HPMA–drug–antibody conjugate	B. Říhová, J. Kopeček, Biological properties of targetable poly[*N*-(2-hydroxypropyl)methacrylamide-antibody conjugates. J. Controlled Release 2 (1985) 289–310.
1994	First combination therapy using polymer-bound drugs	N.L. Krinick, Y. Sun, D. Jonyer, J.D. Spikes, R.C. Straight, J. Kopeček, A polymeric drug delivery system for the simultaneous delivery of drugs activatable by enzymes and/or light. J. Biomat. Sci. Polym. Ed. 5 (1994) 211–222.
1995	First semitelechelic HPMA	S. Kamei, J. Kopeček, Prolonged blood circulation in rats of nanospheres surface-modified with semitelechelic poly[*N*-(2-hydroxypropyl)methacrylamide]. Pharmaceutical Res. 12 (1995) 663–668.
1999	First clinical trials	P.A. Vasey, S.B. Kaye, R. Morrison, C. Twelves, P. Wilson, R. Duncan, A.H. Thomson, L.S. Murray, T.E. Hilditch, T. Murray, S. Burtles, D. Fraier, E. Frigerio, J. Cassidy, and on behalf of the Cancer Research Campaign Phase I/II Committee, Phase I clinical and pharmacokinetic study of PK1 [*N*-(2-hydroxypropyl)methacrylamide copolymer doxorubicin]: first member of a new class of chemotherapeutic agents–drug–polymer conjugates. Clin. Cancer Res. 5 (1999) 83–94.
1999	First ATRP polymerization	M. Teodorescu, K. Matyjaszewski, Atom transfer radical polymerization of (meth)acrylamides. Macromolecules 32 (1999) 4826–4831.
1999	First self-assembly into hybrid hydrogels	C. Wang, R.J. Stewart, J. Kopeček, Hybrid hydrogels assembled from synthetic polymers and coiled-coil protein domains. Nature 397 (1999) 417–420.
2005	First RAFT polymerization	C.W. Scales, Y.A. Vasilieva, A.J. Convertine, A.B. Lowe, C.L. McCormick, Direct, controlled synthesis of the nonimmunogenic, hydrophilic polymer, poly(*N*-(2-hydroxypropyl)methacrylamide) via RAFT in aqueous media. Biomacromolecules 6 (2005) 1846–1850.
2010	First self-assembly of peptide-containing hybrid HPMA copolymers at cell surface	K. Wu, J. Liu, R.N. Johnson, J. Yang, J. Kopeček, Drug-free macromolecular therapeutics: induction of apoptosis by coiled-coil mediated crosslinking of antigens at cell surface. Angew. Chem. Int. Ed. 49 (2010) 1451–1455.
2011	First backbone degradable HPMA copolymer carrier	J. Yang, K. Luo, H. Pan, P. Kopečková, J. Kopeček, Synthesis of biodegradable multiblock copolymers by click coupling of RAFT generated heterotelechelic polyHPMA conjugates. Reactive Functional Polym. 71 (2011) 294–302.
2012	First *in vivo* self-assembly of peptide-containing hybrid HPMA copolymers resulting in tumor cure	K. Wu, J. Yang, J. Liu, J. Kopeček, Coiled-coil based drug-free macromolecular therapeutics: *in vivo* efficacy. J. Controlled Release 157 (2012) 126–131.
2013	First combination therapy targeting both stem cells and differentiated cells	Y. Zhou, J. Yang, J. Rhim, J. Kopeček, HPMA copolymer-based combination therapy toxic to both prostate cancer stem/progenitor cells and differentiated cells induces durable anticancer effect. J. Controlled Release 172 (2013) 946–953.
2014	First *in vivo* self-assembly of oligonucleotide-containing hybrid HPMA copolymers resulting in tumor cure	T.-W. Chu, J. Yang, R. Zhang, M. Sima, J. Kopeček, Cell surface self-assembly of hybrid nanoconjugates via oligonucleotide hybridization induces apoptosis. ACS Nano 8 (2014) 719–730.

antibodies, and antibody fragments. The specific targeting interactions result in biorecognition at the cell surface and enhanced uptake of conjugates by cancer cells through receptor-mediated endocytosis with concomitant improvement in therapeutic efficacy [59,104]. Attachment of several targeting moieties to one macromolecule provides in a multivalency effect resulting in enhanced avidity of the conjugate [105]. Examples include binding several Fab′ antibody fragments [106–108], several saccharide moieties [109,110] or several peptides [111] per HPMA macromolecule. The multivalency effect resulted in enhanced biological activity of the conjugates.

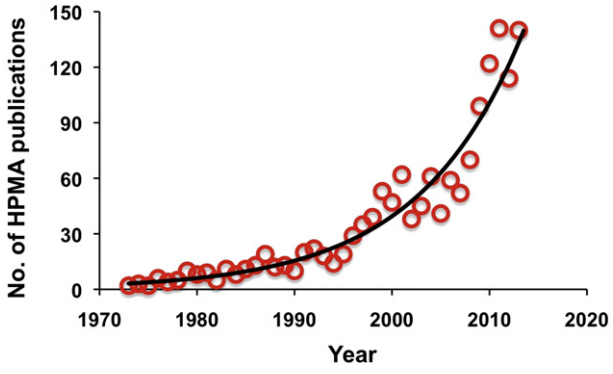

Fig. 1. HPMA publications 1973–present.

3.2.5. Subcellular targeting

The activity of many drugs depends on their subcellular location; consequently, manipulation of their subcellular fate may result in more effective conjugates. For example, mitochondrial targeting can be achieved by exploiting the negative mitochondrial potential and use of positively charged triphenylphosphonium ions as mitochondrial targeting agents [112]. Steroid hormone receptors (SHRs) have been employed to achieve nuclear targeting. SHSs are known to shuttle between the cytoplasm and nucleus of cells. Once a steroid ligand binds to a receptor such as the glucocorticoid receptor (GR), the ligand–receptor complex actively migrates to the nucleus. This concept was used for

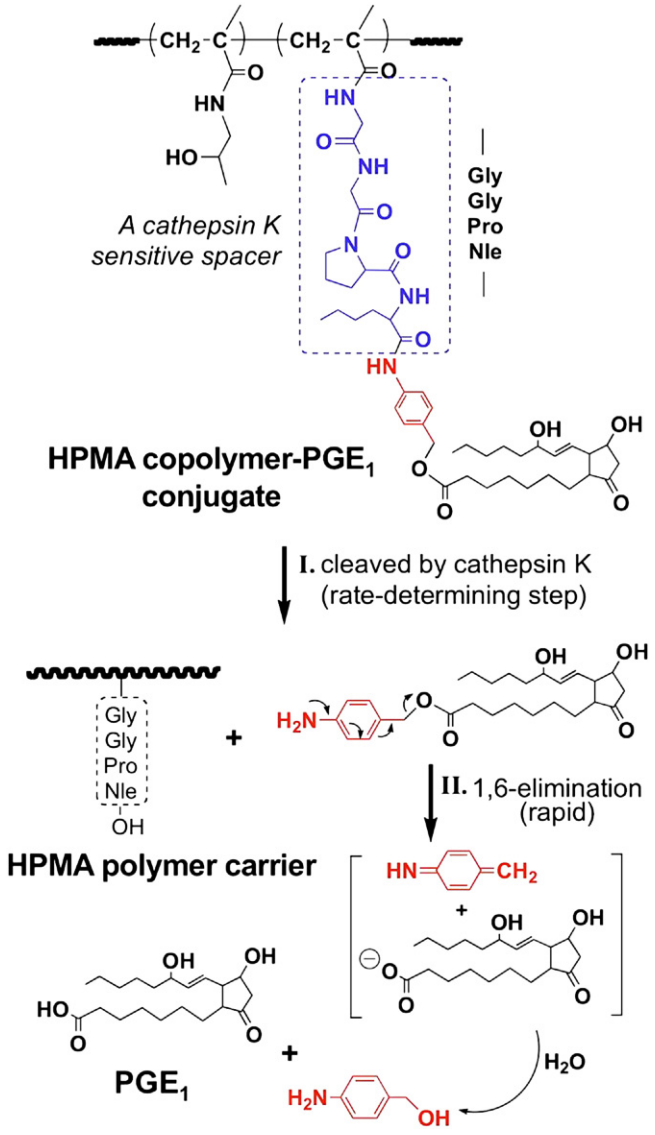

Fig. 2. Example of self-immolative spacer. Scheme of release of unmodified PGE_1 from HPMA copolymer–PGE_1 conjugate by a two-step process — rate controlling enzymatic cleavage followed by fast 1,6-elimination.
Adapted from ref. [103].

nuclear transport of DNA [113] or for a cortisol modified photosensitizer bound to HPMA copolymer via a lysosomally degradable GFLG sequence [114].

Structural factors have impact on the biocompatibility and efficiency of a polymer drug carrier as well as on the cellular uptake and subcellular trafficking. General conclusions on the relationship between structure (charge, molecular weight, hydrophobic/hydrophilic balance) and internalization are known [115–120]. However, depending on the type of the cell and detailed structure of the conjugate the subcellular trafficking may vary. The understanding of the endocytic pathways is important in the design of effective conjugates and should be individually evaluated for each design and target.

3.2.6. Gene delivery

Most approaches for gene delivery using water-soluble polymer carriers focus on polyelectrolyte complexes. These will be covered elsewhere in this volume. However, several designs use covalent attachment of DNA/RNA and will be briefly mentioned:

A) The dynamic polyconjugate technology for siRNA delivery uses covalently attached RNA and fits the scope of this review. The delivery system is composed of: a) a polymeric carrier that contains amine groups in the side chains. The latter provide attachment/release points for masking poly(ethylene glycol) chains, covalent attachment of siRNA via disulfide bonds (reducible in the cytosol) and optionally a targeting moiety. The PEG chains are attached via pH-sensitive maleic amide bonds [84]. Upon internalization the pH will decrease, the PEG molecule will be released from the conjugate exposing amino groups that will destabilize the endosomal membrane resulting in a reductible environment that will release siRNA into the cytoplasm (Fig. 3) [121].

B) Stayton and coworkers used a diblock copolymer that contains a hydrophilic block of HPMA and *N*-(2-(pyridin-2-yldisulfanyl) ethyl)methacrylamide (poly[HPMA-co-PDSMA]) to promote aqueous solubility and permit thiol-disulfide exchange reactions. The second ampholytic block is composed of propylacrylic acid (PAA), dimethylaminoethyl methacrylate (DMAEMA) and butyl methacrylate (BuMA) [122]. This system organizes into micelles. Thiolated siRNA was directly conjugated to the copolymer via thiol exchange reactions with the pyridal disulfide groups present in micelle corona. Excellent silencing activity was observed in HeLa cells [122].

C) Comb-type PEG — siRNA conjugates. A thiol modified siRNA targeting the green fluorescent protein gene was conjugated with reversible addition–fragmentation chain transfer (RAFT) polymerized pyridyl disulfide containing poly(PEG methyl ether acrylate)s. These conjugates demonstrated enhanced serum stability and nuclease resistance when compared with free siRNA [123].

3.2.7. Architecture of conjugates

Polymer architecture has an important impact on the activity of the conjugates. Szóka and Fréchet studied the impact of molecular architecture (hydrodynamic volume, conformation, flexibility, and branching) on the fate of polymers in the organism. They found that molecular architecture has a serious impact on the elimination of the carrier via glomerular filtration, but a much smaller impact on the extravasation of the polymer into the tumor [124,125]. Ulbrich's group studied in detail the relationship between the architecture of HPMA copolymers – linear conjugates, branched conjugates, grafted conjugates, self-assembled micellar conjugates, and grafted dendritic star conjugates – and their activity [126,127]. The linear conjugates with flexible polymer chains were eliminated by glomerular filtration, faster than the highly branched star conjugates with comparable molecular weight. Star conjugates appeared to produce an enhanced number of long-term survivors [128].

Intermolecular and intramolecular aggregation can impact solution properties and activity of macromolecular therapeutics. Multifunctional polymeric drug carriers containing several components, such as targeting modules, drug releasing modules, and endosome disruptive modules, have showed the potential to perform multiple functions within a single structure [55]. Ideally, each component within the delivery system should function independently, without affecting the functionality of the other components. However, the physical and biological properties of multifunctional conjugates can be expected to exert some influence on the other components [103,128]. For example, higher amounts of the hydrophobic drug prostaglandin E_1 bound to polyHPMA macromolecules resulted in a lower rate of drug release [103]. Ding et al. studied the self-association of HPMA copolymers containing an amphipathic CD21-binding heptapeptide (HP = YILIHRN) using FRET, light scattering, and SEC [129]. The process of association, largely the result of intra-polymer hydrophobic interactions, resulted in a unimolecular micelle structure. The degree of self-association increased with increased heptapeptide content. The self-association of HPMA copolymer–peptide conjugate was disrupted by the

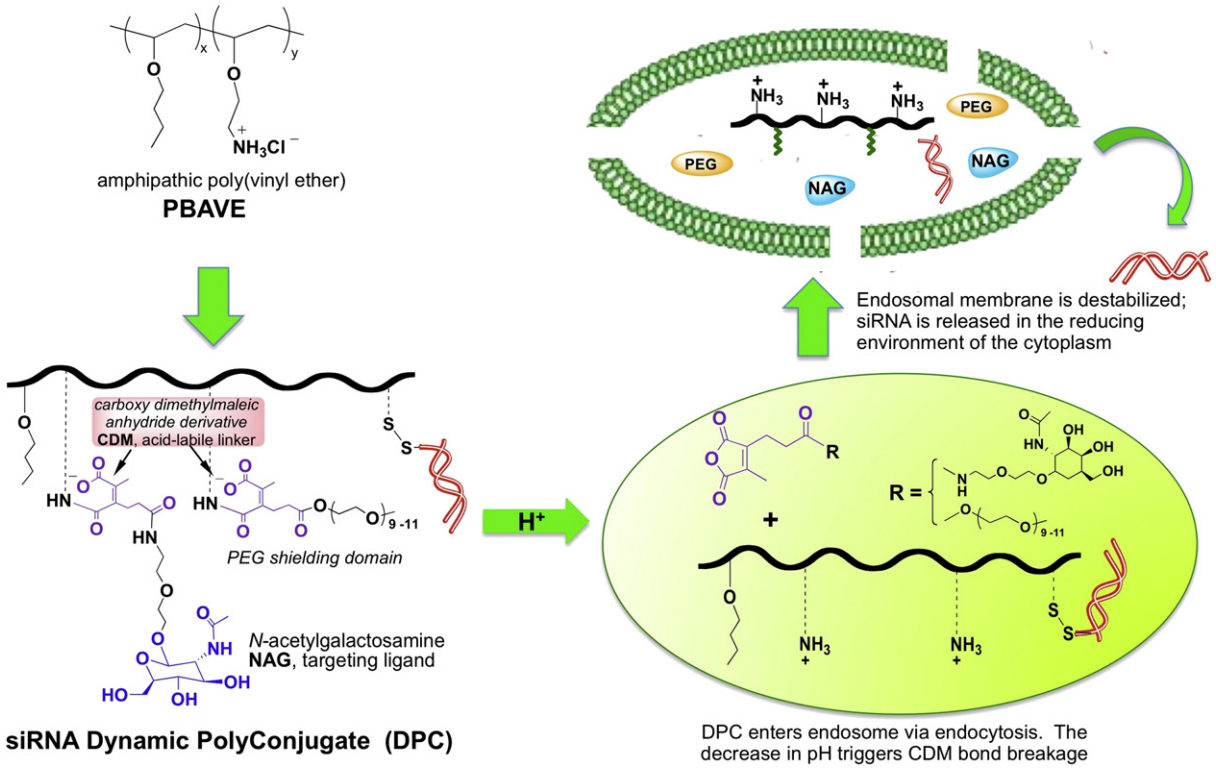

Fig. 3. Design of dynamic conjugates containing siRNA bound via covalent bonds. Scheme of structure of dynamic conjugate, its cellular uptake, release of protecting PEG chains in the endosome and release of siRNA into the cytoplasm following reduction of the disulfide bond. Carboxy dimethylmaleic anhydride (CDM) chemistry was used in the synthesis. Adapted from ref. [121].

incorporation of acrylic acid comonomers into the HPMA copolymer backbone; the ionization of COOH groups along the polymer chains induced a conformational change into an extended conformation. On the other hand the formation of unimolecular micelles (in the absence of ionizable comonomer) resulted in decreased enzyme biorecognizability and accessibility of oligopeptide side-chains (GFLG) by papain [129]. Formation of aggregates of HPMA copolymers by hydrophobic interactions played a major role in blood clearance and body distribution [130]. A better understanding of the relationship between the self-association of polymer conjugates and biological significance is a prerequisite for the rational design of polymeric drug delivery systems.

3.3. Targeted- vs. non-targeted systems

Targeting of polymer–drug conjugates is mostly connected with enhanced biorecognition at the target cell surface mediated by a targeting moiety complementary to a cell surface antigen/receptor. The efficiency of this approach may depend on the type of tumor and structure of the macromolecular therapeutics [27]. For solid tumors the extravasation of long-circulating polymer–drug conjugates via the EPR (enhanced permeability and retention) effect [131,132] might be sufficient to achieve effectiveness. Manipulation of the molecular weight [133,134] or of the architecture [135] may provide a tool to fine-tune the biological properties and efficacy of the conjugates.

For blood tumors, the advantages of targeted conjugates are obvious. Taking into account the limited time a conjugate remains in the bloodstream a biorecognition system can dramatically improve target localization. Examples of treatment of non-Hodgkin lymphoma by targeting to CD20 receptor on B cells will be discussed in Section 4.2.

Targeting may also involve the choice of a drug effective only for a subset of cells. In the section below (Section 3.4) we shall discuss using HPMA copolymer conjugates that target a cell phenotype due to its mechanism of action. Additional incorporation of targeting moieties specific for the particular phenotype would further improve the efficacy.

3.4. Targeting stem cells

A major challenge for the development of effective anti-cancer macromolecular therapeutics is the heterogeneity of cancer cells. Cancer cells are present in various differentiation statuses, such as cancer stem cells (CSC) and differentiated cells [136,137]. Only the CSCs, with the ability to self-renew and differentiate, have the tumorigenic potential and are able to generate phenotypically heterogeneous tumor cell populations that resemble the original organizations of the parent tumor. The hierarchical CSC theory suggests that the unsuccessful treatment of cancers is largely due to the failure of conventional cytotoxic anti-cancer therapies to eliminate CSCs. Therefore, targeting CSCs in combination with traditional anticancer therapeutics represents a promising strategy to improve cancer patient survival [138,139].

Aiming to improve the outcome of prostate cancer treatments by targeting CSCs, we designed a CSC specific nanomedicine. Cyclopamine, a hedgehog (Hh) pathway inhibitor, was attached to the end of GFLG (glycylphenylalanylleucylglycyl) biodegradable tetrapeptide side chains of HPMA copolymer. To be noted, targeting Hh signaling allows *specific interference with malignant CSCs while sparing adult stem cells* [140,141]. We evaluated the CSC inhibitory effects of the HPMA copolymer–cyclopamine conjugate in an *in vitro* prostate cancer epithelial cell model, RC-92a/hTERT cells, with stem cell properties [142]. RC-92a/hTERT cells were chosen since the CD133 +/integrin $\alpha2\beta1^{hi}$/CD44 + putative prostate CSCs within the whole cell line could be enriched to 5%, higher than that reported on primary prostate cancer cells or other established prostate cancer cell lines. Following exposure of RC-92a/hTERT cells to HPMA copolymer–cyclopamine conjugate (P-CYP) or HPMA copolymer docetaxel conjugate (P-DTX), we found that P-CYP reduced the percentage of

CD133 + cancer cells while not decreasing the general cell viability, indicating the preferential toxic effect of P-CYP to CD133 + cell subpopulation. In contrast, P-DTX could not reduce the proportion of CD133 + cells, although toxic to the bulk tumor cells [139].

An important end point for evaluating *in vivo* antitumor efficacy is the tumor growth inhibitory effect in long-term. The combination of P-CYP and P-DTX, as well as the P-CYP or P-DTX single treatment all inhibited the PC-3 prostate tumor growth to certain extent compared to saline group, immediately after three weeks of treatment (Fig. 4) [143]. However, after stopping the treatment at day 21 and continuing monitoring for longer periods, tumors in P-DTX group started to regrow faster on average; tumors in P-CYP group continued to grow progressively; strikingly, the combination of P-CYP and P-DTX showed the most persistent tumor growth inhibition, leading to the longest mice survival on average (Fig. 4A) [143].

We evaluated prostate CSCs in residual tumors: P-CYP and combination treatments resulted in decreased proportion of CD133 + cells compared to saline group; on the contrary, P-DTX failed to reduce the CD133 + cell population (Fig. 4B). Similarly, the number of prostaspheres formed by tumor cells isolated from P-CYP and combination group was significantly smaller than that isolated from P-DTX treated group (Fig. 4C). In short, P-CYP alone or in combination with P-DTX decreased the CD133 + cancer stem/progenitor cell population; this may contribute to more effective long-term tumor growth inhibition. The achievement of a durable anticancer effect by this combination treatment has been reported as the "top story" in "Prostate Cell News" [144].

Obviously, the efficacy of the system could be further improved by CD133 targeting. CD133 is usually expressed in a confined manner; it is present only in the prostate cancer cell population and in certain tissue stem cells [145,146]. In addition, certain epitopes of CD133 on the surface of CSCs are glycosylated and of unique protein folding pattern, different from CD133 molecules that could also be present on other adult cells [147,148]. Thus it appears that antibodies toward glycosylated CD133 epitopes could be suitable targeting moieties for CSC targeted systems.

3.5. Tumor microenvironment as delivery barrier

The tumor microenvironment cannot be ignored when discussing anti-cancer therapeutics and drug delivery [58]. In the past decade, numerous studies have indicated the importance of tumor microenvironment in cancer growth, progression, and metastasis [149]. Cancer cells are embedded in unique extracellular matrix (ECM) and are surrounded by various tumor stromal cells. The whole tumor is constantly remodeling through the reciprocal communications between cancer cells and the various tumor microenvironment components by cell–cell interactions, cell–matrix interactions as well as via secreted growth factors and/or cytokines [58]. We shall demonstrate the importance of the microenvironment in pancreatic cancer as an example.

While drugs, such as gemcitabine exhibit efficacy against human pancreatic ductal adenocarcinoma (PDA) cells transplanted into immunodeficient mice [150], they are far less effective in patients. One potential explanation is the dense accumulation of activated fibroblasts (stellate cells), immune cells and extracellular matrix that is characteristic of PDA [151]. The dense stroma creates an elevated interstitial fluid pressure (IFP) that renders the uniform delivery of therapeutics extremely difficult [152–154]. It is important to note that transplantation and xenograft-based animal models do not reproduce this environment. Relevant models in genetically engineered mice have been developed by tissue-specific manipulation of the *Kras* oncogene and key tumor suppressors mutated in human PDA [155–157]. Such models resemble that of human patients; e.g., gemcitabine has no effect on survival.

Provenzano et al. [153] identified hyaluronic acid (HA) as the primary transport barrier and demonstrated that the use of PEG modified hyaluronidase can ablate stromal HA, normalize IFP, and re-expand the vasculature (Fig. 5). Using combination treatment of PEG-hyaluronidase with gemcitabine they doubled the survival time of experimental animals [153]. Interestingly, treatment of genetically engineered mice with Hh pathway antagonist IPI-926 induced transient increase of blood flow and improved gemcitabine delivery [150]. Also, the Hh antagonist cyclopamine was shown to be synergistic with gemcitabine in elimination of cancer stem cells from a direct pancreatic cancer xenograft from patients [158].

Buckway et al. used traditional animal model of pancreatic cancer and demonstrated that tumor targeting could be achieved when co-administering hyaluronidase [159]. However, decisive experiments to prove the suitability of this approach for macromolecular therapeutics will be those using genetically engineered mouse models and

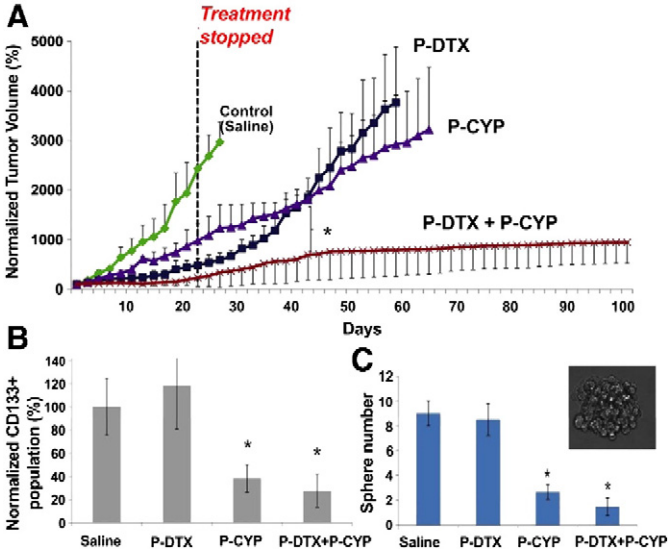

Fig. 4. Treatment of prostate PC-3 tumor bearing nude mice with a combination of two nanomedicines, one targeting cancer stem cells, the other differentiated cells. (A) Tumor growth inhibition by P-CYP (CYP 40 mg/kg, twice per week, 6 doses), P-DTX (DTX 10 mg/kg, single dose), and combination of P-DTX (DTX 10 mg/kg, single dose) and P-CYP (CYP 40 mg/kg, 6 doses) in PC-3 tumor-bearing nude mice. * represents statistically significant difference between single and combination treatment groups ($p < 0.05$); (B) percentage of CD133 + cells in residual tumor cells following *in vivo* treatments; (C) prostasphere forming ability of the residual tumor cells following *in vivo* treatments. *, $p < 0.05$.
Adapted with permission from ref. [143].

combination treatment including hyaluronidase and/or hedgehog pathway inhibitors.

The design of suitable ways for macromolecular therapeutics to overcome the transport barrier of the tumor microenvironment is one of the great challenges waiting to be solved.

3.6. Overcoming of multidrug resistance

The appearance of multidrug resistance (MDR) to anticancer drugs is one of major obstacles in cancer chemotherapy [160,161]. Following exposure to anticancer drugs, MDR is induced by overexpression of the MDR1 gene that encodes the transmembrane protein, P-glycoprotein (Pgp). Pgp is an ATP dependent efflux pump that restricts the transport of drugs into the cell interior (Fig. 6A). The mechanism of drug exclusion [162], i.e., partition of the drug into the Pgp drug binding pocket, ATP binding to Pgp resulting in conformational change and release of drug to extracellular space, indicates that nanomedicines that enter cells by endocytosis have a potential to overcome the Pgp type of multidrug resistance. For example, water-soluble polymer–drug conjugates will be internalized in membrane limited organelles and the drug released from lysosomes in the perinuclear region far from the Pgp, securing efficient intracellular concentration [163]. This hypothesis was validated *in vivo*. We studied the anticancer activities of free DOX and HPMA copolymer-bound DOX [P(GFLG)–DOX] in mouse models of DOX sensitive (A2780) and DOX resistant (A2780/AD) human ovarian carcinoma xenografts [164]. Free DOX was effective only in sensitive tumors, decreasing tumor size about three times, while P(GFLG)–DOX decreased tumor size 28 and 18 times in the sensitive and resistant tumors, respectively (Fig. 6B).

3.7. Combination therapy with macromolecular therapeutics

We have developed a novel concept of using combination therapy with water-soluble polymer-bound drugs. *In vivo* combination chemotherapy and photodynamic therapy (PDT) studies on two cancer models, Neuro 2A neuroblastoma induced in A/J mice [165] and human ovarian carcinoma heterotransplanted in nude mice [104,166,167], demonstrated that combination therapy produced tumor cures which could not be obtained with either chemotherapy or PDT alone. Other combination systems were quantitatively evaluated by combination index (CI) analysis in A498 renal carcinoma cells [168] and in OVCAR-3 ovarian carcinoma cells [169]. The results demonstrated synergistic effects of HPMA copolymer–drug (SOS thiophene, DOX, and chlorin e_6) conjugate combinations in a wide range of concentrations. Recently, the regions of synergism for the combination of backbone degradable HPMA copolymer–gemcitabine and HPMA copolymer–paclitaxel conjugates [170] and backbone degradable HPMA copolymer–gemcitabine and HPMA copolymer–platinum conjugates [171] have been identified.

A detailed comparison of the efficacy of combination therapy of ovarian carcinoma with 1st and 2nd generation HPMA copolymer – PTX and – GEM conjugates clearly demonstrated the advantage of long circulating 2nd generation conjugates – favorable pharmacokinetics, dramatically enhanced inhibition efficacy on tumor growth, and the absence of adverse effects [172].

3.8. Treatment of non-cancerous diseases

Water-soluble polymer–drug conjugates are suitable for the delivery of drugs to other than cancer disease sites. HPMA copolymers have been used in the treatment of musculoskeletal [173–175], inflammatory [175,176], and infectious [177–180] diseases.

Considerable effort has been devoted to the development of macromolecular therapeutics for the treatment of rheumatoid arthritis. This research was stimulated by the demonstration of profound arthrotropism of HPMA copolymers in the adjuvant-induced arthritis (AA) rat model [181]. Consequently, the HPMA copolymer–dexamethasone conjugate provided superior and sustained amelioration of AA in rats [182]. Recently, four dexamethasone nanomedicines, namely liposome, core-crosslinked micelle, slow releasing HPMA copolymer–dexamethasone conjugate and fast-releasing HPMA copolymer–dexamethasone conjugate were compared. After a single i.v. injection, the formulations with a slower drug release kinetics (micelle and slow releasing HPMA copolymer–dexamethasone conjugate) maintained longer duration of AA therapeutic activity than those with fast dexamethasone release [183].

4. Novel approaches

New approaches are needed to achieve translation of macromolecular therapeutics into the clinics [184]. Two examples of designs that have a potential to accomplish this task will be discussed below: a) the synthesis of backbone degradable HPMA copolymer carriers that overcome the molecular weight dilemma; and b) drug-free macromolecular therapeutics, a new paradigm in macromolecular therapeutics — a system based on crosslinking of cell surface receptors, which results in apoptosis. This design was inspired by self-assembling biomaterials studied in our laboratory [185,186]. The

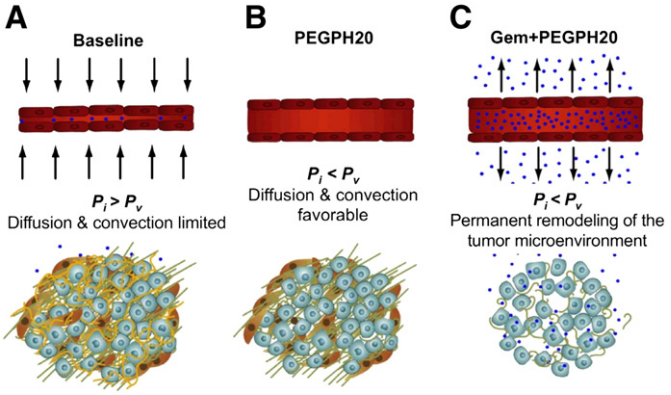

Fig. 5. Altering physicomechanics and remodeling the stroma in pancreatic ductal adenocarcinoma (PDA) to therapeutic advantage. (A) Intratumoral mechanics in PDA impede diffusion and convection of small molecules. (B) Enzymatic degradation of stromal hyaluronic acid decreases interstitial fluid pressure and relieves physical constraints on small molecule perfusion, which can reconstitute in the absence of additional therapy. (C) Combined enzymatic and cytotoxic therapies permanently remodel the tumor microenvironment to favor the delivery and distribution of small molecules. Blue spheres represent chemotherapy molecules, vessels are shown in red, carcinoma cells in light blue, activated pancreatic stromal cells in brown, collagen in green, and hyaluronic acid in yellow. Pi, interstitial fluid pressure; Pv, intravascular fluid pressure.
Adapted with permission from ref. [153].

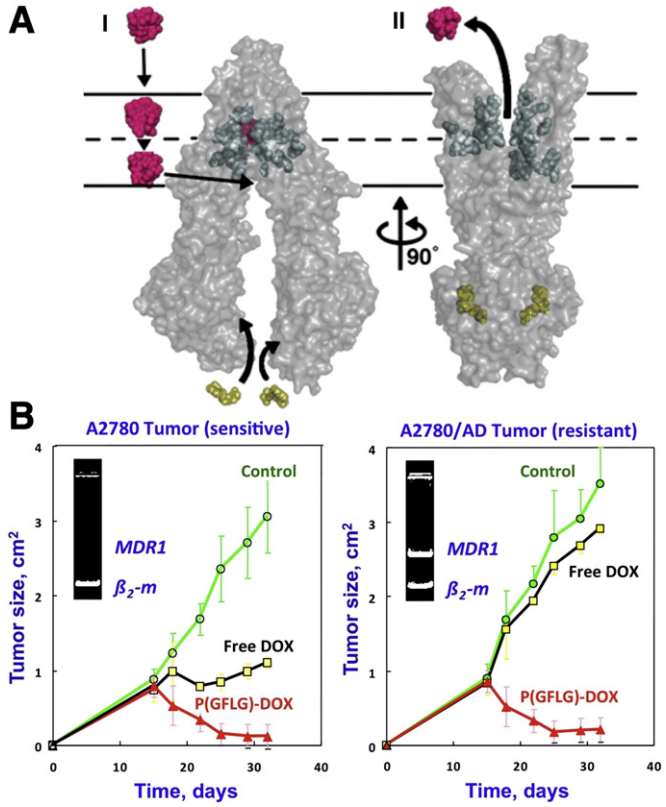

Fig. 6. Multidrug resistance (MDR). (A) Model of substrate transport by P-glycoprotein (Pgp). (B) Efficacy of free doxorubicin (DOX) and HPMA copolymer-bound DOX on the growth of (A) A2780 sensitive, and (B) A2780/AD resistant (expressing the MDR1 gene) human ovarian carcinoma xenografts in mice. Untreated as control. Means ± SD are shown.
(A) Reprinted with permission from ref. [162]. (B) Reprinted with permission from ref. [164].

application of biomaterial design principles on drawing a new strategy of apoptosis induction demonstrates that a bridge between biomaterials and nanomedicines can be created [187].

4.1. Design of backbone degradable long-circulating conjugates

It is well established that high molecular weight (long-circulating) polymer conjugates accumulate efficiently in solid tumor tissue due to the EPR effect [131,132]. To achieve substantial accumulation of the polymer–drug conjugate in solid tumors (due to the EPR effect) a sustained concentration gradient is needed. The concentration depends on the administered dose and the circulation time depends on the molecular weight of the carrier. However, higher molecular weight drug carriers with a nondegradable backbone deposit and accumulate in various organs, impairing biocompatibility.

It was evident a long time ago that polymers with molecular weight above the renal threshold would be advantageous (see p. 193 of ref. [1]). However, previous attempts to design and synthesize long-circulating conjugates produced branched, partially crosslinked copolymers with enzymatically degradable sequences [188]. The synthetic process and the polymer structure were difficult to control; consequently, the process would be difficult to scale-up. Nevertheless, the results proved that a higher molecular weight of polymer carriers transfers into higher accumulation of drugs in the tumor tissue with concomitant enhancement of efficacy [189].

The advances in controlled radical polymerization [190,191] and click chemistry [192–194] offered new vistas for the design and synthesis of long-circulating biocompatible polymer–drug conjugates. To this end we designed new, *second-generation anticancer nanomedicines* based on high molecular weight HPMA copolymer–drug carriers containing enzymatically degradable bonds in the main chain (polymer backbone) [195–197]. The proposed new design permits tailor-made synthesis of well-defined backbone degradable HPMA copolymers. The synthetic process consists of two main steps: first, the synthesis of a telechelic HPMA copolymer by reversible addition–fragmentation chain transfer (RAFT) polymerization, followed in the second step by chain extension using alkyne-azide [195,196] or thiol–ene [197] click reactions. In addition, we synthesized a new RAFT chain transfer agent (CTA), N^{α},N^{ε}-bis(4-cyano-4-(phenylcarbonothioylthio) pentanoylglycylphenylalanylleucylglycyl) lysine (Peptide2CTA), containing an enzymatically degradable oligopeptide capped at both ends with 4-cyano-4-(phenylcarbonothioylthio)pentanoate [197]. During RAFT polymerization the HPMA monomers incorporate at both dithiobenzoate groups of the Peptide2CTA with identical efficiency. When the final polymer was incubated with papain, a thiol proteinase with similar specificity as lysosomal proteinases, the molecular weight decreased to half of the original value. Thus it is possible to prepare a degradable diblock copolymer with narrow molecular weight distribution in one step, eliminating the chain extension reaction [197].

Multiblock polyHPMAs with Mw as high as 300 kDa and containing degradable GFLG sequences were obtained by chain extension followed by fractionation using size exclusion chromatography (SEC). The exposure of the multiblock HPMA copolymer to model enzyme papain or lysosomal cathepsin B (pH 6, 37 °C) resulted in complete degradation of GFLG segments and decrease of the molecular weight of the carrier to half (below the renal threshold) [195–197]. These data support our hypothesis and bode well for the success of the proposed design of backbone degradable HPMA copolymers composed of alternating segments of HPMA copolymer, with molecular weight below the renal threshold, and lysosomally degradable GFLG containing oligopeptides (Fig. 7).

The enhanced activity of 2nd generation conjugates when compared to 1st generation conjugates (non-degradable, Mw below the renal threshold) has been proven *in vivo*. Long-circulating backbone degradable HPMA copolymer conjugates with doxorubicin [198], paclitaxel [199], or gemcitabine (Fig. 8) demonstrated higher efficacy in suppressing the growth of human ovarian carcinoma xenografts in nude mice than 1st generation conjugates. Similarly, bone-targeted long-circulating conjugates containing prostaglandin E_1 had higher accumulation on bone tissue and greater indices of bone formation in an ovariectomized rat osteoporosis model when compared to 1st generation conjugates [200]. Interestingly, *in vivo* experiments on animal models of ovarian cancer have proven that the diblock structure is sufficient to dramatically enhance efficacy when compared with the first generation conjugates [172,198]. This is of importance for the scale-up of the synthesis and translation into the clinics.

4.2. Drug-free macromolecular therapeutics — a new paradigm in nanomedicines

An exciting new development in the nanomedicine research area is the design of drug-free macromolecular therapeutics. The new paradigm in drug delivery is based on the biorecognition of natural (e.g., peptide or oligonucleotide) motifs at cell surface, formation of heterodimers (e.g., antiparallel coiled-coils or hybridization of complementary oligonucleotides), crosslinking of non-internalizing receptors and initiation of apoptosis [201–203].

4.2.1. Biorecognition in hybrid polymer systems

Hybrid polymer systems are composed from at least two distinct classes of macromolecules, for example, synthetic and biological macromolecules. For instance, conjugation of peptide domains to synthetic polymers produces materials with properties superior to individual components. The peptide domain inserts a level of control over structure resulting from self-assembly at a nanometer scale; the synthetic

part may enhance the biocompatibility of the whole system by reducing the immunogenicity of the natural domain [187].

4.2.2. Drug-free macromolecular therapeutics based on formation of antiparallel coiled-coils

The coiled-coil is one of the basic folding patterns of native proteins. It consists of two or more right-handed α-helices winding together to form (usually) a slightly left-handed super-helix [204,205]. The primary structure of the coiled-coil motif is characterized by a sequence of repeating heptads (motif of seven amino acids) designated as $[a, b, c, d, e, f, g]_x$, in which *a* and *d* are usually hydrophobic amino acid residues, while the others are polar. Two helices associate through a hydrophobic interface between *a* and *d*, making *b*, *c*, and *f* face outward. Interhelical electrostatic interactions between residues *e* and *g* contribute to the stability depending on their detailed structure; α-helices may associate as homodimers, heterodimers in parallel or antiparallel alignments, or form higher order (e.g., tetramer) aggregates [206,207]. Hundreds of native proteins, such as muscle proteins, transcription factors, cytoskeletal proteins, cell and viral surface proteins, tumor suppressors, molecular motors, and many disease- and organ-specific auto-antigens have functional coiled-coil domains [208]. A distinctive feature of coiled-coils is the specific spatial recognition, association, and dissociation of helices, making it an ideal model for protein biomaterials in which the higher order structures may be predicted based on the primary sequence. Various functional groups may be exactly positioned into the coiled-coil structure, allowing specific intermolecular interactions to occur.

We have designed hybrid systems composed from hydrophilic HPMA copolymer backbone grafted with two pentaheptad antiparallel coiled-coil forming oligopeptide sequences with opposite charge (CCE and CCK [209]) [185]. A mixture of equimolar solutions of P-CCK (P is the HPMA copolymer backbone) and P-CCE self-assemble into hydrogels. This process is mediated by the recognition of CCE and CCK peptide grafts — they fold into antiparallel coiled-coils [185,186]. The excellent biorecognition of the CCE and CCK peptides [185,210] was an inspiration for the design of new nanomedicines; this created a bridge between the design of biomaterials and the design of nanomedicines.

4.2.2.1. Design. CCK and CCE peptides were engaged in the design of a new CD20+ cell apoptosis induction system, called drug-free macromolecular therapeutics [201,202]. CD20 is an ideal target for immunotherapies. It is an integral membrane protein [211] that is expressed from pre-B cells to terminally differentiated plasma cells and is present

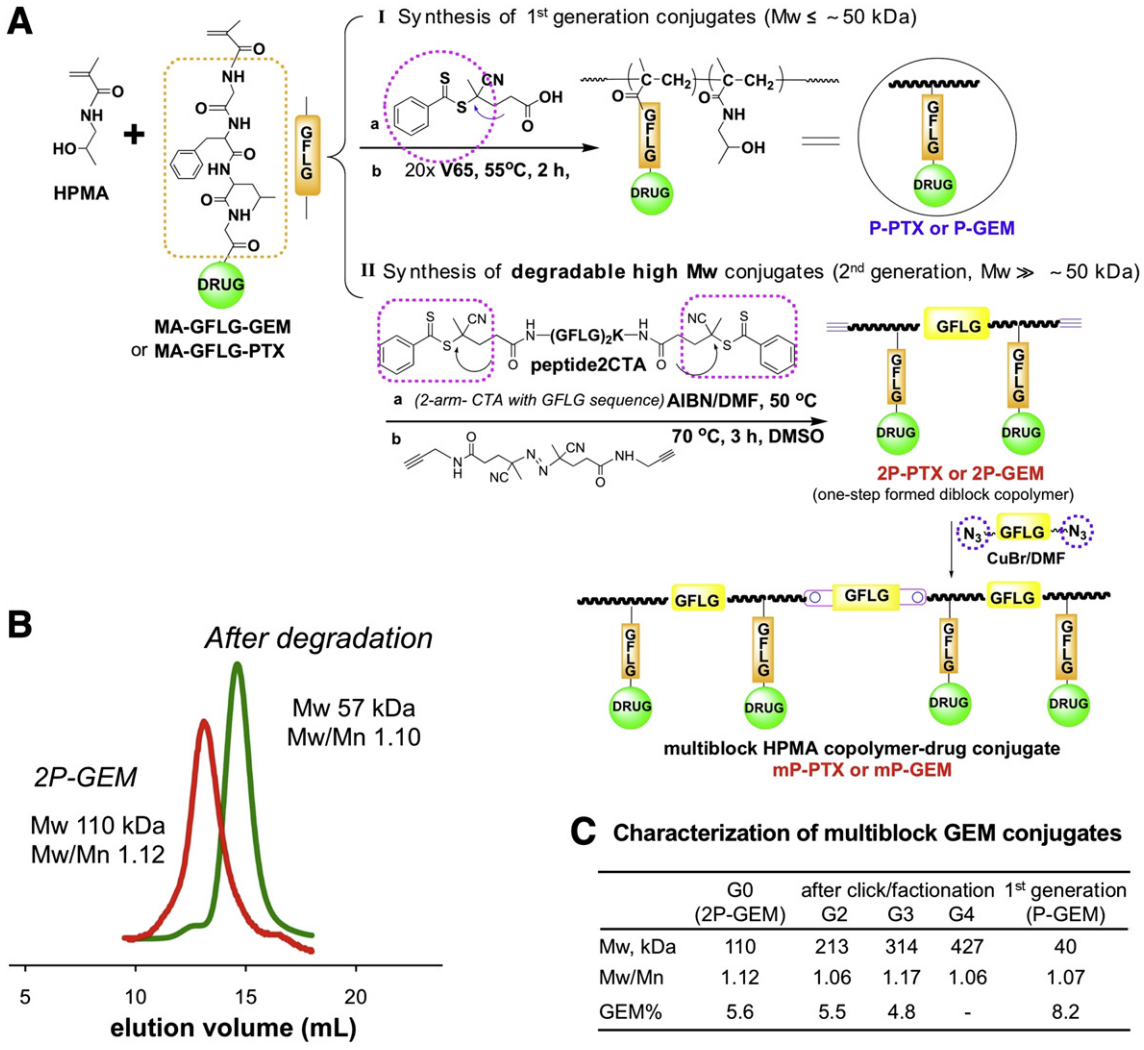

	G0 (2P-GEM)	after click/factionation G2	G3	G4	1st generation (P-GEM)
Mw, kDa	110	213	314	427	40
Mw/Mn	1.12	1.06	1.17	1.06	1.07
GEM%	5.6	5.5	4.8	-	8.2

Fig. 7. Design of backbone degradable long-circulating HPMA copolymer–drug conjugates. Two dithiobenzoate chain transfer agents were linked with lysosomal enzyme cleavable peptide GFLGKGLFG resulting in a biodegradable RAFT agent, peptide2CTA. This permits one-step synthesis of diblock copolymers. (A) Post-polymerization click reaction produces multiblock HPMA copolymer–drug conjugates with different chain lengths; (B) the diblock HPMA copolymer–drug conjugates degraded into half of their initial Mw, indicating the potential to employ diblock conjugates with 100 kDa Mw without impairing their biocompatibility (the degradation products are below the renal threshold); (C) characterization of 1st- and 2nd generation HPMA copolymer–gemcitabine conjugates including molecular weight and drug content [195–197].

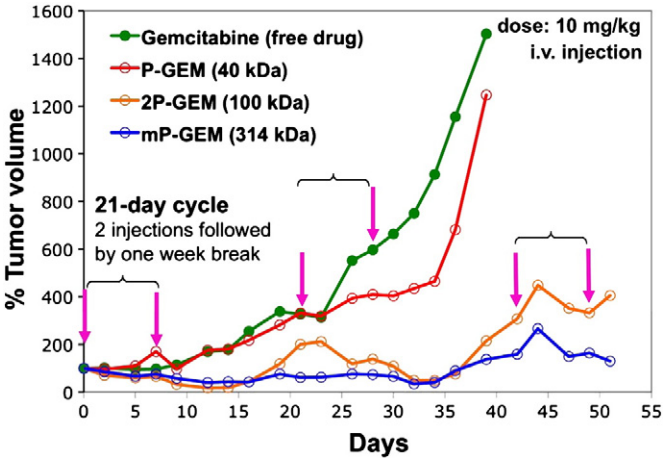

Fig. 8. Comparison of backbone degradable long circulating (second-generation) HPMA copolymer–gemcitabine conjugates (diblock 2P-GEM and multiblock mP-GEM) with low molecular weight (first generation) HPMA copolymer–gemcitabine conjugate (P-GEM): *in vivo* antitumor activity against A2780 human ovarian xenografts in nude mice. Unpublished data from Kopeček laboratory.

on greater than 90% of B-cell malignancies [212]. CD20 is not shed from the cell surface nor is it present in serum under standard physiological conditions. It is a cell cycle regulatory protein [213] that either controls or functions as a store operated calcium channel. The protein forms dynamic dimers and tetramers [214] constitutively associated in lipid rafts of the cell membrane [215].

Indeed, the biorecognition of CCE/CCK peptide motifs at the cellular surface was able to induce apoptosis of CD20 + B cells. Exposure of Raji B cells to a 1F5 anti-CD20 Fab′–CCE conjugate decorated the cell surface with CCE (CD20 is a non-internalizing receptor) through antigen–antibody fragment recognition. Further exposure of the decorated cells to P-CCK (grafted with multiple copies of CCK) resulted in the formation of CCE/CCK coiled-coil heterodimers at the cell surface. This second biorecognition induced the crosslinking of CD20 receptors and triggered the apoptosis of Raji B cells *in vitro* [201] and in a non-Hodgkin lymphoma animal model *in vivo* [202]. High degrees of apoptosis could be achieved *in vitro* [201] and long-term survivors produced in Raji B lymphoma mice model [202]. This is a new concept, where the biological activity of drug-free macromolecular therapeutics is based on the biorecognition of peptide motifs.

4.2.3. Drug-free macromolecular therapeutics based on hybridization of morpholino oligonucleotides

After we proved the concept of the new paradigm in nanomedicine by employing a pair of pentaheptad coiled-coil forming peptides, we focused our attention on a hybrid system where the biorecognition is mediated by the hybridization of complementary morpholino oligonucleotides.

4.2.3.1. HPMA copolymer–oligonucleotide hybrids. A recent new design was based on the biorecognition (hybridization) of a pair of morpholino oligonucleotides with complementary sequences [203]. The system is composed of a 1F5 anti-CD20 Fab′ antibody fragment, a pair of complementary phosphorodiamidate morpholino oligomers (MORF1 and MORF2 [216]), and a linear polymer (P) of HPMA. We hypothesized that [203]: (1) the exposure of malignant CD20 + B-cells to the anti-CD20 Fab′-MORF1 conjugate (Fab′-MORF1) decorates the cell surfaces with MORF1; and (2) further treatment of decorated B-cells with HPMA copolymer grafted with multiple copies of MORF2 (P-MORF2) results in MORF1–MORF2 hybridization at the cell surface with concomitant CD20 crosslinking, which triggers apoptosis. Indeed, this system produced high levels of Raji B cell apoptosis *in vitro* and excellent results *in vivo* (Fig. 9). Treatment of systemically disseminated CD20 + Raji B cell lymphoma in C.B.-17 SCID mice with Fab′-MORF1 and P-MORF2 led to long-term survivors (125 days, Fig. 9C). Eradication of Raji cells after treatment was further confirmed by flow cytometry (Fig. 9D, E), MRI and histology [203]. These results were highlighted in Chemical & Engineering News in January 2014 [217].

The results shown above demonstrate that in the hybridization-mediated system (Fab′-MORF1/P-MORF2), the treatment with equimolar MORF1/MORF2 was sufficient for biorecognition, apoptosis induction, and prevention of lymphoma dissemination. In contrast, for the coiled-coil mediated apoptosis induction a 25× excess of the second conjugate (P-CCK) was needed. In addition, rapid binding kinetics were observed with the oligonucleotide-based system. Other advantages of the MORF oligonucleotides include: (1) specific binding due to a well-defined hydrogen bonding pattern (i.e., base pairing), (2) charge-neutral property that prevents potential off-target effects, and (3) water solubility due to good base-stacking property resulting in favorable pharmacokinetics [203].

The design of drug-free macromolecular therapeutics is a truly novel approach in nanomedicine. It builds on the design of new self-assembling biomaterials [185–187,218,219] and translates the biorecognition principles to nanomedicine [201–203]. The first design of this system was tailored for the non-internalizing CD20 receptor and NHL. CD20 is highly expressed on the surface of malignant and normal B-cells, but not in stem cells or plasma cells. Thus, drug-free macromolecular therapeutics (employing the "B-cell depletion strategy") can be potentially used to treat B-cell derived *hematological neoplastic diseases* and *autoimmune diseases*, without non-reversible impact on normal immune function [220]. Other potential disease targets are (in addition to NHL): chronic lymphocytic leukemia (CLL), rheumatoid arthritis, multiple sclerosis, systemic lupus erythematosus, autoimmune hemolytic anemia, pure red cell aplasia, idiopathic thrombocytopenic purpura, Evans syndrome, vasculitis, bullous skin disorders, type 1 diabetes mellitus, Sjögren's syndrome, Devic's disease, and Graves' ophthalmopathy. All of the above listed diseases have been treated by rituximab anti-CD20 mAb (either approved by FDA or in clinical trials).

Importantly, the concept of drug-free macromolecular therapeutics could be expanded by using different components in the design. For example, the Fab′ fragment can be replaced by antigen binding saccharides [99] or by peptides selected by phage display [221] or by combinatorial methods [222,223].

5. Future prospects

The advantages of polymer-bound drugs (when compared to low-molecular weight drugs) are [55,59]: a) active uptake by fluid-phase

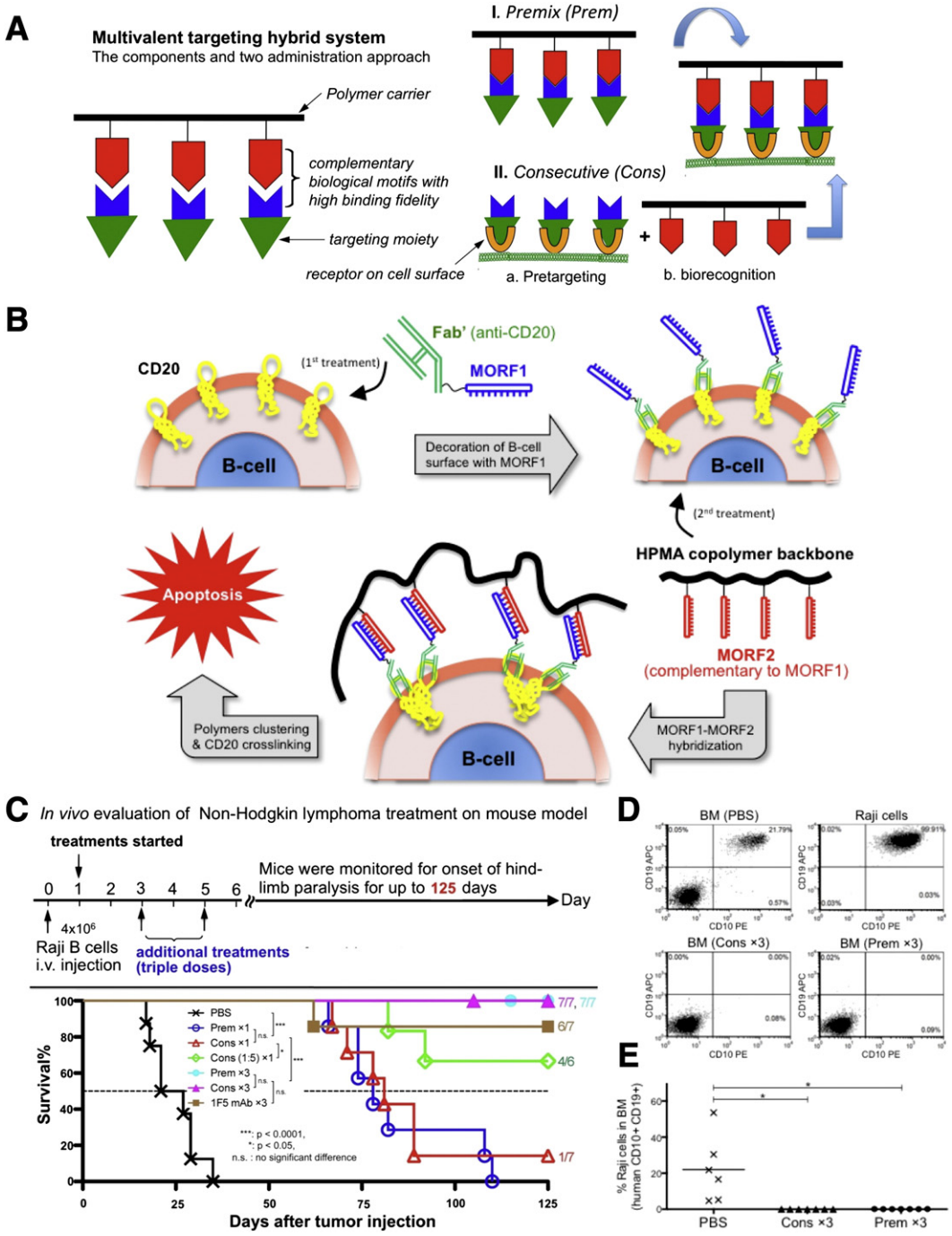

Fig. 9. Drug-free macromolecular therapeutics. (A) General design concept of the therapeutic platform; (B) apoptosis induction of B-cells by crosslinking of the CD20 antigens that is mediated by extracellular hybridization of complementary morpholino oligonucleotides (MORF1–MORF2); (C) treatment schedule and Kaplan–Meier plot with indication of numbers of long-term survivors (7 mice per group); (D) flow cytometry analysis of residual Raji cells in the bone marrow (BM) of the PBS-treated, paralyzed mice (PBS) and the nanomedicine-treated, surviving mice (Cons ×3, Prem ×3). Bone marrow cells isolated from the femur of mice and Raji cells from culture flasks (upper right panel) were stained with PE-labeled mouse anti-human CD10 and APC-labeled mouse anti-human CD19 antibodies. (E) Quantitative comparison of % Raji cells (human CD10+ CD19+) in the bone marrow of control mice (PBS, n = 6) and the nanomedicine-treated mice (Cons ×3 and Prem ×3, n = 7 per group). Statistics was performed by Student's *t* test of unpaired samples (*: $p < 0.05$). Cons. consecutive administration of Fab′-MORF1 first followed 1 h later by P-MORF2; Prem. premixture was administered.
Reprinted with permission from ref. [203].

pinocytosis (non-targeted polymer-bound drugs) or receptor-mediated endocytosis (targeted polymer-bound drug), b) increased *passive* accumulation of the drug at the tumor site by the EPR effect, c) increased *active* accumulation of the drug at the tumor site by targeting, d) long-lasting circulation in the bloodstream, e) decreased non-specific toxicity of the conjugated drugs, f) potential to overcome multidrug resistance, g) decreased immunogenicity of the targeting moiety, h) immunoprotecting and immunomobilizing activities, and i) modulation of the cell signaling and apoptotic pathways. In addition to preclinical evaluation on animal cancer models, the benefits of macromolecular therapeutics over free (unbound) drugs have been demonstrated in preclinical and clinical arrangements [224,225]. Results from clinical trials with 1st generation HPMA conjugates indicated a significant decrease of adverse effects

when compared to small molecule drugs; however, the therapeutic efficacy did not match the data in preclinical animal studies.

Here we present data that show the advantage of the second generation conjugates over both, first generation conjugates and free drugs [198–200]. These new conjugates are backbone degradable and long-circulating; they are composed from enzymatically cleavable sequences and synthetic segments in an alternating arrangement [195–197]. These conjugates have a clear translational potential. In addition to enhanced efficacy, the synthesis of biodegradable diblock HPMA copolymer conjugates using a RAFT chain transfer agent that contains a degradable peptide sequence flanked by two dithiobenzoate groups, is clearly a scalable process.

The new paradigm in nanomedicine–drug-free macromolecular therapeutics [201–203] seems to address the challenges of treating blood borne cancers. It avoids the use of low molecular weight, potentially toxic drugs, is triggered by specific recognition at the molecular level and offers the possibility of pretargeting.

Thus on the design side the area of macromolecular therapeutics is well advanced. The major challenge, however, is to merge the knowledge of design principles of conjugates with the understanding of the biological features of cancer, including heterogeneity of cancer cells, tumor microenvironment and metastasis [58]. The design of conjugates targeting stem cells [143] and their use in combination with conjugates targeting differentiated cells as well as destabilization of stroma [153] surrounding the tumor tissue will enhance the efficiency of treatment. The development of non-invasive imaging technologies will undoubtedly contribute to progress [226–228]. Imaging can provide valuable feedback to fine tune the conjugate design and treatment protocol.

The scientific knowledge and experience from preclinical and clinical research accumulated in the last 30 years form the basis for the possible translation of macromolecular therapeutics into the clinics within the next decade.

Acknowledgments

The research in the authors' laboratory was supported in part by the National Institutes of Health (recently grants CA51578, CA132831, GM69847, EB5288, GM95606, and CA156933), U.S. Department of Defense grant W81XWH-04-1-0900, and the University of Utah Research Foundation (grant No. 51003599). We also acknowledge support in conjunction with grant P30 CA042014 awarded to the Huntsman Cancer Institute, University of Utah. We thank all past and present coworkers and numerous collaborators. We are truly indebted to all of them; their scientific contributions are reflected in the references.

References

[1] J. Kopeček, Soluble biomedical polymers, Polim. Med. 7 (1977) 191–221.
[2] Blood Substitutes, Preparation, Physiology, and Medical Applications, in: K.C. Lowe (Ed.), VCH Weinheim, ISBN: 3-527-26556-2, 1988.
[3] A. Billiau, J.J. Muyembe, P. De Somer, Interferon-inducing polycarboxylates: mechanism of protection against virus infection in mice, Infect. Immun. 5 (1972) 854–857.
[4] E.B. Tazulakhova, O.V. Parshina, T.S. Guseva, F.I. Ershov, Russian experience in screening, analysis, and clinical application of novel interferon inducers, J. Interferon Cytokine Res. 21 (2001) 65–73.
[5] K.F. Mück, H. Rolly, K. Burg, Herstellung und antiviralle Wirksamkeit von Polyacrylsäure und Polymethacrylsäure, Makromol. Chem. 178 (1977) 2773–2784.
[6] G. Pasut, F.M. Veronese, State-of-the-art in PEGylation: the great versatility achieved after forty years of research, J. Control. Release 161 (2012) 461–472.
[7] V. Levy, M.S. Hershfield, C. Fernandez-Mejia, S.H. Polmar, D. Scrudiery, M. Berger, R. U. Sorensen, Adenosine deaminase deficiency with late onset or recurrent infections: response to treatment with polyethylene glycol modified adenosine deaminase, J. Pediatr. 113 (1988) 312–317.
[8] L.M. Graham, Pegaspargase: a review of clinical studies, Adv. Drug Deliv. Rev. 55 (2003) 1293–1302.
[9] K.R. Reddy, M.W. Modi, S. Pedder, Use of peginterferon α2a (40 kD) (Pegasys®) for the treatment of hepatitis C, Adv. Drug Deliv. Rev. 54 (2002) 571–586.
[10] Y.S. Wang, S. Youngster, M. Grace, J. Bausch, R. Bordens, D.F. Wyss, Structural and biological characterization of pegylated recombinant interferon α2b and its therapeutic implications, Adv. Drug Deliv. Rev. 54 (2002) 547–570.
[11] O. Kinstler, G. Moulinex, M. Treheit, D. Ladd, C. Gegg, Mono-*N*-terminal poly(ethylene glycol)–protein conjugates, Adv. Drug Deliv. Rev. 54 (2002) 477–485.
[12] A.M. Nesbitt, S. Stephens, E.K. Chartash, Certolizumab pegol: a PEGylated antitumor necrosis factor alpha biological agent, in: F.M. Veronese (Ed.), PEGylated Protein Drugs: Basic Science and Clinical Applications, Birkhäuser Verlag, Basel, Switzerland, 2009, pp. 229–254.
[13] M.R. Sherman, M.G. Saifer, F. Perez-Ruiz, PEG-uricase in the management of treatment-resistant gout and hyperuricemia, Adv. Drug Deliv. Rev. 60 (2008) 59–68.
[14] Z.-R. Lu, P. Kopečková, J. Kopeček, Semitelechelic poly[*N*-(2-hydroxypropyl)-methacrylamide] for biomedical applications, in: R.M. Ottenbrite, S.W. Kim (Eds.), Polymeric Drugs & Delivery Systems, Technomics Publishing Co., Lancaster, PA, 2001, pp. 1–14.
[15] Z.-R. Lu, P. Kopečková, Z. Wu, J. Kopeček, Functionalized semitelechelic poly[*N*-(2-hydroxypropyl)methacrylamide] for protein modification, Bioconjug. Chem. 9 (1998) 793–804.
[16] A. Lääne, A. Aaviksaar, M. Haga, V. Chytrý, J. Kopeček, Preparation of polymer-modified enzymes of prolonged circulation times. Poly[*N*-(2-hydroxypropyl) methacrylamide] bound acetylcholinesterase, Makromol. Chem. Suppl. 9 (1985) 35–42.
[17] V. Chytrý, A. Vrána, J. Kopeček, Synthesis and activity of a polymer which contains insulin covalently bound on a copolymer of *N*-(2-hydroxypropyl)methacrylamide and *N*-methacryloylglycylglycine 4-nitrophenyl ester, Makromol. Chem. 179 (1978) 329–336.
[18] J.H. Lee, G. Sabnis, A. Nan, Synthesis and *in vitro* characterization of semitelechelic poly[*N*-(2-hydroxypropyl)methacrylamide]-trastuzumab conjugates targeted to breast cancer, Macomol. Biosci. 12 (2012) 55–60.
[19] T.X. Viegas, M.D. Bentley, J.M. Harris, Z. Fang, K. Yoon, B. Dizman, R. Weimer, A. Mero, G. Pasut, F.M. Veronese, Polyoxazolines: chemistry, properties, and applications in drug delivery, Bioconjug. Chem 22 (2011) 976–986.
[20] K. Knop, R. Hoogenboom, D. Fischer, U.S. Schubert, Poly(ethylene glycol) in drug delivery: pros and cons as well as potential alternatives, Angew. Chem. Int. Ed. 49 (2010) 6288–6308.
[21] T. Ishigara, T. Maeda, H. Sakamoto, N. Takasaki, M. Shigyo, T. Ishida, H. Kiwada, Y. Mizushima, T. Mizuahima, Evasion of nanoparticle accelerated blood clearance phenomenon by coating of nanoparticles with various hydrophilic polymers, Biomacromolecules 11 (2010) 2700–2706.
[22] A. Abuchowski, J.R. McCoy, N.C. Palczuk, T. van Es, F.F. Davis, Effect of covalent attachment of polyethylene glycol on immunogenicity and circulation time of bovine liver catalase, J. Biol. Chem. 252 (1977) 3582–3586.
[23] S. Kamei, J. Kopeček, Prolonged blood circulation in rats of nanospheres surface-modified with semitelechelic poly[*N*-(2-hydroxypropyl)methacrylamide], Pharm. Res. 12 (1995) 663–668.
[24] T. Safra, F. Muggia, S. Jeffers, D.D. Tsao-Wei, S. Groshen, O. Lyas, R. Henderson, G. Berry, A. Gabizon, Pegylated liposomal doxorubicin (Doxil): reduced cardiotoxicity in patients reaching or exceeding cumulative doses of 500 mg/m^2, Ann. Oncol. 11 (2000) 1029–1033.
[25] M.T. Peracchia, E. Fattal, D. Desmaele, M. Besnard, J.P. Noël, J.M. Gomis, M. Appel, J. d'Angelo, P. Couvreur, Stealth PEGylated polycyanoacrylate nanoparticles for intravenous administration and splenic targeting, J. Control. Release 60 (1999) 121–128.
[26] Y. Ma, Q. Yang, L. Wang, X. Zhou, Y. Zhao, Y. Deng, Repeated injections of PEGylated liposomal topotecan induces accelerated blood clearance phenomenon in rats, Eur. J. Pharm. Sci. 45 (2012) 539–545.
[27] J. Kopeček, Polymer–drug conjugates: origins, progress to date and future directions, Adv. Drug Deliv. Rev. 65 (2013) 49–59.
[28] J. Kopeček, Soluble polymers in medicine, in: D.F. Williams (Ed.), Systemic Aspects of Biocompatibility, Vol. II, CRC Press, Boca Raton, Florida, 1981, pp. 159–180.
[29] H. Jatzkewitz, Peptamin (glycyl-L-leucyl-mescaline) bound to blood plasma expander (polyvinylpyrrolidone) as a new depot form of a biologically active primary amine (mescaline), Z. Naturforsch. 10b (1955) 27–31.
[30] N.I. Givetal, S.N. Ushakov, E.F. Panarin, G.O. Popova, Experimental studies on penicillin polymer derivatives (in Russian), Antibiotiki 10 (1965) 701–706.
[31] K.I. Shumikina, E.F. Panarin, S.N. Ushakov, Experimental study of polymer salts of penicillins (in Russian), Antibiotiki 11 (1966) 767–770.
[32] E.F. Panarin, S.N. Ushakov, Synthesis of polymer salts and amidopenicillins (in Russian), Khim. Pharm. Zhur. 2 (1968) 28–31.
[33] G. Mathé, T.B. Loc, J. Bernard, Effect sur la leucémie L1210 de la souris d'une combinaison par diazotation d'a méthoptérine et de γglobulines de hamsters porteurs de cette leucémie par hétérogreffe, CR Acad. Sci. 3 (1958) 1626–1628.
[34] C. De Duve, T. De Barsy, B. Poole, A. Trouet, P. Tulkens, F. van Hoof, Lysosomotropic agents, Biochem. Pharmacol. 23 (1974) 2495–2531.
[35] H. Ringsdorf, Structure and properties of pharmacologically active polymers, J. Polym. Sci. Polym. Symp. 51 (1975) 135–153.
[36] L. Šprincl, J. Vacík, J. Kopeček, D. Lím, Biological tolerance of poly(*N*-substituted methacrylamides), J. Biomed. Mater. Res. 5 (1971) 197–205.
[37] J. Kopeček, L. Šprincl, H. Bažilová, J. Vacík, Biological tolerance of poly(*N*-substituted acrylamides), J. Biomed. Mater. Res. 7 (1973) 111–121.
[38] L. Šprincl, J. Kopeček, D. Lím, Effect of porosity of heterogeneous poly(glycol monomethacrylate) gels on the healing-in of test implants, J. Biomed. Mater. Res. 5 (1971) 447–458.
[39] L. Šprincl, J. Vacík, J. Kopeček, D. Lím, Biological tolerance of ionogenic hydrophilic gels, J. Biomed. Mater. Res. 7 (1973) 123–136.
[40] K. Ulbrich, L. Šprincl, J. Kopeček, Biocompatibility of poly(2,4-pentadiene-1ol), J. Biomed. Mater. Res. 8 (1974) 155–161.

[41] J. Kopeček, L. Šprincl, Relationship between the structure and biocompatibility of hydrophilic gels, Polim. Med. 4 (1974) 109–117.
[42] J. Kopeček, L. Šprincl, D. Lím, New types of synthetic infusion solutions. I. Investigation of the effect of solutions of some hydrophilic polymers on blood, J. Biomed. Mater. Res. 7 (1973) 179–191.
[43] L. Šprincl, J. Exner, O. Štěrba, J. Kopeček, New types of synthetic infusion solutions. III. Elimination and retention of poly[*N*-(2-hydroxypropyl)methacrylamide] in a test organism, J. Biomed. Mater. Res. 10 (1976) 953–963.
[44] E. Paluska, J. Činátl, L. Korčáková, O. Štěrba, J. Kopeček, A. Hrubá, J. Nezvalová, R. Staněk, Immunosuppressive effect of a synthetic polymer–poly[*N*-(2-hydroxypropyl) methacrylamide] (Duxon), Folia Biol. 26 (1980) 304–311.
[45] E. Paluska, A. Hrubá, O. Štěrba, J. Kopeček, Effect of a synthetic poly[*N*-(2-hydroxypropyl)methacrylamide] (Duxon) on haemopoiesis and graft versus host reaction, Folia Biol. 32 (1986) 91–102.
[46] J. Kopeček, H. Bažilová, Poly[*N*-(2-hydroxypropyl)methacrylamide]. 1. Radical polymerization and copolymerization, Europ. Polym. J. 9 (1973) 7–14.
[47] M. Bohdanecký, H. Bažilová, J. Kopeček, Poly[*N*-(2-hydroxypropyl)methacrylamide]. II. Hydrodynamic properties of diluted polymer solutions, Europ. Polym. J. 10 (1974) 405–410.
[48] J. Kopeček, K. Ulbrich, J. Vacík, J. Strohalm, V. Chytrý, J. Drobník, J. Kálal, Copolymers based on N-substituted acrylamides, N-substituted methacrylamides and N,N-disubstituted acrylamides and the method of their manufacturing, U.S. Patent 4,062,831 (Dec.13,1977).
[49] J. Drobník, J. Kopeček, J. Labský, P. Rejmanová, J. Exner, J. Kálal, Preparation of biologically active substances bearing NH_2 groups in a form releasable by enzymatic cleavage, U.S. Patent 4,097,470 (June 27, 1978).
[50] P. Rejmanová, J. Kopeček, R. Duncan, J.B. Lloyd, Stability in rat plasma and serum of lysosomally degradable oligopeptide sequences in *N*-(2-hydroxypropyl) methacrylamide copolymers, Biomaterials 6 (1985) 45–48.
[51] P. Rejmanová, J. Pohl, M. Baudyš, V. Kostka, J. Kopeček, Polymers containing enzymatically degradable bonds. 8. Degradation of oligopeptide sequences in *N*-(2-hydroxypropyl)methacrylamide copolymers by bovine spleen cathepsin B, Makromol. Chem. 184 (1983) 2009–2020.
[52] B. Říhová, J. Kopeček, Biological properties of targetable poly[*N*-(2-hydroxypropyl)methacrylamide]–antibody conjugates, J. Control. Release 2 (1985) 289–310.
[53] B. Říhová, P. Kopečková, J. Strohalm, P. Rossmann, V. Větvička, J. Kopeček, Antibody directed affinity therapy applied to the immune system: *in vivo* effectiveness and limited toxicity of daunomycin conjugates to HPMA copolymers and targeting antibody, Clin. Immunol. Immunopathol. 46 (1988) 100–114.
[54] Z.-R. Lu, J.-G. Shiah, S. Sakuma, P. Kopečková, J. Kopeček, Design of novel bioconjugates for targeted drug delivery, J. Control. Release 78 (2002) 165–173.
[55] J. Kopeček, P. Kopečková, Design of polymer–drug conjugates, in: F. Kratz, P. Senter, H. Steinhagen (Eds.), Drug Delivery in Oncology, Vol. 2, Wiley-VCH, Weinheim, Germany, 2012, pp. 485–512.
[56] T.M. Allen, Ligand-targeted therapeutics in anticancer therapy, Nat. Rev. Cancer 2 (2002) 750–763.
[57] R. Duncan, Polymer therapeutics as nanomedicines: new perspectives, Curr. Opin. Biotechnol. 22 (2011) 492–501.
[58] Y. Zhou, J. Kopeček, Biological rationale for the design of polymeric anti-cancer nanomedicines, J. Drug Target. 21 (2013) 1–26.
[59] J. Kopeček, P. Kopečková, HPMA copolymers: origins, early developments, present, and future, Adv. Drug Deliv. Rev. 62 (2010) 122–149.
[60] B.S. Tucker, B.S. Sumerlin, Poly(*N*-(2-hydroxypropyl) methacrylamide)-based nanotherapeutics, Polym. Chem. 5 (2014) 1566–1572.
[61] J. Nakamura, N. Nakajima, K. Matsumura, S.H. Hyon, Water-soluble taxol conjugates with dextran and targets tumor cells by folic acid immobilization, Anticancer Res. 30 (2010) 903–909.
[62] K. Inoue, E. Kumazawa, H. Kuga, H. Susaki, N. Masabuch, T. Kajimura, CM–dextran–polyalcohol–camptothecin conjugate: DE-310 with a novel carrier system and its preclinical data, Adv. Exp. Med. Biol. 519 (2003) 145–153.
[63] C. Li, R.A. Newman, Q.P. Wu, S. Ke, W. Chen, T. Hutto, Z. Kan, M.D. Brannan, C. Charnsangavej, S. Wallace, Biodistribution of paclitaxel and poly(L-glutamic acid)–paclitaxel conjugate in mice with ovarian OCa-1 tumor, Cancer Chemother. Pharmacol. 46 (2000) 416–422.
[64] J.W. Singer, S. Shaffer, B. Baker, A. Bernareggi, S. Stromatt, D. Nienstedt, M. Besman, Paclitaxel poliglumex (XYOTAX; CT-2103): an intracellularly targeted taxane, Anticancer Drugs 16 (2005) 243–254.
[65] P. Sabbatinin, C. Aghajanian, D. Dizon, S. Anderson, J. Dupont, J.V. Brown, W.A. Peters, A. Jacobs, A. Mehdi, S. Rivkin, A.J. Eisenfeld, D. Spriggs, Phase II study of CT-2103 in patients with recurrent epithelial, ovarian, fallopian tube, or primary peritoneal carcinoma, J. Clin. Oncol. 22 (2004) 4523–4531.
[66] H. Ding, G. Helguera, J.A. Rodriguez, J. Markman, R. Luria-Pérez, P. Gangalum, J. Portilla-Arias, S. Inoue, T.R. Daniels-Wells, K. Black, E. Holler, M.L. Penichet, J.Y. Ljubimova, Polymalic acid nanobioconjugate for simultaneous immunostimulation and inhibition of tumor growth in HER2/neu-positive breast cancer, J. Control. Release 171 (2013) 322–329.
[67] H. Ding, J. Portilla-Arias, R. Patil, K.L. Black, J.Y. Ljubimova, E. Holler, Distinct mechanisms of membrane permeation induced by two polymalic acid copolymers, Biomaterials 34 (2013) 217–225.
[68] R. Tomlinson, J. Heller, S. Brocchini, R. Duncan, Polyacetal–doxorubicin conjugates designed for pH-dependent degradation, Bioconjug. Chem. 14 (2003) 1096–1106.
[69] R.M. England, E. Masiá, V. Giménez, R. Lucas, M.J. Vicent, Polyacetal–stilbene conjugates — the first examples of polymer therapeutics for the inhibition of HIF-1 in the treatment of solid tumors, J. Control. Release 164 (2012) 314–322.
[70] A. Kakinoki, Y. Kaneo, Y. Ikeda, T. Tanaka, K. Fujita, Synthesis of poly(vinyl alcohol)–doxorubicin conjugates containing cis-aconityl acid-cleavable bond and its isomer dependent doxorubicin release, Biol. Pharm. Bull. 31 (2008) 103–110.
[71] A. Kakinoki, Y. Kaneo, T. Tanaka, Y. Hosokawa, Synthesis and evaluation of water-soluble poly(vinyl alcohol)–paclitaxel conjugate as a macromolecular prodrug, Biol. Pharm. Bull. 31 (2008) 963–969.
[72] W.J. Kim, M.S. Kang, H.K. Kim, Y. Kim, T. Chang, T. Ohulchanskyy, P.N. Prasad, K.S. Lee, Water-soluble porphyrin–polyethylene glycol conjugate with enhanced cellular uptake for photodynamic therapy, J. Nanosci. Nanotechnol. 9 (2009) 7130–7135.
[73] P. Chadna, J.J. Khandare, E. Ber, L. Rodriguez-Rodriguez, T. Minko, Multifunctional tumor-targeted polymer–peptide–drug delivery system for treatment of primary and metastatic cancers, Pharm. Res. 27 (2011) 2296–2306.
[74] I. Conejos-Sánchez, I. Cardoso, M.J. Saraiva, M.J. Vicent, Targeting a rare amyloidotic disease through rationally designed polymer conjugates, J. Control. Release 178 (2014) 95–100.
[75] S. Van, S.K. Das, X. Wang, Z. Feng, Y. Jin, Z. Hou, F. Chen, A. Pham, N. Jiang, S.B. Howell, L. Yu, Synthesis, characterization, and biological evaluation of poly(L-γ-glutamyl-glutamine)–paclitaxel conjugate, Int. J. Nanomedicine 5 (2010) 825–837.
[76] P.A. Vasey, S.B. Kaye, R. Morrison, C. Twelves, P. Wilson, R. Duncan, A.H. Thomson, L.S. Murray, T.E. Hilditch, T. Murray, S. Burtles, D. Fraier, E. Frigerio, J. Cassidy, and on behalf of the Cancer Research Campaign Phase I/II Committee, Phase I clinical and pharmacokinetic study of PK1 [*N*-(2-hydroxypropyl)methacrylamide copolymer doxorubicin]: first member of a new class of chemotherapeutic agents–drug–polymer conjugates, Clin. Cancer Res. 5 (1999) 83–94.
[77] L.W. Seymour, D.R. Ferry, D. Anderson, S. Hesslewood, P.J. Julyan, R. Poyner, J. Doran, A.M. Young, S. Burtles, D.J. Kerr, Hepatic drug targeting: phase I evaluation of polymer-bound doxorubicin, J. Clin. Oncol. 20 (2002) 1668–1676.
[78] J.M. Rademaker-Lakhai, C. Terret, S.B. Howell, C.M. Baud, R.F. De Boer, D. Pluim, J.H. Beijnen, J.H. Schellens, J.P. Droz, A phase I and pharmacological study of the platinum polymer AP5280 given as an intravenous infusion once every 3 weeks in patients with solid tumors, Clin. Cancer Res. 10 (2004) 3386–3395.
[79] J.B. Lloyd, Lysosomal membrane permeability: implications for drug delivery, Adv. Drug Deliv. Rev. 41 (2000) 189–200.
[80] K. Ulbrich, V. Šubr, Polymeric anticancer drugs with pH-controlled activation, Adv. Drug Deliv. Rev. 56 (2004) 1023–1050.
[81] H. Nakamura, T. Etrych, P. Chytil, M. Ohkubo, J. Fang, K. Ulbrich, H. Maeda, Two step mechanism of tumor selective delivery of N-(2-hydroxypropyl) methacrylamide copolymer conjugated with piarubicin via an acid-cleavable linkage, J. Control. Release 174 (2014) 81–87.
[82] T. Etrych, M. Jelínková, B. Říhová, K. Ulbrich, New HPMA copolymers containing doxorubicin bound via pH-sensitive linkage: synthesis and preliminary *in vitro* and *in vivo* properties, J. Control. Release 73 (2001) 89–102.
[83] W.-C. Shen, H.J.-P. Ryser, Cis-aconityl spacer between daunomycin and macromolecular carriers: a model of pH-sensitive linkage releasing drug from a lysosomotropic conjugate, Biochem. Biophys. Res. Commun. 102 (1981) 1048–1054.
[84] D.B. Rozema, K. Ekena, D.L. Lewis, A.G. Loomis, J.A. Wolff, Endosomolysis by masking of a membrane-active agent (EMMA) for cytoplasmic release of macromolecules, Bioconjug. Chem. 14 (2003) 51–57.
[85] J. Kopeček, P. Rejmanová, Enzymatically degradable bonds in synthetic polymers, in: S.D. Bruck (Ed.), Controlled Drug Delivery, vol. I, CRC Press, Boca Raton, Florida, 1983, pp. 81–124.
[86] J. Kopeček, Biodegradation of polymers for biomedical use, in: H. Benoit, P. Rempp (Eds.), IUPAC Macromolecules, Oxford, Pergamon Press, 1982, pp. 305–320.
[87] J. Kopeček, P. Rejmanová, V. Chytrý, Polymers containing enzymatically degradable bonds 1. Chymotrypsin catalyzed hydrolysis of p-nitroanilides of phenylalanine and tyrosine attached to side-chains of copolymers of *N*-(2-hydroxypropyl) methacrylamide, Makromol. Chem. 182 (1981) 799–809.
[88] K. Ulbrich, J. Strohalm, J. Kopeček, Polymers containing enzymatically degradable bonds. 3. Poly[*N*-(2-hydroxypropyl)methacrylamide] chains connected by oligopeptide sequences cleavable by trypsin, Makromol. Chem. 182 (1981) 1917–1928.
[89] K. Ulbrich, E.I. Zacharieva, B. Obereigner, J. Kopeček, Polymers containing enzymatically degradable bonds. 5. Hydrophilic polymers degradable by papain, Biomaterials 1 (1980) 199–204.
[90] J. Kopeček, Controlled degradability of polymers — a key to drug delivery systems, Biomaterials 5 (1984) 19–25.
[91] J. Kopeček, I. Cífková, P. Rejmanová, J. Strohalm, B. Obereigner, K. Ulbrich, Polymers containing enzymatically degradable bonds. 4. Preliminary experiments *in vivo*, Makromol. Chem. 182 (1981) 2941–2949.
[92] R. Duncan, H.C. Cable, J.B. Lloyd, P. Rejmanová, J. Kopeček, Polymers containing enzymatically degradable bonds. 7. Design of oligopeptide side-chains in poly[*N*-(2-hydroxypropyl)methacrylamide] copolymers to promote efficient degradation by lysosomal enzymes, Makromol. Chem. 184 (1983) 1997–2008.
[93] V. Šubr, J. Kopeček, J. Pohl, M. Baudyš, V. Kostka, Cleavage of oligopeptide side-chains in *N*-(2-hydroxypropyl)methacrylamide copolymers by mixtures of lysosomal enzymes, J. Control. Release 8 (1988) 133–140.
[94] A. Nan, H. Ghandehari, C. Harbert, H. Siavash, N. Nikitakis, M. Reynolds, J.J. Sauk, Water-soluble polymers for targeted drug delivery to human squamous carcinoma of head and neck, J. Drug Target. 13 (2005) 190–197.
[95] M. Manea, J. Tóvári, M. Tejeda, A. Schulcz, B. Kapuvári, B. Voncze, G. Mezo, *In-vivo* antitiumour effect of daunorubicin–GnRH-III derivative conjugates on colon carcinoma-bearing mice, Anticancer Drugs 23 (2012) 90–97.

[96] Z.H. Peng, M. Sima, M.E. Salama, P. Kopečková, J. Kopeček, Spacer length impacts the efficacy of targeted docetaxel conjugates in prostate-specific membrane antigen expressing prostate cancer, J. Drug Target. 21 (2013) 968–980.
[97] S.O. Doronina, T.D. Bovee, D.W. Meyer, J.B. Miyamoto, M.E. Anderson, C.A. Morris-Tilden, P.D. Senter, Novel peptide linkers for highly potent antibody–auristatin conjugate, Bioconjug. Chem. 19 (2008) 1960–1963.
[98] P.J. Burke, P.D. Senter, D.W. Meyer, J.B. Miyamoto, M. Anderson, B.E. Toki, G. Manikumar, M.C. Wani, D.J. Krol, S.C. Jeffrey, Design, synthesis, and biological evaluation of antibody–drug conjugates comprised of potent camptothecin analogues, Bioconjug. Chem. 20 (2009) 1242–1250.
[99] P.L. Carl, P.K. Chakravarty, J.A. Katzenellenbogen, A novel connector linkage applicable in prodrug design, J. Med. Chem. 24 (1981) 479–480.
[100] F.M. de Groot, W.J. Loos, R. Koekkoek, L.W. van Berkom, G.F. Busscher, A.E. Seelen, C. Albrecht, P. de Bruijn, H.W. Scheeren, Elongated multiple electronic cascade and cyclization spacer systems in activatible anticancer prodrugs for enhanced drug release, J. Org. Chem. 66 (2001) 8815–8830.
[101] B.E. Toki, C.G. Cerveny, A.F. Wahl, P.D. Senter, Protease-mediated fragmentation of p-amidobenzyl ethers: a new strategy for the activation of anticancer prodrugs, J. Org. Chem. 67 (2002) 1866–1872.
[102] S. Gao, Z. Lu, B. Petri, P. Kopečková, J. Kopeček, Colon-specific 9-aminocamptothecin–HPMA copolymer conjugates containing a 1,6-elimination spacer, J. Control. Release 110 (2006) 323–331.
[103] H.Z. Pan, P. Kopečková, D. Wang, J. Yang, S. Miller, J. Kopeček, Water-soluble HPMA copolymer–prostaglandin conjugates containing a cathepsin K sensitive spacer, J. Drug Target. 14 (2006) 425–435.
[104] J.-G. Shiah, Y. Sun, P. Kopečková, C.M. Peterson, R.C. Straight, J. Kopeček, Combination chemotherapy and photodynamic therapy of targetable *N*-(2-hydroxypropyl) methacrylamide copolymer–doxorubicin/mesochlorin e_6–OV-TL16 antibody immunoconjugates, J. Control. Release 74 (2001) 249–253.
[105] M. Mammen, S.K. Choi, G.M. Whitesides, Polyvalent interactions in biological systems: implications for design and use of multivalent ligands and inhibitors, Angew. Chem. Int. Ed. 3 (1998) 2754–2794.
[106] R.N. Johnson, P. Kopečková, J. Kopeček, Synthesis and evaluation of multivalent branched HPMA copolymer–Fab′ conjugates targeted to the B-cell antigen, Bioconjug. Chem. 20 (2009) 129–137.
[107] T.W. Chu, J. Yang, J. Kopeček, Anti-CD20 multivalent HPMA copolymer–Fab′ conjugates for the direct induction of apoptosis, Biomaterials 33 (2012) 7174–7181.
[108] R.N. Johnson, P. Kopečková, J. Kopeček, Biological activity of anti-CD20 multivalent HPMA copolymer–Fab′ conjugates, Biomacromolecules 13 (2012) 727–735.
[109] A. David, P. Kopečková, A. Rubinstein, J. Kopeček, Enhanced biorecognition and internalization of HPMA copolymers containing multi- or multivalent carbohydrate side-chains by human hepatocarcinoma cells, Bioconjug. Chem. 12 (2001) 890–899.
[110] A. David, P. Kopečková, T. Minko, A. Rubinstein, J. Kopeček, Design of multivalent galactoside ligand for selective targeting of HPMA copolymers–doxorubicin conjugates to human colon cancer cells, Eur. J. Cancer 40 (2004) 148–157.
[111] A. Tang, P. Kopečková, J. Kopeček, Binding and cytotoxicity of HPMA copolymers to lymphocytes mediated by receptor-binding epitopes, Pharm. Res. 20 (2003) 360–367.
[112] V. Cuchelkar, P. Kopečková, J. Kopeček, Novel HPMA copolymer-bound constructs for combined tumor and mitochondrial targeting, Mol. Pharm. 5 (2008) 696–709.
[113] A. Rebuffat, A. Bernasconi, M. Ceppi, H. Wehrli, S. Brenz Verca, M. Ibrahim, B.M. Frey, F.J. Frey, S. Rusconi, Selective enhancement of gene transfer by steroid-mediated gene delivery, Nat. Biotechnol. 19 (2001) 1155–1161.
[114] V. Cuchelkar, Ph.D. Dissertation, University of Utah, Department of Bioengineering, 2008.
[115] R. Duncan, P. Rejmanová, J. Kopeček, J.B. Lloyd, Pinocytic uptake and intracellular degradation of *N*-(2-hydroxypropyl)methacrylamide copolymers. A potential drug delivery system, Biochim. Biophys. Acta 678 (1981) 143–150.
[116] R. Duncan, H.C. Cable, P. Rejmanová, J. Kopeček, J.B. Lloyd, Tyrosinamide residues enhance pinocytic capture of *N*-(2-hydroxypropyl)methacrylamide copolymers, Biochim. Biophys. Acta 799 (1984) 1–8.
[117] J. Liu, P. Kopečková, P. Bühler, P. Wolf, H. Pan, H. Bauer, U. Elsässer-Beile, J. Kopeček, Biorecognition and subcellular trafficking of HPMA copolymer–anti-PMSA antibody conjugates by prostate cancer cells, Mol. Pharm. 6 (2009) 959–970.
[118] J. Callahan, P. Kopečková, J. Kopeček, The intracellular trafficking and subcellular distribution of a large array of HPMA copolymer conjugates, Biomacromolecules 10 (2009) 1704–1714.
[119] M. Tijerina, P. Kopečková, J. Kopeček, Correlation of subcellular compartmentalization of HPMA copolymer–Mce_6 conjugates with chemotherapeutic activity in human ovarian carcinoma cells, Pharm. Res. 20 (2003) 728–737.
[120] M. Tijerina, P. Kopečková, J. Kopeček, Mechanism of cytotoxicity in human ovarian carcinoma cells exposed to free Mce_6 or HPMA copolymer–Mce_6 conjugates, Photochem. Photobiol. 77 (2003) 645–652.
[121] D.B. Rozema, D.L. Lewis, D.H. Wakefield, S.C. Wong, J.J. Klein, P.L. Roesch, S.L. Bertin, T.W. Reppen, Q. Chu, A.V. Blokhin, J.E. Hagstrom, J.A. Wolff, Dynamic polyconjugates for targeted *in vivo* delivery of siRNA to hepatocytes, Proc. Natl. Acad. Sci. U. S. A. 104 (2007) 12982–12987.
[122] B.B. Lundy, A. Convertine, M. Miteva, P.S. Stayton, Neutral polymeric micelles for RNA delivery, Bioconjug. Chem. 24 (2013) 398–407.
[123] K. Gunasekaran, T.H. Nguyen, H.D. Maynard, T.P. Davis, V. Bulmus, Conjugation of siRNA with comb-type PEG enhances serum stability and gene silencing efficiency, Macromol. Rapid Commun. 32 (2011) 654–659.
[124] M.E. Fox, F.C. Szóka, J.M. Fréchet, Soluble polymer carriers for the treatment of cancer: the importance of molecular architecture, Acc. Chem. Res. 42 (2009) 1141–1151.
[125] B. Chen, D.G. van der Poll, K. Jerger, W.C. Floyd, J.M. Fréchet, F.C. Szóka, Synthesis and properties of star-comb polymers and their doxorubicin conjugates, Bioconjug. Chem. 22 (2011) 617–624.
[126] K. Ulbrich, V. Šubr, Structural and chemical aspects of HPMA copolymers as drug carriers, Adv. Drug Deliv. Rev. 62 (2010) 150–166.
[127] T. Etrych, V. Šubr, J. Strohalm, M. Šírová, B. Říhová, K. Ulbrich, HPMA copolymer–doxorubicin conjugates: the effects of molecular weight and architecture on biodistribution and *in vivo* activity, J. Control. Release 164 (2012) 346–354.
[128] K. Ulbrich, Č. Koňák, Z. Tuzar, J. Kopeček, Solution properties of drug carriers based on poly[*N*-(2-hydroxypropyl)methacrylamide] containing biodegradable bonds, Makromol. Chem. 188 (1987) 1261–1272.
[129] H. Ding, P. Kopečková, J. Kopeček, Self-association properties of HPMA copolymers containing an amphipathic heptapeptide, J. Drug Target. 15 (2007) 465–474.
[130] M. Allmeroth, D. Mederegger, B. Biesalski, K. Koynov, F. Rösch, O. Thews, R. Zentel, Modifying the body distribution of HPMA-based copolymers by molecular weight and aggregate formation, Biomacromolecules 12 (2011) 2841–2849.
[131] H. Maeda, Tumor-selective delivery of macromolecular drugs via the EPR effect: background and future prospects, Bioconjug. Chem. 21 (2010) 797–802.
[132] Y. Matsumura, H. Maeda, A new concept for macromolecular therapeutics in cancer therapy: mechanism of tumoritropic accumulation of proteins and the antitumor agent SMANCS, Cancer Res. 46 (1986) 6387–6392.
[133] L.W. Seymour, R. Duncan, J. Strohalm, J. Kopeček, Effect of molecular weight of *N*-(2-hydroxypropyl)methacrylamide copolymers on body distribution and rate of excretion after subcutaneous, intraperitoneal and intravenous administration, J. Biomed. Mater. Res. 21 (1987) 1341–1358.
[134] Y. Noguchi, J. Wu, R. Duncan, J. Strohalm, K. Ulbrich, T. Akaike, H. Maeda, Early phase tumor accumulation of macromolecules: a great difference in clearance rate between tumor and normal tissues, Jpn. J. Cancer Res. 89 (1998) 307–314.
[135] T. Etrych, J. Strohalm, B. Chytil, B. Říhová, K. Ulbrich, Novel star HPMA-based polymer conjugates for passive targeting to solid tumors, J. Drug Target. 19 (2011) 874–889.
[136] J.P. Medema, Cancer stem cells: the challenges ahead, Nat. Cell Biol. 15 (2013) 338–344.
[137] Y. Zhou, J. Yang, J. Kopeček, Cancer stem cells: potential target for anti-cancer nanomedicines, in: C. Scholz, J. Kressler (Eds.), Tailored polymer architectures for pharmaceutical and biomedical applications, ACS Symposium Series, 1135, American Chemical Society, Washington, D.C., 2013, pp. 127–149.
[138] A. Dubrovska, J. Elliott, R.J. Salamone, S. Kim, L.J. Aimone, J.R. Walker, J. Watson, M. Sauveur-Michel, C. Garcia-Echeverria, C.Y. Cho, V.A. Reddy, P.G. Schultz, Combination therapy targeting both tumor-initiating and differentiated cell populations in prostate carcinoma, Clin. Cancer Res. 16 (2010) 5692–5702.
[139] Y. Zhou, J. Yang, J. Kopeček, Selective inhibitory effect of HPMA copolymer–cyclopamine conjugate on prostate cancer stem cells, Biomaterials 33 (2012) 1863–1872.
[140] J. Gao, S. Graves, U. Koch, S. Liu, V. Jankovic, S. Buonamici, A.E.I. Andaloussi, S.D. Nimer, B.L. Kee, R. Taichman, F. Radtke, I. Aifantis, Hedgehog signaling is dispensable for adult hematopoietic stem cell function, Cell Stem Cell 4 (2009) 548–558.
[141] I. Hofmann, E.H. Stover, D.E. Cullen, J. Mao, K.J. Morgan, B.H. Lee, M.G. Kharas, P.G. Miller, M.G. Cornejo, R. Okabe, S.A. Armstrong, N. Ghilardi, S. Gould, F.J. de Sauvage, A.P. McMahon, D.G. Gilliland, Hedgehog signaling is dispensable for adult murine hematopoietic stem cell function and hematopoiesis, Cell Stem Cell 4 (2009) 559–567.
[142] Y. Gu, H. Li, J. Miki, K.H. Kim, B. Furusato, I.A. Sesterhenn, W.S. Chu, D.G. McLeod, S. Srivastava, C.M. Ewing, W.B. Isaacs, J.S. Rhim, Phenotypic characterization of telomerase-immortalized primary nonmalignant and malignant tumor-derived human prostate epithelial cell lines, Exp. Cell Res. 312 (2006) 831–843.
[143] Y. Zhou, J. Yang, J.S. Rhim, J. Kopeček, HPMA copolymer-based combination therapy toxic to both prostate cancer stem/progenitor cells and differentiated cells induces durable anti-tumor effects, J. Control. Release 172 (2013) 946–953.
[144] "Top story", Prostate Cell News 4.36 September 20, 2013.
[145] J. Miki, B. Furusato, H. Li, Y. Gu, H. Takahashi, S. Egawa, I.A. Sesterhenn, D.G. McLeod, S. Srivastava, J.S. Rhim, Identification of putative stem cell markers, CD133 and CXCR4, in hTERT-immortalized primary nonmalignant and malignant tumor-derived human prostate epithelial cell lines and in prostate cancer specimens, Cancer Res. 67 (2007) 3153–3161.
[146] G.D. Richardson, C.N. Robson, S.H. Lang, D.E. Neal, N.J. Maitland, A.T. Collins, CD133, a novel marker for human prostatic epithelial stem cells, J. Cell Sci. 117 (2004) 7180–7185.
[147] K. Kemper, M.R. Sprick, M. de Bree, A. Scopelliti, L. Vermeulen, M. Hoek, J. Zeilstra, S.T. Pals, H. Mehmet, G. Stassi, J.P. Medema, The AC133 epitope, but not the CD133 protein, is lost upon cancer stem cell differentiation, Cancer Res. 70 (2010) 719–729.
[148] B. Campos, C.C. Herold-Mende, Insight into the complex regulation of CD133 in glioma, Int. J. Cancer 128 (2011) 501–510.
[149] P. Friedl, S. Alexander, Cancer invasion and the microenvironment: plasticity and reciprocity, Cell 147 (2011) 992–1009.
[150] K.P. Olive, M.A. Jacobetz, C.J. Davidson, A. Gopinathan, D. McIntyre, D. Honess, B. Madhu, M.A. Goldgraben, M.E. Caldwell, D. Allard, K.K. Frese, G. Denicola, C. Feig, C. Combs, S.P. Winter, H. Ireland-Zecchini, S. Reichelt, W.J. Howat, A. Chang, M. Dhara, L. Wang, F. Rückert, R. Grützmann, C. Pilarsky, K. Izeradjene, S.R. Hingorani, P. Huang, S.E. Davies, W. Plunkett, M. Egorin, R.H. Hruban, N. Whitebread, K. McGovern, J. Adams, C. Iacobuzio-Donahu, J. Griffiths, D.A. Tuveson, Inhibition of

hedgehog signaling enhances delivery of chemotherapy in a mouse model of pancreatic cancer, Science 324 (2009) 1457–1461.
[151] C. Whatcott, H. Han, R.G. Posner, D.D. Von Hoff, Tumor–stromal interactions in pancreatic cancer, Crit. Rev. Oncog. 18 (2013) 135–151.
[152] P.P. Provenzano, S.R. Hingorani, Hyaluronan, fluid pressure, and stromal resistance in pancreas cancer, Brit. J. Cancer 108 (2013) 1–8.
[153] P.P. Provenzano, C. Cuevas, A.E. Chang, V.K. Goel, D.D. Von Hoff, S.R. Hingorani, Enzymatic targeting of the stroma ablates physical barriers to treatment of pancreatic ductal adenocarcinoma, Cancer Cell 21 (2012) 418–429.
[154] M.A. Jacobetz, D.S. Chan, A. Neesse, T.E. Bapiro, N. Cook, K.K. Frese, C. Feig, T. Nakagawa, M.E. Caldwell, H.I. Zecchini, M.P. Lolkema, P. Jiang, A. Kultti, C.B. Thompson, D.C. Maneval, D.I. Jodrell, G.I. Frost, H.M. Shepard, J.N. Skepper, D.A. Tuveson, Hyaluronan impairs vascular function and drug delivery in a mouse model of pancreatic cancer, Gut 62 (2013) 112–120.
[155] L.C. Murtaugh, Pathogenesis of pancreatic cancer: lessons from animal models, Toxicol. Pathol. 42 (2014) 217–228.
[156] N. Cook, K.P. Olive, K. Frese, D.A. Tuveson, K-Ras-driven pancreatic cancer mouse model for anticancer inhibitor analyses, Meth. Enzymol. 439 (2008) 73–85.
[157] J.P. Morton, P. Timpson, S.A. Karim, R.A. Ridgway, D. Athineos, B. Doyle, N.B. Jamieson, K.A. Oien, A.M. Lowy, V.G. Brunton, M.C. Frame, T.R. Evans, O.J. Sansom, Mutant p53 drives metastasis and overcomes growth arrest/senescence in pancreatic cancer, Proc. Natl. Acad. Sci. U. S. A. 107 (2010) 246–251.
[158] A. Jimeno, G. Feldmann, A. Suarez-Gauthier, Z. Rasheed, A. Solomon, G.M. Zou, B. Rubio-Viqueira, E. García-García, F. López-Ríos, W. Matsui, A. Maitra, M. Hidalgo, A direct pancreatic cancer xenograft model as a platform for cancer stem cell therapeutic development, Mol. Cancer Ther. 8 (2009) 310–314.
[159] B. Buckway, Y. Wang, A. Ray, H. Ghandehari, Overcoming the stromal barrier for targeted delivery of HPMA copolymers to pancreatic tumors, Int. J. Pharm. 456 (2013) 202–211.
[160] M.M. Gottesman, T. Fojo, S.F. Bates, Multidrug resistance in cancer: role of ATP-dependent transporters, Nat. Rev. Cancer 2 (2002) 48–58.
[161] J.I. Fletcher, M. Haber, M.J. Henderson, M.D. Norris, ABC transporters in cancer: more than just drug efflux pumps, Nat. Rev. Cancer 10 (2010) 147–156.
[162] S.G. Aller, J. Yu, A. Ward, S. Chittaboina, R. Zhuo, P.M. Harrell, Y.T. Trinh, Q. Zhang, I.L. Urbatsch, G. Chang, Structure of P-glycoprotein reveals a molecular basis for poly-specific drug binding, Science 323 (2009) 1718–1722.
[163] V. Omelyanenko, P. Kopečková, C. Gentry, J. Kopeček, Targetable HPMA copolymer–adriamycin conjugates. Recognition, internalization, and subcellular fate, J. Control. Release 53 (1998) 25–37.
[164] T. Minko, P. Kopečková, J. Kopeček, Efficacy of chemotherapeutic action of HPMA copolymer-bound doxorubicin in a solid tumor model of ovarian carcinoma, Int. J. Cancer 86 (2000) 108–117.
[165] N.L. Krinick, Y. Sun, D. Joyner, J.D. Spikes, R.C. Straight, J. Kopeček, A polymeric drug delivery system for the simultaneous delivery of drugs activatable by enzymes and/or light, J. Biomater. Sci. Polym. Ed. 5 (1994) 303–324.
[166] C.M. Peterson, J.M. Lu, Y. Sun, C.A. Peterson, J.-G. Shiah, R.C. Straight, J. Kopeček, Combination chemotherapy and photodynamic therapy with *N*-(2-hydroxypropyl)methacrylamide copolymer-bound anticancer drugs inhibit human ovarian carcinoma heterotransplanted in nude mice, Cancer Res. 56 (1996) 3980–3985.
[167] J.-G. Shiah, Y. Sun, C.M. Peterson, R.C. Straight, J. Kopeček, Antitumor activity of HPMA copolymer–meso chlorin e_6 and adriamycin conjugates in combination treatments, Clin. Cancer Res. 6 (2000) 1008–1015.
[168] J. Hongrapipat, P. Kopečková, S. Prakongpan, J. Kopeček, Enhanced antitumor activity of combinations of free and HPMA copolymer-bound drugs, Int. J. Pharm. 351 (2008) 259–270.
[169] J. Hongrapipat, P. Kopečková, J. Liu, S. Prakongpan, J. Kopeček, Combination chemotherapy and photodynamic therapy with Fab′ fragment targeted HPMA copolymer conjugates in human ovarian carcinoma cells, Mol. Pharm. 5 (2008) 696–709.
[170] N. Larson, J. Yang, A. Ray, D.L. Cheney, H. Ghandehari, J. Kopeček, Ovarian cancer combination therapy using biodegradable multiblock poly[*N*-(2-hydroxypropyl)-methacrylamide gemcitabine and paclitaxel conjugates, Int. J. Pharm. 454 (2013) 435–443.
[171] A. Duangjai, K. Luo, Y. Zhou, J. Yang, J. Kopeček, Combination cytotoxicity of backbone degradable HPMA copolymer gemcitabine and platinum conjugates toward human ovarian carcinoma cells, Eur. J. Pharm. Biopharm. (2014) (http://dx.doi.org/10.1016/j.ejpb.2013.11.008).
[172] R. Zhang, J. Yang, M. Sima, Y. Zhou, J. Kopeček, Sequential Combination Therapy of Ovarian Cancer with Backbone Degradable HPMA Copolymer Paclitaxel and Gemcitabine Conjugates, 2014. (submitted for publication).
[173] S.A. Low, J. Kopeček, Targeting polymer therapeutics to bone, Adv. Drug Deliv. Rev. 64 (2012) 1189–1204.
[174] D. Wang, S. Miller, P. Kopečková, J. Kopeček, Bone-targeting macromolecular therapeutics, Adv. Drug Deliv. Rev. 57 (2005) 1049–1076.
[175] X.M. Liu, S.C. Miller, D. Wang, Beyond oncology — application of HPMA copolymers in non-cancerous diseases, Adv. Drug Deliv. Rev. 62 (2010) 258–271.
[176] F. Yuan, L.D. Quan, L. Cui, S.R. Goldring, D. Wang, Development of macromolecular prodrug for rheumatoid arthritis, Adv. Drug Deliv. Rev. 64 (2012) 1205–1219.
[177] A. Nan, N.P. Nanayakkara, L.A. Walker, V. Yardley, S.L. Croft, H. Ghandehari, *N*-(2-hydroxypropyl)methacrylamide (HPMA) copolymers for targeted delivery of 8-aminoquinoline antileishmanial drugs, J. Control. Release 77 (2001) 233–243.
[178] A. Nan, S.L. Croft, V. Yardley, H. Ghandehari, Targetable water-soluble polymer–drug conjugates for the treatment of visceral leishmaniasis, J. Control. Release 94 (2004) 115–127.
[179] S. Nicoletti, K. Seifert, I.H. Gilbert, *N*-(2-hydroxypropyl)methacrylamide–amphotericin B (HPMA–AmB) copolymer conjugates as antileishmanial agents, Int. J. Antimicrob. Agents 33 (2009) 441–448.
[180] S. Nicoletti, K. Seifert, I.H. Gilbert, Water-soluble polymer–drug conjugates for combination chemotherapy against visceral leishmaniasis, Bioorg. Med. Chem. 18 (2010) 2559–2565.
[181] D. Wang, S.C. Miller, M. Sima, D. Parker, H. Buswell, K.C. Goodrich, P. Kopečková, J. Kopeček, The arthrotropism of macromolecules in adjuvant-induced arthritis rat model: a preliminary study, Pharm. Res. 21 (2004) 1741–1749.
[182] L.D. Quan, P.E. Purdue, X.M. Liu, M.D. Boska, S.M. Lele, G.M. Thiele, T.R. Mikuls, H. Dou, S.R. Goldring, D. Wang, Development of a macromolecular prodrug for the treatment of inflammatory arthritis: mechanism involved in arthrotropism and sustained therapeutic efficacy, Arthritis Res. Ther. 12 (2010) R170, http://dx.doi.org/10.1186/ar3130.
[183] L. Quan, Y. Zhang, B.J. Crielaard, A. Dusad, S.M. Lele, C.J. Rijcken, J.M. Metsalaar, H. Kostková, T. Etrych, K. Ulbrich, F. Kiessling, T.R. Mikuls, W.E. Hennink, G. Storm, T. Lammers, D. Wang, Nanomedicines for inflammatory arthritis: head-to-head comparison of glucocorticoid-containing polymers, micelles, and liposomes, ACS Nano 8 (2014) 458–466.
[184] J. Kopeček, Biomaterials and drug delivery — past, present, and future, Mol. Pharm. 7 (2010) 922–925.
[185] J. Yang, C. Xu, C. Wang, J. Kopeček, Refolding hydrogels self-assembled from HPMA graft copolymers by antiparallel coiled-coil formation, Biomacromolecules 7 (2006) 1187–1195.
[186] J. Yang, K. Wu, Č. Koňák, J. Kopeček, Dynamic light scattering study of the self-assembly of HPMA hybrid graft copolymers, Biomacromolecules 9 (2008) 510–517.
[187] J. Kopeček, J. Yang, Smart, self-assembled hybrid hydrogel materials, Angew. Chem. Int. Ed. 51 (2012) 7396–7417.
[188] M. Dvořák, P. Kopečková, J. Kopeček, High-molecular weight HPMA copolymer–adriamycin conjugates, J. Control. Release 60 (1999) 321–332.
[189] J.-G. Shiah, M. Dvořák, P. Kopečková, Y. Sun, C.M. Peterson, J. Kopeček, Biodistribution and antitumor efficacy of long-circulating *N*-(2-hydroxypropyl) methacrylamide copolymer–doxorubicin conjugates in nude mice, Eur. J. Cancer 37 (2001) 131–139.
[190] G. Moad, E. Rizzardo, S.H. Thang, Toward living radical polymerization, Acc. Chem. Res. 41 (2008) 1133–1142.
[191] C.W. Scales, Y.A. Vasilieva, A.J. Convertine, A.B. Lowe, C.L. McCormick, Direct, controlled synthesis of the nonimmunogenic, hydrophilic polymer, poly(*N*-(2-hydroxypropyl)methacrylamide) via RAFT in aqueous media, Biomacromolecules 6 (2005) 1846–1850.
[192] C.D. Hein, X.M. Liu, D. Wang, Click chemistry, a powerful tool for pharmaceutical sciences, Pharm. Res. 25 (2008) 2216–2230.
[193] J.C. Jewett, C.R. Bertozzi, Cu-free click cycloaddition reactions in chemical biology, Chem. Soc. Rev. 39 (2010) 1272–1279.
[194] C.E. Hoyle, C.N. Bowman, Thiol–ene click chemistry, Angew. Chem. Int. Ed. 49 (2010) 1540–1573.
[195] J. Yang, K. Luo, H. Pan, P. Kopečková, J. Kopeček, Synthesis of biodegradable multiblock copolymers by click coupling of RAFT-generated heterotelechelic polyHPMA conjugates, React. Funct. Polym. 71 (2011) 294–302.
[196] K. Luo, J. Yang, P. Kopečková, J. Kopeček, Biodegradable multiblock *N*-(2-hydroxypropyl)methacrylamide copolymers via reversible addition–fragmentation chain transfer polymerization and click chemistry, Macromolecules 44 (2011) 2481–2488.
[197] H. Pan, J. Yang, P. Kopečková, J. Kopeček, Backbone degradable multiblock *N*-(2-hydroxypropyl)methacrylamide copolymer conjugates via reversible addition–fragmentation chain transfer polymerization and thiol–ene coupling reaction, Biomacromolecules 12 (2011) 247–252.
[198] H. Pan, M. Sima, J. Yang, J. Kopeček, Synthesis of long-circulating, backbone degradable HPMA copolymer–doxorubicin conjugates and evaluation of molecular-weight-dependent antitumor efficacy, Macromol. Biosci. 13 (2013) 155–160.
[199] R. Zhang, K. Luo, J. Yang, M. Sima, Y. Sun, M.M. Janát-Amsbury, J. Kopeček, Synthesis and evaluation of a backbone biodegradable multiblock HPMA copolymer nanocarrier for the systemic delivery of paclitaxel, J. Control. Release 166 (2013) 66–74.
[200] H. Pan, M. Sima, S.C. Miller, P. Kopečková, J. Yang, J. Kopeček, Efficiency of high molecular weight backbone degradable HPMA copolymer–prostaglandin E1 conjugate in promotion of bone formation in overiectomized rats, Biomaterials 34 (2013) 6528–6538.
[201] K. Wu, J. Liu, R.N. Johnson, J. Yang, J. Kopeček, Drug-free macromolecular therapeutics: induction of apoptosis by coiled-coil-mediated cross-linking of antigens on the cell surface, Angew. Chem. Int. Ed. 49 (2010) 1451–1455.
[202] K.G. Wu, J. Yang, J. Liu, J. Kopeček, Coiled-coil based drug-free macromolecular therapeutics: *in vivo* efficacy, J. Control. Release 157 (2012) 126–131.
[203] T.W. Chu, J. Yang, R. Zhang, M. Sima, J. Kopeček, Cell surface self-assembly of hybrid nanoconjugates via oligonucleotide hybridization induces apoptosis, ACS Nano 8 (2014) 719–730.
[204] D.A. Parry, R.D. Fraser, J.M. Squire, Fifty years of coiled-coils and α-helical bundles: a close relationship between sequence and structure, J. Struct. Biol. 163 (2008) 258–269.
[205] J.Y. Su, R.S. Hodges, C.M. Kay, Effect of chain length on the formation and stability of synthetic alpha-helical coiled coils, Biochemistry 33 (1994) 15501–15510.
[206] M.G. Oakley, J.J. Hollenbeck, The design of antiparallel coiled-coils, Curr. Opin. Struct. Biol. 11 (2001) 450–457.
[207] Y.B. Yu, Coiled-coils: stability, specificity, and drug delivery potential, Adv. Drug Deliv. Rev. 54 (2002) 1113–1129.

[208] J. Walshaw, D.N. Woolfson, Socket: a program for identifying and analyzing coiled-coil motifs within protein structures, J. Mol. Biol. 307 (2001) 1427–1460.
[209] *CCE*: CYGG E VSALEKE VSALEKK NSALEKE VSALEKE VSALEK; *CCK*: CYGG K VSALKEK VSALKEE VSANKEK VSALKEK VSALKE.
[210] S. Lv, Y. Cao, H. Li, Tandem modular protein-based hydrogels constructed using a novel two-component approach, Langmuir 28 (2012) 2269–2274.
[211] D.A. Einfeld, J.P. Brown, M.A. Valentine, E.A. Clark, J.A. Ledbetter, Molecular cloning of the human B cell CD20 receptor predicts a hydrophobic protein with multiple transmembrane domains, EMBO J. 7 (1988) 711–717.
[212] O.W. Press, J. Howell-Clark, S. Anderson, I. Bernstein, Retention of B-cell-specific monoclonal antibodies by human lymphoma cells, Blood 83 (1994) 1390–1397.
[213] J.T. Golay, E.A. Clark, P.C. Beverley, The CD20 (Bp35) antigen is involved in activation of B cells from the G0 to the G1 phase of the cell cycle, J. Immunol. 135 (1985) 3795–3801.
[214] J.K. Bubien, L.J. Zhou, P.D. Bell, R.A. Frizzell, T.F. Tedder, Transfection of the CD20 cell surface molecule into ectopic cell types generates a Ca^{2+} conductance found constitutively in B lymphocytes, J. Cell Biol. 121 (1993) 1121–1132.
[215] J.P. Deans, H. Li, M. Polyak, CD20-mediated apoptosis: signaling through lipid rafts, Immunology 107 (2002) 176–182.
[216] *MORF1*: 5'-GAGTAAGCCAAGGAGAATCAATATA-linker-amine-3′ (MW = 8630.5 Da); *MORF2*: 5′-TATATTGATTCTCCTTGGCTTACTC-linker-amine-3′ (MW =8438.5 Da).
[217] L.K. Boerner, Nanoconjugates trigger cell suicide, Chem. Eng. News (January 7, 2014) http://cen.acs.org/articles/92/web/2014/01/Nanoconjugates-Trigger-Cancer-Cell-Suicide.html .
[218] J. Kopeček, Hydrogel biomaterials: a smart future? Biomaterials 28 (2007) 5185–5192.
[219] J. Kopeček, Hydrogels: from soft contact lenses and implants to self-assembled nanomaterials, J. Polym. Sci. A Polym. Chem. 47 (2009) 5929–5946.
[220] E. Kimby, Tolerability and safety of rituximab (MabThera), Cancer Treat. Rev. 31 (2005) 456–473.
[221] H. Ding, W.M. Prodinger, J. Kopeček, Identification of CD21-binding peptides with phage display and investigation of binding properties of HPMA copolymer–peptide conjugates, Bioconjug. Chem. 17 (2006) 514–523.
[222] H. Ding, W.M. Prodinger, J. Kopeček, Two-step fluorescence screening of CD21-binding peptides with one-bead one-compound library and investigation of binding properties of HPMA copolymer–peptide conjugates, Biomacromolecules 7 (2006) 3037–3046.
[223] L. Peng, R. Liu, J. Marik, X. Wang, Y. Takada, K.S. Lam, Combinatorial chemistry identifies high-affinity peptidomimetics against α4β1 integrin for *in vivo* tumor imaging, Nat. Chem. Biol. 2 (2006) 381–389.
[224] C. Li, S. Wallace, Polymer–drug conjugates: recent development in clinical oncology, Adv. Drug Deliv. Rev. 60 (2008) 886–898.
[225] R. Duncan, M.J. Vicent, Polymer therapeutics — prospects for 21st century: the end of the beginning, Adv. Drug Deliv. Rev. 65 (2013) 60–70.
[226] Z.-R. Lu, Molecular imaging of HPMA copolymers: visualizing drug delivery in cell, mouse and man, Adv. Drug Deliv. Rev. 62 (2010) 246–257.
[227] M.A. Pysz, S.S. Gambhir, J.K. Willman, Molecular imaging: current status and emerging strategies, Clin. Radiol. 65 (2010) 500–516.
[228] M.J. Pittet, R. Weissleder, Intravital imaging, Cell 147 (2011) 983–991.

Journal of Controlled Release 218 (2015) 36–44

Contents lists available at ScienceDirect

Journal of Controlled Release

journal homepage: www.elsevier.com/locate/jconrel

FRET-trackable biodegradable HPMA copolymer-epirubicin conjugates for ovarian carcinoma therapy

Jiyuan Yang [a], Rui Zhang [a], D. Christopher Radford [b], Jindřich Kopeček [a,b,*]

[a] Department of Pharmaceutics and Pharmaceutical Chemistry/CCCD, University of Utah, Salt Lake City, UT 84112, USA
[b] Department of Bioengineering, University of Utah, Salt Lake City, UT 84112, USA

ARTICLE INFO

Article history:
Received 10 June 2015
Received in revised form 17 September 2015
Accepted 23 September 2015
Available online 26 September 2015

Keywords:
N-(2-hydroxypropyl)methacrylamide (HPMA)
Epirubicin
Ovarian carcinoma
FRET

ABSTRACT

To develop a biodegradable polymeric drug delivery system for the treatment of ovarian cancer with the capacity for non-invasive fate monitoring, we designed and synthesized *N*-(2-hydroxypropyl)methacrylamide (HPMA) copolymer-epirubicin (EPI) conjugates. The polymer backbone was labeled with acceptor fluorophore Cy5, while donor fluorophores (Cy3 or EPI) were attached to HPMA copolymer side chains via an enzyme-cleavable GFLG linker. This design allows elucidating separately the fate of the drug and of the polymer backbone using fluorescence resonance energy transfer (FRET). The degradable diblock conjugate (2P-EPI) was synthesized by reversible addition-fragmentation chain transfer (RAFT) polymerization using a bifunctional chain transfer agent (Peptide2CTA). The pharmacokinetics (PK) and therapeutic effect of 2P-EPI (Mw ~100 kDa) were determined in mice bearing human ovarian carcinoma A2780 xenografts. Compared to 1st generation conjugate (P-EPI, Mw <50 kDa), 2P-EPI demonstrated remarkably improved PK such as fourfold terminal half-life (33.22 ± 3.18 h for 2P-EPI vs. 7.55 ± 3.18 h for P-EPI), which is primarily attributed to the increased molecular weight of the polymer carrier. Notably, complete tumor remission and long-term inhibition of tumorigenesis (100 days) were achieved in mice (n = 5) treated with 2P-EPI. Moreover, in vitro cell uptake and intracellular drug release were determined via FRET intensity changes. The results establish a solid foundation for future in vivo tracking of drug delivery and chain scission of polymeric conjugates by FRET imaging.

1. Introduction

Polymer-drug conjugates have a long history. The concept of polymer-drug conjugates was developed to address sub-optimal bioactivity and non-specificity of low molecular weight drugs in the human body [1–4]. Loading drugs on soluble macromolecules can improve pharmacokinetics and accumulation of drugs in solid tumors, resulting in enhanced therapeutic efficacy and reduced adverse side effects [5–7]. As the first example entering clinical trials for cancer treatment, (*N*-(2-hydroxypropyl)methacrylamide) (HPMA) copolymer-doxorubicin (DOX) conjugate demonstrated significant reduction of nonspecific toxicity. Maximum tolerated dose (MTD) of HPMA copolymer-DOX conjugate in humans was 320 mg/m^2 of DOX equivalent, whereas MTD of free (unbound) DOX in humans is 60–80 mg/m^2. The enhanced MTD of the polymer-bound DOX is primarily attributed to low uptake in heart tissue [8]. The use of polymeric drug delivery systems has become an established approach for improvement of cancer chemotherapy [9,10]. To gain more insight into the relationship between structure of polymer carrier and antitumor activity of polymer-conjugates, various fluorescent dyes have been exploited to investigate cellular uptake and drug release [11,12].

Recently we designed 2nd generation backbone-degradable HPMA copolymer carriers [13–15]. The combination therapy of A2780 human ovarian carcinoma xenografts with long-circulating HPMA copolymer-paclitaxel/gemcitabine conjugates showed distinct advantages over 1st generation conjugates [16]. Similarly, the backbone degradable HPMA copolymers possessed enhanced efficacy (when compared to 1st generation conjugates) in ovarian carcinoma xenografts in mice [17,18] and in a rat osteoporosis model [19].

Epirubicin (EPI), the 4′-epimer of the anthracycline DOX, is an antineoplastic agent that inhibits DNA replication, transcription and repair by binding to nucleic acids [20]. Epirubicin has been regarded as one of the most active drugs for the patients with cancer, particularly with metastatic disease [21]. It has shown equivalent cytotoxic effects to DOX in human ovarian cancer cells, but decreased cardiotoxicity and myelotoxicity than DOX at equimolar doses [22]. Thus, epirubicin is thought to have a better therapeutic index than DOX. Recently, EPI has been bound to various polymer carriers to improve its properties and delivery. For example, dextran [23], polyethylene glycol (PEG) [24], dendritic PEG [25], human monoclonal antibodies [26], polyHPMA [27,28] and polysialic acid [28] were used as (targetable) carriers.

* Corresponding author at: Center for Controlled Chemical Delivery, University of Utah, 20 S 2030 E, BPRB 205B, Salt Lake City, UT 84112-9452, USA.
E-mail address: jindrich.kopecek@utah.edu (J. Kopeček).

http://dx.doi.org/10.1016/j.jconrel.2015.09.045
0168-3659/

Taking advantage of the inherent fluorescence of EPI, we synthesized 2nd generation HPMA copolymer-EPI conjugates aiming to develop a biodegradable polymeric drug delivery system with the capacity for non-invasive fate monitoring. Fluorescence resonance energy transfer (FRET) was used as a tool to track chain scission of the conjugates and to elucidate separately the fate of the polymer backbone and the drug. The in vitro cytotoxicity, pharmacokinetics (PK), and in vivo antitumor activity of the conjugates were first evaluated on human ovarian carcinoma xenografts. The backbone of FRET polymers was labeled with Cy5, whereas model drug Cy3 or EPI was attached to HPMA copolymer backbone via an enzyme-cleavable GFLG linker. The cell uptake and drug release were analyzed by changes in FRET intensity.

2. Materials and methods

2.1. Materials

Common solvents methanol, acetonitrile, dimethylformamide (DMF), dichloromethane (DCM) were from Fisher Scientific (Pittsburgh, PA) as HPLC grade and used directly. Diisopropylethylamine (DIPEA), trifluoroacetic acid (TFA), papain (EC 3.4.22.2, from papaya latex) and cathepsin B (EC 3.4.22.1, from bovine spleen) were from Sigma-Aldrich (St. Louis, MO). Epirubicin (EPI) was a kind gift from Prof. Kui Luo (Sichuan University, China). HATU was from AAPPTEC (Louisville, KY). 2,2-azobis[2-(2-imidazolin-2-yl)propane] dihydrochloride (VA-044) and 2,2-azobis(2,4-dimethyl valeronitrile) (V-65) were obtained from Wako Chemicals (Richmond, VA). ^{125}Iodine was from Perkin-Elmer (Waltham, MA). Cy3−/Cy5-NHS ester and Cy5-amine were purchased from Lumiprobe (Hallandale Beach, FL). Various monomers including *N*-(2-hydroxypropyl)methacrylamide (HPMA) [29], *N*-methacryloylglycyl phenylalanylleucylglycine (MA-GFLG-OH) [30], 3-(*N*-methacryloylglycyl phenylalanylleucylglycyl) thiazolidine-2-thione (MA-GFLG-TT) [31], *N*-methacryloyltyrosinamide (MA-Tyr-NH_2) [32], 2-(*N*-methacryloylglycyl phenylalanylleucylglycine)-N′-Boc-ethylenediamine (MA-GFLG-NH-Boc) [16], and RAFT agents, 4-cyanopentanoic acid dithiobenzoate (CPA) [33] and peptide2CTA (N^{α},N^{ε}-bis(4-cyano-4-(phenylcarbonothioylthio)pentanoylglycylphenylalanylleucylglycyl)lysine) [15], were synthesized as previously described.

2.2. Cell culture

A2780 human ovarian cancer cells (ATCC) were maintained at 37 °C in a humidified atmosphere containing 5% CO_2 in RPMI-1640 medium (Gibco) supplemented with 10% FBS and a mixture of antibiotics (100 units/mL penicillin, 0.1 mg/mL streptomycin).

2.3. Synthesis and characterization of HPMA copolymer conjugates

2.3.1. Synthesis of polymerizable derivative of epirubicin (MA-GFLG-EPI)

N-(methacryloylglycylphenylalanylleucylglycyl) epirubicin (MA-GFLG-EPI) was synthesized by the reaction of MA-GFLG-OH with EPI in DMF using HATU/DIPEA as coupling agent. In brief, EPI (54 mg, 0.1 mmol) was first dissolved in 0.2 mL DMF. MA-GFLG-OH (50 mg, 0.11 mmol) was dissolved in 0.5 mL DMF, followed by addition of HATU (38 mg, 0.1 mmol) and DIPEA (45 μL, 0.25 mmol). After activation at room temperature for 2 min, MA-GFLG-OH/HATU/DIPEA solution was added to the vial containing EPI solution. The system was kept stirring in dark overnight. The reaction solution (10 μL, diluted with methanol) was then loaded onto an analytical column (Zorbax C18, 4.6 × 250 mm) and checked by HPLC. The peak of free EPI (15.34 min) disappeared, whereas a new peak showed up (20.14 min) indicating the reaction had finished. The solvent was removed by rotary evaporator under vacuum. The crude product was purified by column chromatography (silica gel 60 Å, 200–400 mesh) with elution 6:1 dichloromethane/methanol. A dark red powder was obtained after removal of the solvents with a yield of 70 mg (70%). The structure of the monomer (MA-GFLG-EPI) was confirmed by MALDI ToF MS (LTQ-FT, ThermoElectron) ($[M + Na]^+$ 1024.43), and the purity was verified by HPLC (Agilent 1100 series).

2.3.2. Synthesis of HPMA copolymer-epirubicin conjugates (P-EPI/2P-EPI and P-Tyr-EPI/2P-Tyr-EPI

HPMA copolymer-epirubicin conjugates (P-EPI and 2P-EPI) were synthesized by the copolymerization of HPMA with MA-GFLG-EPI using VA044 as initiator and 4-cyanopentanoic acid dithiobenzoate (CTA) or Peptide2CTA as chain transfer agent, respectively. As an example, HPMA (138 mg, 0.965 mmol) and MA-GFLG-EPI (35 mg, 0.035 mmol) were dissolved in 0.3 mL methanol under N_2 atmosphere. Peptide2CTA (60 μL with conc. 8.5 mg/mL in methanol, [M]/[CTA] = 1400) and VA044 at a molar ratio of 3:1 were added using a syringe. The ampoule was bubbled with N_2 in ice bath for 5 min then sealed and polymerization was carried out at 40 °C for 24 h. The copolymer was precipitated in acetone. The resultant orange-color copolymer was re-dissolved in methanol and re-precipitated in acetone to remove unreacted monomers. The dithiobenzoate end group was replaced by radical-induced end-modification using excess of V-65 in methanol at 55 °C for 2 h. The final product (2P-EPI) was isolated by precipitation and dried under vacuum at room temperature with yield of 80 mg (50%). Similarly, P-EPI was obtained when CTA was used as RAFT agent with [M]/[CTA] = 550 (Scheme 1).

The molecular weight and molecular weight distribution of the conjugates were determined by size-exclusion chromatography (SEC) on an ÄKTA FPLC system (GE Healthcare) equipped with miniDAWN and OptilabEX detectors (Wyatt) with acetate/30% acetonitrile (pH 6.5) as mobile phase. Superose 6 HR10/30 column was used. The drug content in conjugates was determined by enzyme cleavage of free drug from polymer side chain GFLG linker using papain according to the procedure described previously [15].

To synthesize a radioisotope ^{125}I labeled conjugate, comonomer MA-Tyr-NH_2 (1.5% molar ratio in feed) was added and the same procedure shown above was used to produce P-Tyr-EPI/2P-Tyr-EPI.

2.3.3. Synthesis of polymer conjugates containing fluorophore Cy3 and/or Cy5

To synthesize polymer conjugates suitable for FRET evaluation, P-Cy3-Cy5/2P-Cy3-Cy5, the polymer precursor containing side chain thiazolidine-2-thione (TT) and GFLG linker terminated with protected amino group was first synthesized by RAFT copolymerization of the amino-protected monomer (MA-GFLG-NH-Boc [16]), HPMA and MA-GG-TT (Scheme 2A). After chain end-modification, the content of TT groups in the copolymer was determined by UV (ε_{305} = 10,900 M^{-1} cm^{-1} in methanol) [31]. Cy5-NH_2 was dissolved in DMSO and reacted with polymer precursor. Unbound dye was removed using PD10 column. To incorporate the second dye, Cy3, the polymer was dissolved in water followed by addition of trifluoroacetic acid. The sample was kept stirring in ice-bath for 30 min, then condensed under reduced pressure and precipitated in precooled ether/acetone. The side-chain amino content in the deprotected polymer was analyzed by ninhydrin assay. Cy3-NHS was used to attach Cy3 to the polymer backbone via GFLG enzyme-cleavable linker. The content of Cy3 and Cy5 in the polymer chain was determined via UV–vis spectroscopy.

As control, HPMA copolymers containing fluorophore Cy3 or Cy5 (P-Cy3 or P-Cy5) were synthesized by polymer analogous reaction of HPMA polymer precursor containing pendant amino groups with Cy3−/Cy5-NHS ester (Scheme 2B). Free dye was removed using PD10 column (Amersham Biosciences). The content of Cy3/Cy5 in polymer conjugates was determined via UV–vis spectroscopy (Varian Cary 400 Bio UV–visible spectrophotometer).

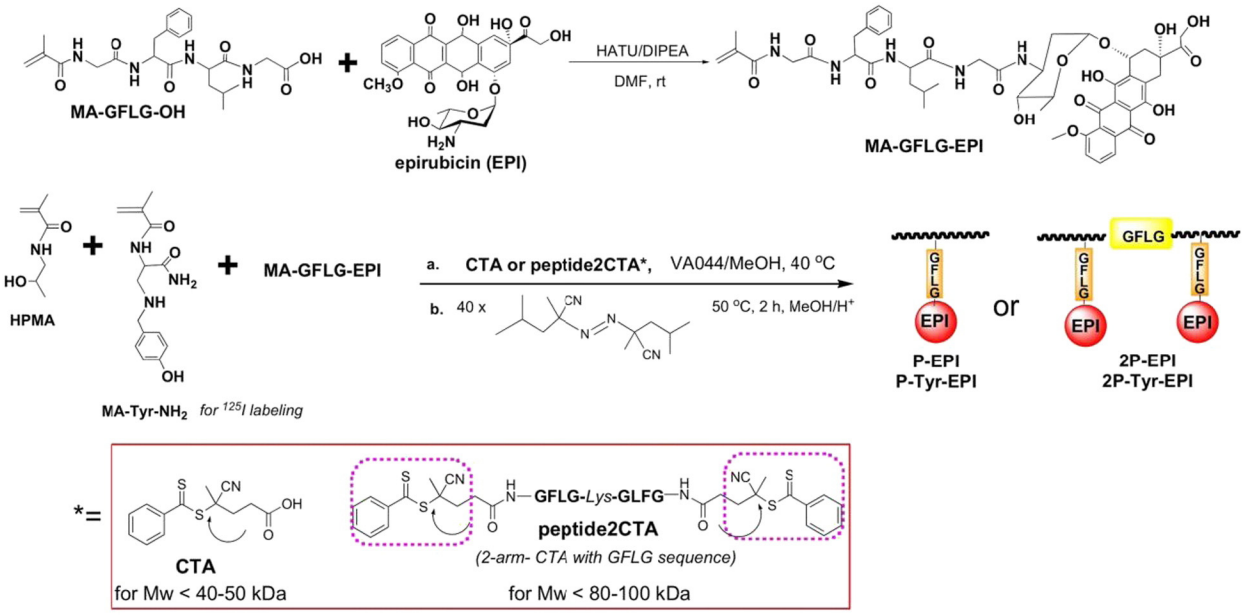

Scheme 1. Synthesis of HPMA copolymer-epirubicin conjugates.

2.3.4. Synthesis of HPMA copolymer-epirubicin conjugate containing fluorophore Cy5

FRET polymer P-EPI-Cy5 was synthesized in two steps (Scheme 3): First, RAFT copolymerization of HPMA (134 mg, 0.94 mmol), MA-GFLG-EPI (33 mg, 0.035 mmol) and MA-GG-TT (7.5 mg, 0.025 mmol) was conducted in methanol at 40 °C as described above. The dithiobenzoate end group was removed by addition of 40× V65 to the polymer solution at 55 °C for 2 h. The TT group was then aminolyzed by Cy5-NH_2. The free dye was removed using PD10 column. The final contents of EPI and Cy5 were determined by UV–vis spectroscopy.

2.4. FRET measurements

The concentration of fluorophore-labeled conjugate solution was first determined by UV–vis spectroscopy. Typically, 1.5 mg/mL conjugate in methanol was scanned within range of 400–800 nm. The solution was further diluted into ~100 μg/mL, and the fluorescence intensity of each sample was measured in duplicates using Infinite®M1000 PRO (TECAN) with excitation wavelengths of 445 nm for EPI (P-EPI), 548 nm for Cy3 (P-Cy3) and 646 nm for Cy5 (P-Cy5), respectively. For FRET measurements, the donor was excited at 520 nm for Cy3 [34] and 445 nm for EPI; the emission spectra of the donor-acceptor were recorded at the range of 400 to 800 nm.

To compare the fluorescence intensity changes of the conjugate P-Cy3-Cy5 before and after cleavage of the donor Cy3, the conjugate was incubated in McIlvaine's buffer (50 mM citrate/0.1 M phosphate, pH 6) in the presence of papain (5 mg/mL, preactivated with 10 mM glutathione) at 37 °C for 1 h. The cleaved conjugate was diluted into methanol and determined with Ex 520 nm.

2.5. FRET change measurement in cancer and normal cells

To determine the cathepsin B dependence of drug release capability in our conjugates, FRET model conjugates, P-Cy3-Cy5 and 2P-Cy3-Cy5, were incubated with A2780 ovarian cancer cells (cathepsin B over-expressing) and NIH3T3 normal cells (cathepsin B low expression). The cells were first incubated with the conjugate (P-Cy3-Cy5 or 2P-Cy3-Cy5) at 37 °C for 4 h, then cells were washed with fresh medium and subsequently cultured in fresh medium without conjugate for another 8 or 20 h. Cell lysates at different time intervals were measured by fluorescence spectrometer. FRET ratio = I_{Cy3}/I_{FRET}, where I_{Cy3} and I_{FRET} are the fluorescence intensity at 562 nm and 664 nm, respectively (excitation 520 nm). The data were presented as mean ± standard deviation (n = 3).

2.6. Confocal microscopy of FRET changes in A2780 cancer cells

To visualize the FRET changes in cancer cells, A2780 cells were first incubated with conjugate P-Cy3-Cy5 at 37 °C. After 4 h incubation, the cells were washed and fresh medium was added. Then a portion of treated cells was fixed with 4% paraformaldehyde immediately while the other cells were incubated for another 20 h and then were fixed. The fixed cells were observed under confocal microscope using the standard acceptor Cy5 photobleaching FRET method (the cells were exposed to high excitation intensity at an excitation wavelength of 646 nm for a 20 min period. In this experiment, both pre-bleach and post-bleach images were collected).

2.7. EPI release inside cultured cells

The release of drug EPI from Cy5-labeled polymeric conjugate was determined using FRET, with EPI serving as the donor fluorophore, and Cy5 as the acceptor. The conjugate P-EPI-Cy5 was incubated with A2780 cells at 37 °C for 4 h. Then the treated cells were cultured in fresh medium for another 20 h. The cell lysate was measured by fluorescence spectrometer, before and after the 20 h additional culture. The "relative" FRET efficiency, also known as the FRET ratio, was calculated with the following equation FRET ratio = I_{EPI}/I_{FRET}, where I_{EPI} and I_{FRET} are the fluorescence intensity at 590 nm and 664 nm, respectively (excitation 490 nm).

Table 1
Characterization of HPMA copolymer-epirubicin conjugates.

	Mn (kDa)	Mw (kDa)	Mw/Mn	EPI % (wt)
P-EPI	39	43	1.10	7.4
P-Tyr-EPI	26	28	1.08	6.5
2P-EPI	76	106	1.39	5.9
2P-Tyr-EPI	61	84	1.38	6.4

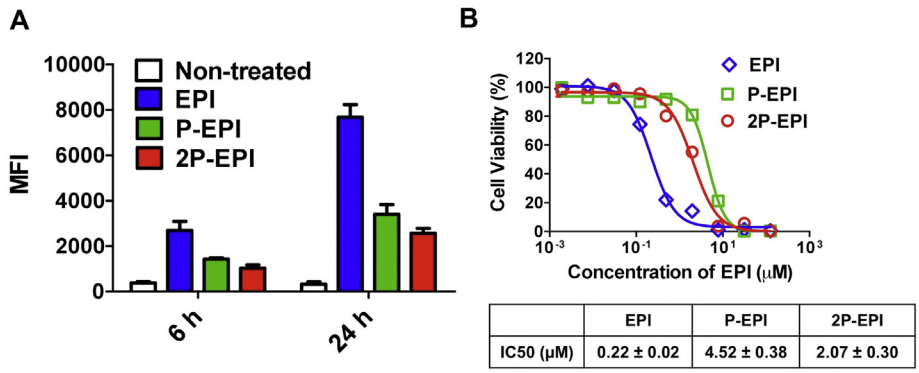

	EPI	P-EPI	2P-EPI
IC50 (μM)	0.22 ± 0.02	4.52 ± 0.38	2.07 ± 0.30

Fig. 1. Cell uptake and cytotoxicity of free drug EPI and its conjugates (P-EPI, 2P-EPI) in A2780 human ovarian cancer cells. (A) Flow cytometry analysis of cell uptake in the A2780 cells incubated with medium alone (non-treated), free EPI, or its conjugates (P-EPI, 2P-EPI) at 37 °C for 6 and 24 h. MFI, mean fluorescence intensity. (B) In vitro cytotoxicity of free drug EPI and its HPMA conjugates (P-EPI, 2P-EPI) toward A2780 human ovarian carcinoma cells. The data are presented as mean ± standard deviation (n = 3–4).

2.8. Cell uptake study

Cellular uptake of the EPI and its conjugates (P-EPI and 2P-EPI) was analyzed using flow cytometry. A2780 human ovarian cancer cells (2×10^5) were seeded in 6-well plates. After 24 h culture, the cells were treated with free EPI, P-EPI, or 2P-EPI (EPI concentration: 100 nM) for 6 or 24 h. Untreated cells served as a negative control for background fluorescence. Thereafter, the cells were harvested and washed. An average of 1×10^4 cells was determined using flow cytometry (BD Biosciences) and FlowJo software (Tree star). EPI uptake was analyzed based on the EPI fluorescence intensity (n = 3).

2.9. In vitro cytotoxicity study

The cytotoxicity of free drug EPI and its polymeric conjugates (P-EPI, 2P-EPI) against A2780 human ovarian cancer cells was measured by CCK-8 assay (Dojindo). The cells were seeded in 96-well plates at the density of 10,000 cells/well in RMPI-1640 media containing 10% FBS. The cells were washed after 24 h, then incubated with media containing the drug EPI or its polymeric conjugates (P-EPI, 2P-EPI) at a series of drug concentrations. After 48 h of incubation, the number of viable cells was estimated using CCK-8 kit according to manufacturer's protocol. In brief, medium was discarded and replaced with 100 μL fresh growth medium in each well, followed by the addition of 50 μL 5× diluted CCK-8 solution. Dehydrogenase activities in live cells converted the water-soluble tetrazolium salt WST-8 into a soluble yellow-color formazan dye. After the incubation of cells at 37°°C, 5% CO_2 for 2 h, the absorbance was measured using a microplate reader at 450 nm (630 nm as reference). Untreated control cells were set as 100% viable.

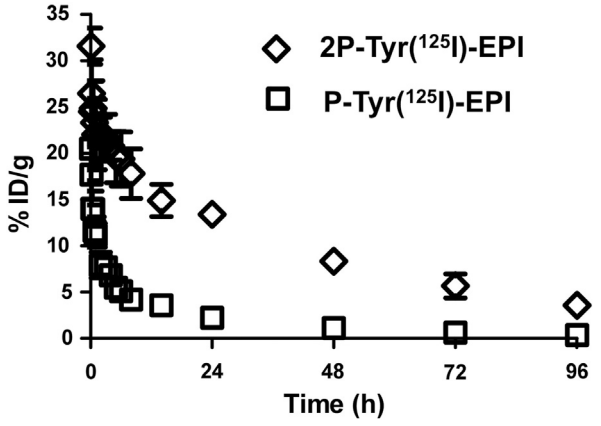

Fig. 2. Pharmacokinetic profiles of ^{125}I-labeled conjugates P-EPI and 2P-EPI in mice. The data represent the mean radioactivity expressed as a percentage of the injected dose per gram of blood (n = 5).

2.10. Radiolabeling and pharmacokinetics study

HPMA copolymer-EPI conjugates containing tyrosinamide were reacted with $Na^{125}I$ (Perkin Elmer) at room temperature in 0.01 M phosphate buffer containing chloramine-T for 30 min and then purified with PD-10 columns (GE Healthcare). The specific activity of the hot samples was in the range 40–60 μCi/mg. The ^{125}I labeling of polymer conjugates was conducted immediately before use. After radiolabeling, 6- to 8-week-old healthy female nude mice (22–25 g; Charles River Laboratories) were intravenously injected 0.5 mg (20 μCi/mouse) ^{125}I-labeled HPMA copolymer-drug conjugates (P-EPI and 2P-EPI, five mice per group). At predetermined intervals, blood samples (10 μL) were taken from the tail vein, and the radioactivity of each sample was measured with Gamma Counter (Packard). The blood pharmacokinetic parameters for the radiotracer were analyzed using a two-compartmental model with WinNonlin 5.0.1 software (Pharsight).

2.11. Tumor model

All animal studies were carried out in accordance with the University of Utah IACUC guidelines under approved protocols. A2780 human ovarian cancer cells (5×10^6) in 100 μL of phosphate buffered saline were subcutaneously inoculated in right flank of 6- to 8-week-old syngeneic female nude mice (22–25 g, Charles River Laboratories). When tumor reached approximately 4–5 mm in diameter (average 3 weeks after inoculation) treatment started.

2.12. In vivo antitumor activity

Female nude mice bearing subcutaneous A2780 ovarian tumors were randomly assigned to four groups (n = 5 for each group). P-EPI and 2P-EPI were administered via tail vein with dose 5 mg/kg EPI equivalent on day 0, 4, and 8. Free drug EPI was also used for comparison. The mice in the control group were treated with saline. The day that mice received EPI or its conjugates treatment was set as day 0. The tumor size was measured to monitor the tumor growth. The tumor volume at day 0 was normalized to 100%. All subsequent tumor volumes and body weight were then expressed as the percentage relative to those at day 0. Mice were sacrificed at signs of sickness such as body weight loss >20%. Otherwise mice were sacrificed at 100 days.

2.13. Statistical analysis

The Student's t test was used to test differences in therapeutic efficiency, cell uptakes, pharmacokinetic parameters, and toxicity among

Table 2
Comparison of pharmacokinetic parameters for ^{125}I-labeled conjugates in mice.

	P-EPI	P-PTX[a]	P-GEM[a]	2P-EPI	2P-PTX[a]	2P-GEM[a]
$T_{1/2,\alpha}$ (h)	0.33 ± 0.07	*0.88 ± 0.11*	*0.26 ± 0.02*	0.18 ± 0.06	*1.13 ± 0.13*	*1.45 ± 0.36*
$T_{1/2,\beta}$ (h)	7.55 ± 1.55	*13.30 ± 1.28*	*6.36 ± 0.66*	33.22 ± 3.18	*37.90 ± 3.55*	*32.07 ± 2.50*
AUC (%ID h/mL blood)	110.10 ± 14.06	*420.95 ± 26.05*	*108.66 ± 6.74*	1060.48 ± 88.83	*1206.42 ± 85.97*	*1481.23 ± 83.06*
CL (mL/h)	0.91 ± 0.12	*0.24 ± 0.01*	*0.92 ± 0.06*	0.09 ± 0.01	*0.08 ± 0.01*	*0.07 ± 0.004*
MRT (h)	10.34 ± 2.09	*18.25 ± 1.71*	*8.49 ± 0.88*	47.79 ± 4.57	*52.86 ± 4.95*	*45.39 ± 3.43*
Vss (mL)	9.39 ± 0.82	*4.34 ± 0.16*	*7.82 ± 0.38*	4.51 ± 0.11	*4.38 ± 0.16*	*3.06 ± 0.10*

different conjugates. Comparison among groups was performed using one-way ANOVA. The significance level was set at 0.05.

3. Results and discussion

3.1. Synthesis of HPMA copolymer-epirubicin conjugates

As an isomer of DOX, EPI has been reported to have different metabolic degradation and faster clearance from plasma after i.v. injection. As a result, EPI has less side effects compared with DOX at doses producing equivalent antitumor effects [35]. EPI therefore has been nanosized to various formulations such as micelles [36], liposomes [37], nanoparticles [38,39], and, most interesting for us, water-soluble conjugates to improve its therapeutic index. In general, polymer-EPI conjugates were produced via polymeranalogous reaction in which EPI is attached to polymer through active ester [27] or in the presence of coupling agents [25,28]. Here we report a different way to synthesize the conjugates - RAFT copolymerization. The polymerizable EPI derivative was synthesized first, and then copolymerized with HPMA with option of using MA-Tyr-NH_2 for isotope labeling. The major advantage of this approach is reproducibility with predetermined molecular weight and narrow polydispersity. In addition, the polymer is relatively pure without detectable free drug (Fig. S1). Previously we have reported synthesis of long-circulating 2P-PTX and 2P-GEM in one step using a two-arm enzyme-cleavable chain transfer agent [16]. To assess this universal approach, we synthesized the 1st generation and 2nd generation HPMA copolymer-EPI conjugates; their molecular weight (including molecular weight distribution) and drug content are listed in Table 1.

3.2. Cell uptake and in vitro cytotoxicity

The cell uptake of the conjugates (P-EPI and 2P-EPI) was analyzed using flow cytometry with EPI fluorescence signal. The free drug EPI was used as a control. A2780 human ovarian cancer cells were incubated with different EPI formulations, respectively. Free EPI showed a higher cell uptake than the two conjugates. This difference is likely due to their distinct entry pathways – diffusion (free drugs) vs. endocytosis (conjugates). In addition, the cytotoxicity of free EPI and its HPMA copolymer conjugates (P-EPI and 2P-EPI) against A2780 human ovarian cancer cells was determined. Fig. 1A shows the representative cell-growth inhibition curves. Overall, free drug EPI and its conjugates (P-EPI, 2P-EPI) showed a dose-dependent cytotoxicity against A2780 cells. On the basis of the IC_{50} values (Fig. 1B), both HPMA copolymer-EPI conjugates had less in vitro cytotoxicity than free EPI, due to the different mechanism of cell uptake [4,7].

3.3. Pharmacokinetic study of ^{125}I-labeled conjugates

It has been reported that conjugation of free drug to HPMA polymer carrier markedly slows its blood clearance [40]. For example, the fast initial clearance of DOX ($t_{1/2}$) is 4 min, however, there was still 55% polymer-bound drug in circulation 1 h after injection of P-DOX (Mw 25 kDa) [40]. In this study, we compared pharmacokinetic profiles of 1st generation conjugate (P-(Tyr)-EPI, Mw 28 kDa) and 2nd generation conjugate (2P-(Tyr)-EPI, Mw 84 kDa) to highlight the effect of molecular weight on plasma concentration and circulation time. Tyrosine moiety was inserted into the conjugates for radiolabeling (^{125}I) in order to

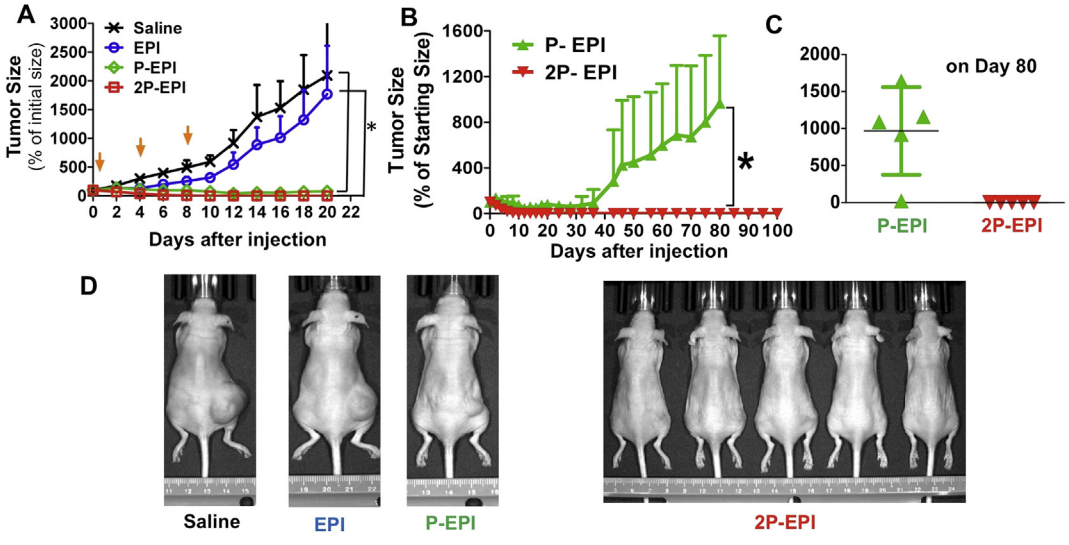

Fig. 3. Comparison of in vivo anti-tumor activity on female nude mice bearing A2780 human ovarian carcinoma xenografts. (A) The mice were intravenously injected with 3 doses of EPI or HPMA copolymer-EPI conjugates (P-EPI and 2P-EPI). Free drug and untreated groups were stopped on day 20 due to large size of tumors. (B) Long-term monitoring of tumor growth in conjugate treatments. (C) The tumor size on day 80 of the polymer conjugates, and (D) End point photographs of tumor-bearing mice from various treatments.

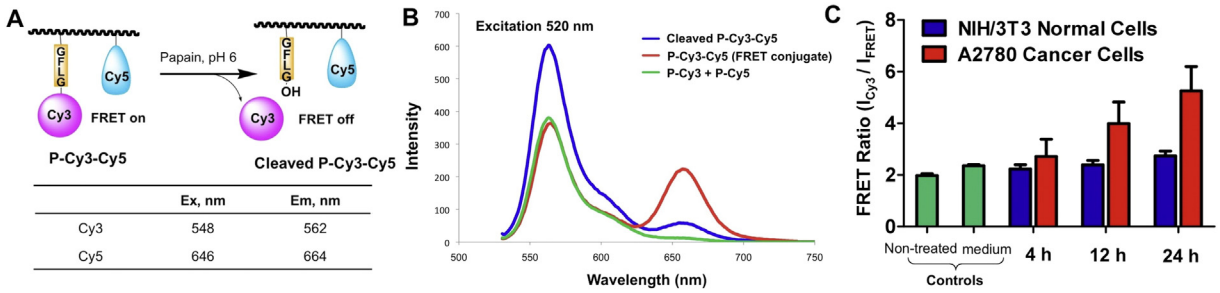

Fig. 4. (A) Cartoon illustration of FRET principle of dual-labeled enzyme-cleavable polymer conjugates containing Cy3 (donor) and Cy5 (acceptor). (B) Fluorescence spectra of conjugate P-Cy3-Cy5 before and after cleavage by papain. The mixture of conjugates P-Cy5/P-Cy3 was measured as control (excitation 520 nm using methanol as solvent). (C) FRET ratios of P-Cy3-Cy5 in NIH3T3 mouse fibroblast cells (low cathepsin B expression) and A2780 ovarian cancer cells (high cathepsin B expression) at different time intervals. The cells were incubated with P-Cy3-Cy5 at 37 °C for 4 h and then cultured in fresh medium for another 0, 8, or 20 h. Then cell lysate was measured by fluorescence spectroscopy. FRET ratio = I_{Cy3}/I_{FRET}, was calculated to quantify the FRET change, where I_{Cy3} and I_{FRET} are the fluorescence intensity at 562 nm and 664 nm, respectively (excitation 520 nm). Increase of the ratio revealed effective payload release following enzyme exposure.

enhance accuracy and sensitivity of the analysis. The blood radioactivity-time profiles were determined and illustrated in Fig. 2. The pharmacokinetic parameters of the two conjugates in mice are listed in Table 2, and the previously reported half-lives of 2P-PTX/P-PTX and 2P-GEM/P-GEM are cited here for comparison [16]. Higher Mw 2P-EPI conjugate showed a longer terminal half-life (33.22 h) than low Mw conjugate P-EPI (7.55 h). 2P-EPI (AUC = 1060.48%ID/mL) had a 10-fold higher systemic exposure than P-EPI (110.10%ID/mL) ($p < 0.001$). The increased exposure of 2P-EPI is mainly attributed to its significantly slower systemic clearance (CL) (2P-EPI: 0.09 mL/h vs. P-EPI: 0.91 mL/h) ($p < 0.001$). Taken all together, the 2nd generation conjugate 2P-EPI having an increased Mw possesses an improved pharmacokinetic profile.

Although individual drugs (EPI, PTX, and GEM) have different metabolism and clearance time [41], the new generation conjugate 2P-EPI showed significant improved pharmacokinetics with parameters similar to 2P-PTX and 2P-GEM, such as terminal half life, total body clearance, and steady-state volume of distribution (Table 2), which indicates that conjugation of drug to polymer carrier can improve its stability in plasma, and the elimination rate of the conjugates is primarily determined by the polymer carrier.

3.4. In vivo anti-tumor activity

The therapeutic potential of the backbone degradable long-circulating HPMA copolymer-EPI conjugate (2P-EPI) was evaluated in female nude mice bearing A2780 human ovarian carcinoma xenografts. The mice were intravenously injected with three doses of 5 mg/kg EPI equivalent on days 0, 4, and 8. Free drug EPI and the 1st generation conjugate P-EPI were also administered for comparison. Tumor growth was closely monitored during and after treatment. At day 20, complete tumor regression was achieved in the five mice treated with conjugate 2P-EPI (Fig. 3); the tumors treated with P-EPI shrank to 80 ± 37% of the initial size. In contrast, free drug EPI at equivalent doses only slightly delayed tumor growth when compared with saline (control), and mice had to be sacrificed on day 20 as the tumor had reached 1772 ± 840% of the baseline. However, there was no significant difference between

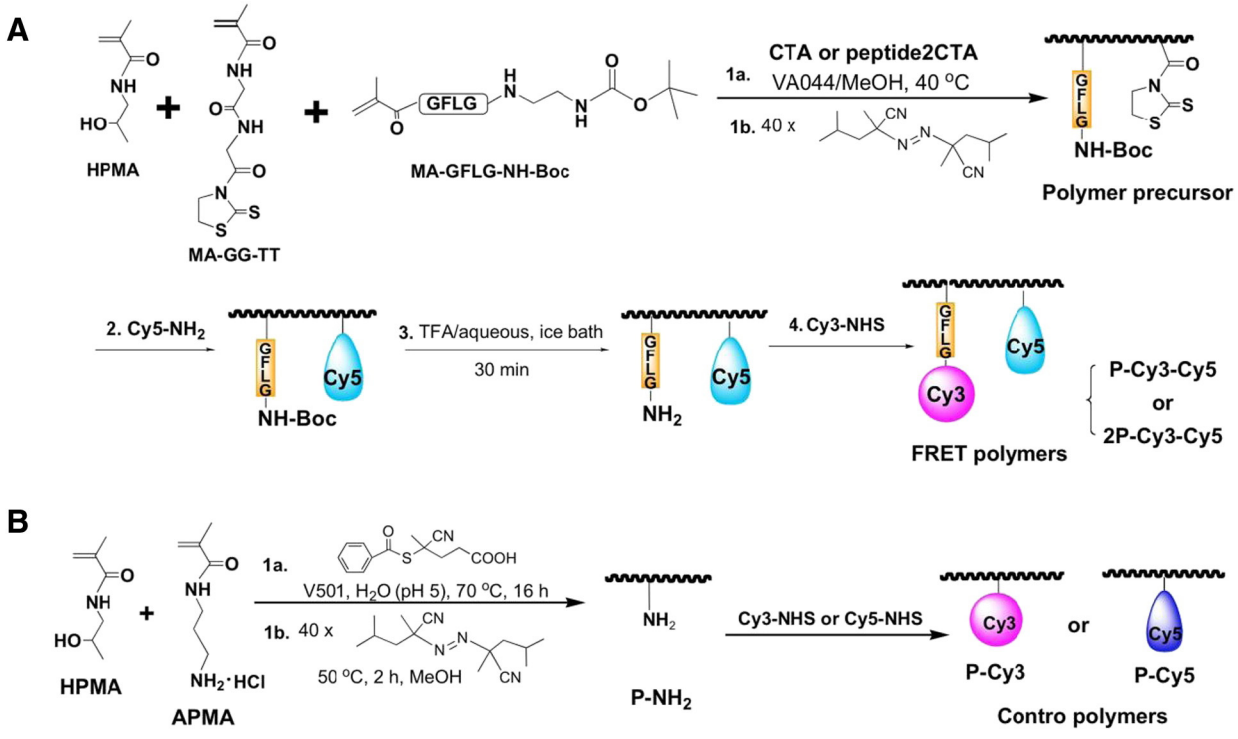

Scheme 2. Synthesis of polymer conjugates containing fluorophores.

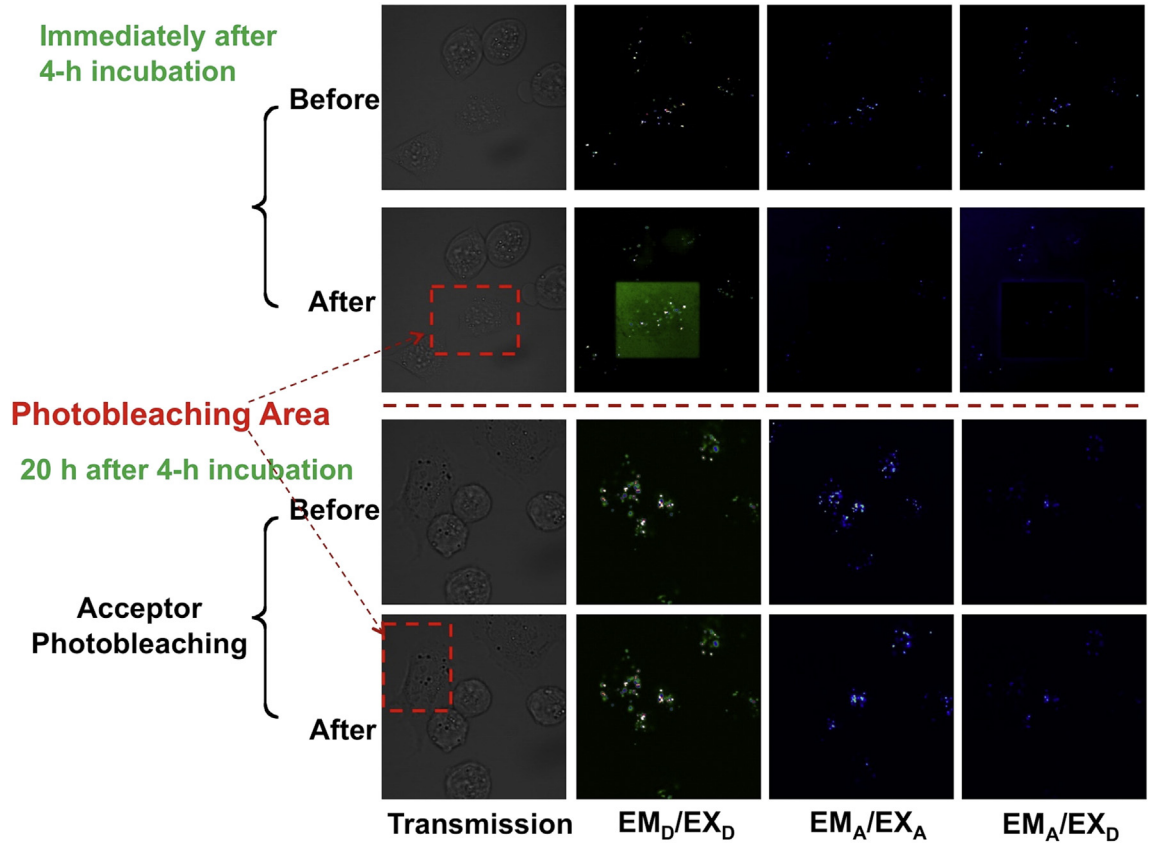

Fig. 5. Visualization of payload Cy3 release from conjugate P-Cy3-Cy5 in cathepsin B over-expressing A2780 human ovarian cancer cells by FRET. The cells were first incubated with P-Cy3-Cy5 at 37 °C for 4 h and then were washed. Half of the cells were fixed immediately, while the other half were incubated with fresh medium at 37 °C for another 20 h and fixed. The fixed cells were observed under confocal microscope using the standard acceptor Cy5 photobleaching method. Bleached areas are indicated by red boxes. Representative images of pre- and post-bleaching are shown.

treatment with 2P-EPI and P-EPI until day 35 when tumor started re-growth in P-EPI group, and four of the tumors grew back to ~1200% at day 80 ($p < 0.01$) (Fig. 3). On the contrary, no observable tumor was detected in the mice treated with 2P-EPI at day 100. These results demonstrate the importance of long-term experiments for evaluation of tumor growth inhibitory effect. The results also indicated that 2P-EPI is highly superior to both P-EPI and free EPI. The complete tumor regression and long-term inhibition of tumorigenesis by 2P-EPI treatment are attributed to long circulation time and sufficient extravasation of the conjugates at the tumor site by the enhanced permeability and retention (EPR) effect. In addition, this result also suggests that 2P-EPI conjugate may be able to arrest both tumor progenitor cells and differentiated cells as we observed in another scenarios [42].

For safety concern, body weight of the mice was closely recorded during and after treatment (Fig. S2). The body weights of the mice temporarily decreased (less than 10%) when P-EPI and 2P-EPI were administered as multiple dosages but recovered gradually and remained stable after withdrawal, which suggests the doses used were tolerable.

3.5. Potential to track chain degradation and intracellular drug release via FRET

Similar to DOX, the fluorescence signal from EPI has been used for cellular uptake studies [39,43]. However, the polymer conjugation can affect the fluorescence emission [28]. Consequently, the data only from drug fluorescence may be misinterpreted.

Herein we propose to use FRET imaging as a tool to monitor drug release from HPMA copolymer conjugates. Initially, we designed and prepared a HPMA copolymer conjugate containing a popular FRET pair Cy3/Cy5 — the donor fluorophore Cy3 was attached to HPMA polymer backbone as model drug via a cleavable (by lysosomal proteases)

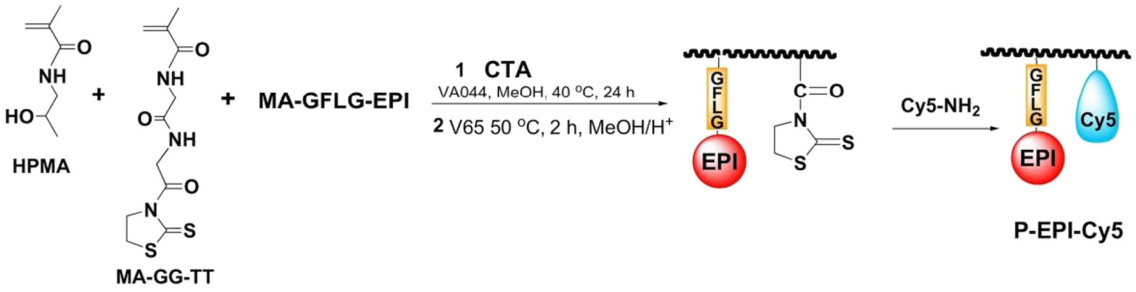

Scheme 3. Synthesis of polymer conjugates containing epirubicin and Cy5 (P-EPI-Cy5).

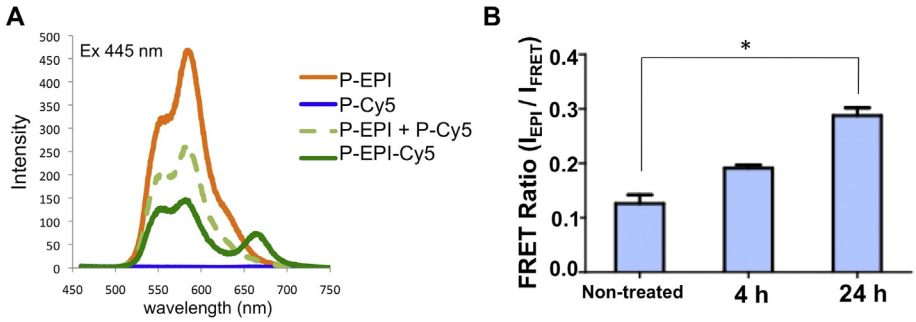

Fig. 6. (A) Fluorescence spectra of FRET conjugate P-EPI-Cy5 compared with P-EPI, P-Cy5 and their mixture P-Cy5 + P-EPI. (B) The change in FRET ratio of P-EPI-Cy5 conjugate revealed effective EPI release in A2780 ovarian cancer cells. The cathepsin B over-expressing A2780 cells were incubated with P-EPI-Cy5 at 37 °C for 4 h and then were cultured in fresh medium for another 20 h. Then cell lysates at different time intervals were measured by fluorescence spectrometer. FRET ratio = I_{EPI}/I_{FRET}, where I_{EPI} and I_{FRET} are the fluorescence intensity at 590 nm and 664 nm, respectively (excitation 490 nm). The data are presented as mean ± standard deviation (n = 3). *, $p < 0.01$.

tetrapeptide linker Gly-Phe-Leu-Gly (GFLG), while the acceptor Cy5 was directly labeled on the HPMA backbone as a tag (Fig. 4A, Scheme 2). To characterize its FRET property, the conjugate was determined using fluorescence spectrometry before and after exposure to papain, a thiol proteinase with specificity similar to lysosomal cathepsin B. Ex 520 nm was selected to minimize direct emission of Cy5. As shown in Fig. 4B, detectable FRET occurred in the original non-treated conjugate, but not in the same conjugate incubated with papain. Loss of FRET was due to the cleavage of the linker GFLG by enzyme, and consequently, the release of Cy3 from backbone.

The FRET property of conjugates (P-Cy3-Cy5 and 2P-Cy3-Cy5) was further elucidated in living cells. Human ovarian cancer A2780 cells that overexpress cathepsin B were incubated with the FRET conjugate, and NIH3T3 mouse fibroblast cells (low cathepsin B expression) were used as control. The release of model drug Cy3 will result in decrease of FRET intensity that can be investigated via cell lysis using fluorescence spectrometry. According to the previous reports [44–46], the ratio, I_{Cy3}/I_{FRET}, was calculated to quantify the FRET change, where I_{Cy3} and I_{FRET} are the fluorescence intensity at 562 nm and 664 nm, respectively (excitation 520 nm). For the conjugate P-Cy3-Cy5, the ratio in medium alone was 2.35, and in initial stock was 1.97. When the conjugate was incubated with A2780 cancer cells, the ratio increased to 2.71 at 4 h, then gradually increased to 3.99 at 12 h and 5.25 at 24 h, whereas in NIH3T3 cells, the ratio only increased to 2.73 at 24 h (Fig. 4C). A similar FRET change in the 2nd generation conjugate (2P-Cy3-Cy5) was also observed (Fig. S3). There was significant difference in the release efficacy between cancer and normal cells. This observation suggests an effective release of Cy3 from the conjugate, which is highly dependent on the cathepsin B level. Compared to normal cells, cathepsin B level is much higher in malignant tumors, such as ovarian cancer, breast cancer, and melanoma. It acts as an important proteinase of matrix materials to degrade surrounding proteins and other tissue components so that cancer cells can invade and metastasize [47]. Therefore, high expression of cathepsin B in tumor cells can induce a fast release of drugs from conjugates and thereby mediates a relatively high concentration of active free drug inside the tumor cells.

The conjugate P-Cy3-Cy5 was also evaluated using FRET confocal microscopy, which is a more straightforward approach for performing FRET. In this experiment, pre-bleach and post-bleach images were collected. To do the photobleaching, the cells were exposed to high excitation intensity at an excitation wavelength of 646 nm (Ex of Cy5) for a 20 min period. After high-energy laser treatment, there was a dramatic reduction of Cy5 intensity in the bleached regions (Fig. 5). In the cells immediately following 4 h incubation, it was found that bleaching the acceptor Cy5 resulted in FRET intensity significantly decreased, and donor Cy3 fluorescence substantial increase, because the acceptor can no longer accept energy from the donor. However, those intensity changes did not occur in the same batch of cells after additional 20 h culture (Fig. 5). It indicated that the model drug Cy3 had been released from the backbone after cellular internalization and lysosomal cleavage.

Following the same principle, we synthesized the conjugate P-EPI-Cy5 (Scheme 3). The conjugate was characterized using FRET spectra. The cell uptake and the drug EPI release were determined by FRET intensity changes. In A2780 cancer cells, the ratio decreased from 0.89 (initial stock) to 0.84 at 4 h and gradually decreased to 0.77 at 24 h (Fig. 6). The reduction of FRET ratio indicates that EPI molecules could be released from the conjugate inside A2780 cancer cells over time. These results showed potential to use FRET as a tool for future in vivo real-time monitoring drug delivery, tracking chain scission of HPMA copolymer-drug conjugates, and for improved cancer diagnostics and therapy.

4. Conclusions

We have developed a biodegradable polymeric drug delivery system with the capacity for non-invasive fate monitoring using FRET-based methodology. Epirubicin served as both fluorescence donor and antineoplastic agent. The degradable diblock HPMA copolymer-EPI conjugate (2P-EPI) produced complete tumor remission and long-term inhibition of tumorigenesis (100 days) when treating mice bearing human ovarian carcinoma A2780 xenografts. This and PK data provide strong evidence that 2nd generation backbone degradable HPMA copolymer-drug conjugates remarkably enhance circulation time and treatment efficacy. Moreover, in vitro cell uptake and intracellular drug release determined via FRET intensity changes clearly demonstrated cathepsin B levels are decisive and responsible for drug anti-tumor activity. This aspect will be further investigated ex vivo and in vivo using near-infrared FRET pairs to ensure deeper tissue penetration and better imaging quality.

Acknowledgments

The research was supported in part by Department of Defense grant W81XWH-13-1-0160 and NIH grant CA156933.

Appendix A. Supplementary data

Supplementary data to this article can be found online at http://dx.doi.org/10.1016/j.jconrel.2015.09.045.

References

[1] C. De Duve, T. De Barsy, B. Poole, A. Trouet, P. Tulkens, F. van Hoof, Lysosomotropic agents, Biochem. Pharmacol. 23 (1974) 2495–2531.
[2] H. Ringsdorf, Structure and properties of pharmacologically active polymers, J. Polym. Sci. Polym. Symp. 51 (1975) 135–153.
[3] J. Kopeček, Polymer – drug conjugates: origins, progress to date and future directions, Adv. Drug Deliv. Rev. 65 (2013) 49–59.

[4] J. Yang, J. Kopeček, Macromolecular therapeutics, J. Control. Release 190 (2014) 288–303.
[5] Y. Zhou, J. Kopeček, Biological rationale for the design of polymeric anti-cancer nanomedicines, J. Drug Target. 21 (2013) 1–26.
[6] H. Maeda, Tumor-selective delivery of macromolecular drugs via the EPR effect: background and future prospects, Bioconjug. Chem. 21 (2010) 797–802.
[7] T. Minko, P. Kopečková, J. Kopeček, Comparison of the anticancer effect of free and HPMA copolymer-bound Adriamycin in human ovarian carcinoma cells, Pharm. Res. 16 (1999) 986–996.
[8] P.A. Vasey, S.B. Kaye, R. Morrison, C. Twelves, P. Wilson, R. Duncan, A.H. Thomson, L.S. Murray, T.E. Hilditch, T. Murray, S. Burtles, D. Fraier, E. Frigerio, J. Cassidy, on behalf of the Cancer Research Campaign Phase I/II Committee, Phase I clinical and pharmacokinetic study of PK1 [*N*-(2-hydroxypropyl)methacrylamide copolymer doxorubicin]: first member of a new class of chemotherapeutic agents-drug-polymer conjugates, Clin. Cancer Res. 5 (1999) 83–94.
[9] C. Li, S. Wallace, Polymer-drug conjugates: recent development in clinical oncology, Adv. Drug Deliv. Rev. 60 (2008) 886–898.
[10] R. Duncan, M.J. Vicent, Polymer therapeutics — prospects for 21st century: the end of the beginning, Adv. Drug Deliv. Rev. 65 (2013) 60–70.
[11] P. Chytil, E. Koziolová, O. Janoušková, L. Kostka, K. Ulbrich, T. Etrych, Synthesis and properties of star HPMA copolymer nanocarriers synthesised by RAFT polymerisation designed for selective anticancer drug delivery and imaging, Macromol. Biosci. 15 (2015) 839–850.
[12] P. Chytil, S. Hoffmann, L. Schindler, L. Kostka, K. Ulbrich, H. Caysa, T. Mueller, K. Mäder, T. Etrych, Dual fluorescent HPMA copolymers for passive tumor targeting with pH-sensitive drug release II: impact of release rate on biodistribution, J. Control. Release 172 (2013) 504–512.
[13] J. Yang, K. Luo, H. Pan, P. Kopečková, J. Kopeček, Synthesis of biodegradable multiblock copolymers by click coupling of RAFT-generated heterotelechelic polyHPMA conjugates, React. Funct. Polym. 71 (2011) 294–302.
[14] K. Luo, J. Yang, P. Kopečková, J. Kopeček, Biodegradable multiblock *N*-(2-hydroxypropyl)methacrylamide copolymers via reversible addition-fragmentation chain transfer polymerization and click chemistry, Macromolecules 44 (2011) 2481–2488.
[15] H. Pan, J. Yang, P. Kopečková, J. Kopeček, Backbone degradable multiblock *N*-(2-hydroxypropyl)methacrylamide copolymer conjugates via reversible addition-fragmentation chain transfer polymerization and thiol-ene coupling reaction, Biomacromolecules 12 (2011) 247–252.
[16] R. Zhang, J. Yang, M. Sima, Y. Zhou, J. Kopeček, Sequential combination therapy of ovarian cancer with degradable *N*-(2-hydroxypropyl)methacrylamide copolymer paclitaxel and gemcitabine conjugates, Proc. Natl. Acad. Sci. U. S. A. 111 (2014) 12181–12186.
[17] R. Zhang, K. Luo, J. Yang, M. Sima, Y. Sun, M.M. Janát-Amsbury, J. Kopeček, Synthesis and evaluation of a backbone biodegradable multiblock HPMA copolymer nanocarrier for the systemic delivery of paclitaxel, J. Control. Release 166 (2013) 66–74.
[18] H. Pan, M. Sima, J. Yang, J. Kopeček, Synthesis of long-circulating backbone degradable HPMA copolymer-doxorubicin conjugates and evaluation of molecular weight dependent antitumor efficacy, Macromol. Biosci. 13 (2013) 155–160.
[19] H. Pan, M. Sima, S.C. Miller, P. Kopečková, J. Yang, J. Kopeček, Promotion of bone formation in ovariectomized rats by high molecular weight backbone degradable HPMA copolymer – prostaglandin E_1 conjugate, Biomaterials 34 (2013) 6528–6538.
[20] S.V. Ontrust, L.R. Wiseman, K.L. Goa, Epirubicin: a review of its intravesical use in superficial bladder cancer, Drugs Aging 15 (1999) 307–333.
[21] H. Havsteen, K. Bertelsen, C.C. Gadeberg, A. Jacobsen, C. Kamby, E. Sandberg, L. Sengelov, A phase 2 study with epirubicin as second-line treatment of patients with advanced epithelial ovarian cancer, Gynecol. Oncol. 63 (1996) 210–215.
[22] G.L. Plosker, D. Faulds, Epirubicin: a review of its pharmacodynamic and pharmacokinetic properties, and therapeutic use in cancer chemotherapy, Drugs 45 (1993) 788–856.
[23] M. Marquez, J. Du, M. Edgren, S. Nilsson, L. Lennartsson, J. Hiltunen, J.E. Westlim, T. Tammela, M. Raitanen, M. Laato, G. Jönsson, A.R. Holmberg, Development of dextran derivatives with cytotoxic effects in human urinary cancer cell lines, Anticancer Res. 22 (2002) 741–744.
[24] F. Canal, M.J. Vicent, G. Pasut, O. Schiavon, Relevance of folic acid/polymer ratio in targeted PEG-epirubicin conjugates, J. Control. Release 146 (2010) 388–399.
[25] G. Pasut, S. Scaramuzza, O. Schiavon, R. Mendichi, F.M. Veronese, PEG-epirubicin conjugates with high drug loading, J. Bioact. Compat. Polym. 20 (2005) 213–230.
[26] H. Takahashi, K. Adachi, F. Yamaguchi, A. Teramoto, Experimental treatment of malignant gliomas with human monoclonal antibody-drug conjugates, Anticancer Res. 19 (1999) 4151–4155.
[27] B. Říhová, Clinical experience with anthracycline antibiotics-HPMA copolymer-human immunoglobulin conjugates, Adv. Drug Deliv. Rev. 61 (2009) 1149–1158.
[28] F. Greco, I. Arif, R. Botting, C. Fante, L. Quintieri, C. Clementi, O. Schiavon, G. Pasut, Polysialic acid as drug carrier: evaluation of a new polysialic acid-epirubicin conjugate and its comparison against established drug carriers, Polym. Chem. 4 (2013) 1600–1609.
[29] J. Kopeček, H. Bažilová, Poly[N-(2-hydroxypropyl)methacrylamide]. 1. Radical polymerization and copolymerization, Eur. Polym. J. 9 (1973) 7–14.
[30] J. Kopeček, P. Rejmanová, J. Strohalm, K. Ulbrich, B. Říhová, V. Chytrý, J.B. Lloyd, R. Duncan, Synthetic polymeric drugs. US Patent 5037883 (1991).
[31] V. Šubr, K. Ulbrich, Synthesis and properties of new *N*-(2-hydroxypropyl)methacrylamide copolymers containing thiazolidine-2-thione reactive groups, React. Funct. Polym. 66 (2006) 1525–1538.
[32] R. Duncan, H.C. Cable, P. Rejmanová, J. Kopeček, J.B. Lloyd, Tyrosinamide residues enhance pinocytic capture of *N*-(2-hydroxypropyl)methacrylamide copolymers, Biochim. Biophys. Acta 799 (1984) 1–8.
[33] Y. Mitsukami, M.S. Donovan, A.B. Lowe, C.L. McCormick, Water-soluble polymers. 81. Direct synthesis of hydrophilic styrenic-based homopolymers and block copolymers in aqueous solution via RAFT, Macromolecules 34 (2001) 2248–2256.
[34] Y.L. Chiu, S.A. Chen, J.H. Chen, K.J. Chen, H.L. Chen, H.W. Sung, A dual-emission forster resonance energy transfer nanoprobe for sensing/imaging pH changes in the biological environment, ACS Nano 4 (2012) 7467–7474.
[35] G.N. Hortobagyi, H.Y. Yap, S.W. Kau, G. Franchini, M.S. Ewer, S.P. Chawla, R. Benjamin, A comparative study of doxorubicin and epirubicin in patients with metastatic breast cancer, Am. J. Clin. Oncol. 12 (1989) 57–62.
[36] Y. Yamamoto, I. Hyodo, Y. Koga, R. Tsumura, R. Sato, T. Obonai, H. Fuchigami, F. Furuya, M. Yasunaga, M. Harada, Y. Kato, A. Ohtsu, Y. Matsumura, Enhanced antitumor effect of anti-tissue factor antibody-conjugated epirubicin-incorporating micelles in xenograft models, Cancer Sci. 106 (2015) 627–634.
[37] Q. Yang, T. Zhang, C. Wang, J. Jiao, J. Li, Y. Deng, Coencapsulation of epirubicin and metformin in PEGylated liposomes inhibits the recurrence of murine sarcoma S180 existing CD133+ cancer stem-like cells, Eur. J. Pharm. Biopharm. 88 (2014) 737–745.
[38] M. Tariq, M.A. Alam, A.T. Singh, Z. Iqbal, A.K. Panda, S. Talegaonkar, Biodegradable polymeric nanoparticles for oral delivery of epirubicin: in vitro, ex vivo, and in vivo investigations, Colloids Surf. B: Biointerfaces 128 (2015) 448–456.
[39] X. Wang, X.C. Low, W. Hou, L.N. Abdullah, T.B. Toh, M.M.A. Rashid, D. Ho, E.K.H. Chow, Epirubicin-adsorbed nanodiamonds kill chemoresistant hepatic cancer stem cells, ACS Nano 8 (2014) 12151–12166.
[40] L. Seymour, K. Ulbrich, J. Strohalm, J. Kopeček, R. Duncan, The pharmacokinetics of polymer-bound Adriamycin, Biochem. Pharmacol. 39 (1990) 1125–1131.
[41] S. Fogli, R. Danesi, A. Gennari, S. Donati, P.F. Conte, M. Del Tacca, Gemcitabine, epirubicin and paclitaxel: pharmacokinetic and pharmacodynamic interactions in advanced breast cancer, Ann. Oncol. 13 (2002) 919–927.
[42] Y. Zhou, J. Yang, J. Rhim, J. Kopeček, HPMA copolymer-based combination therapy toxic to both prostate cancer stem/progenitor cells and differentiated cells induces durable anti-tumor effects, J. Control. Release 172 (2013) 946–953.
[43] I. Matai, A. Sachdev, P. Gopinath, Self-assembled hybrids of fluorescent carbon dots and PAMAM dendrimers for epirubicin delivery and intracellular imaging, ACS Appl. Mater. Interfaces 7 (2015) 11423–11435.
[44] S.J. Hauff, S.C. Raju, R.K. Orosco, A.M. Gross, J.A. Diaz-Perez, E. Savariar, N. Nashi, J. Hasselman, M. Whitney, J.N. Myers, S.M. Lippman, R.Y. Tsien, T. Ideker, Q.T. Nguyen, Matrix-metalloproteinases in head and neck carcinoma—cancer genome atlas analysis and fluorescence imaging in mice, Otolaryngol. Head Neck Surg. 151 (2014) 612–618.
[45] T. Hussain, E.N. Savariar, J.A. Diaz-Perez, K. Messer, M. Pu, R.Y. Tsien, Q.T. Nguyen, Surgical molecular navigation with ratiometric activatable cell penetrating peptide for intraoperative identification and resection of small salivary gland cancers, Head Neck (2015) http://dx.doi.org/10.1002/hed.23946.
[46] E.N. Savariar, C.N. Felsen, N. Nashi, T. Jiang, L.G. Ellies, P. Steinbach, R.Y. Tsien, Q.T. Nguyen, Real-time in vivo molecular detection of primary tumors and metastases with ratiometric activatable cell-penetrating peptides, Cancer Res. 73 (2013) 855–864.
[47] H. Nishikawa, Y. Ozaki, T. Nakanish, K. Blomgren, T. Tada, A. Arakawa, K. Suzumori, The role of cathepsin B and cystatin C in the mechanisms of invasion by ovarian cancer, Gynecol. Oncol. 92 (2004) 881–886.

Design and Synthesis of FRET-Trackable HPMA-Based Biodegradable Conjugates for Drug/Gene Delivery

Jiyuan Yang[1], Rui Zhang[1], D. Christopher Radford[2], and Jindřich Kopeček[1,2]

Departments of [1]Pharmaceutics and Pharmaceutical Chemistry/CCCD and [2]Bioengineering,
University of Utah, Salt Lake City, Utah 84112, USA

SIPCD III Sep 16-19, 2014
Suzhou, China

INTRODUCTION

Recently we designed 2nd generation backbone-degradable *N*-(2-hydroxypropyl)methacrylamide (HPMA) copolymer carriers.[1] The combination therapy of A2780 human ovarian carcinoma xenografts with long-circulating HPMA copolymer-paclitaxel/gemcitabine conjugates showed distinct advantages over 1st generation conjugates (Fig. 1A).[2] We used fluorescence resonance energy transfer (FRET) as a tool to track chain scission of the conjugates and to elucidate the fate of the polymer backbone and the drug, respectively (Fig. 1B). Herein we report a rational design and synthesis of conjugates double-labeled with a pair of fluorophores: the polymer backbone was labeled with Cy5, whereas the enzyme-cleavable linker was labeled with Cy3 as drug model or with epirubicin (EPR).

Another application of the FRET technique in our studies was to visualize at cellular level the fate of the HPMA copolymer-based endosomolytic carrier that we developed for delivery of miRNA (Fig.2).

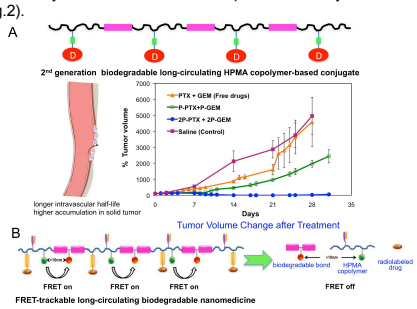

Figure 1. (A) Sequential combination therapy of ovarian cancer with degradable HPMA copolymer paclitaxel (PTX) and gemcitabine (GEM) conjugates. (B) Illustration of simultaneous tracking of the fate of the carrier and drug by FRET and nuclear imaging

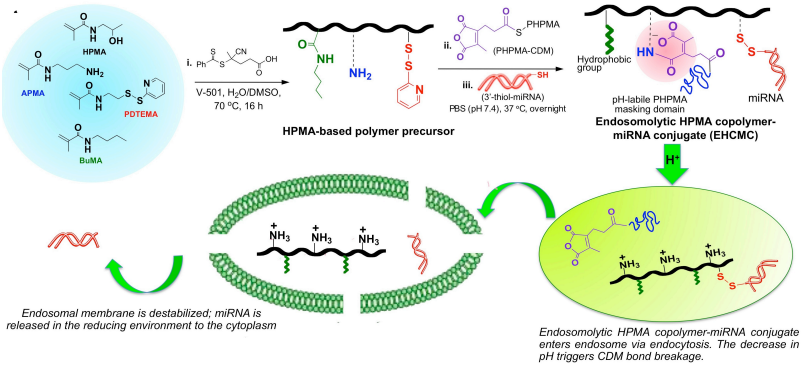

Figure 2. Rational design, synthesis and mechanism of endosomolytic nanomedicines for siRNA/miRNA delivery

EXPERIMENTAL

Synthesis of a FRET nanoprobe conjugate for drug release tracking (P-Cy3-Cy5)

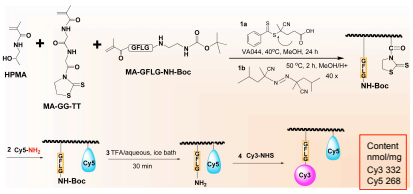

As control, P-Cy5 and P-Cy3 were synthesized:

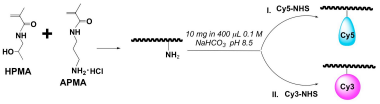

Synthesis of HPMA copolymer-epirubicin (EPR) conjugate

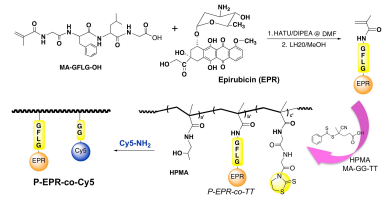

Synthesis of amino-reactive acid-labile semitelechelic polyHPMA

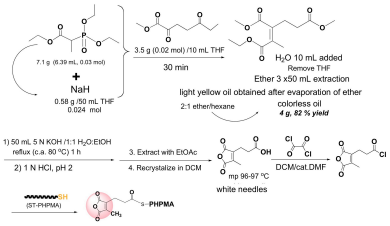

RESULTS

In vitro FRET study of P-Cy3-Cy5

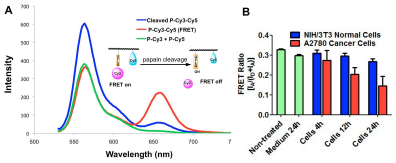

Figure 3. Fluorescence spectra and FRET ratios of conjugate P-Cy3-Cy5 revealed effective payload release following enzyme exposure. (A). Fluorescence spectra of conjugate P-Cy3-Cy5 before or after cleavage by papain (excitation 520 nm). (B). FRET ratios of P-Cy3-Cy5 in NIH3T3 normal cells (low cathepsin B expression) and A2780 ovarian cancer cells (high cathepsin B expression) at different time intervals. The cells were incubated with P-Cy3-Cy5 at 37°C for 4 h and then cultured in fresh medium for another 0, 8, or 20 h. Then cell lysis was measured by fluorescence spectroscopy. FRET ratio = IA / (IA+ID). IA and ID are the fluorescence intensity at 662 nm and 564 nm, respectively (excitation 520nm).

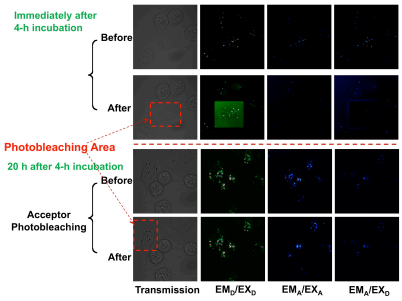

Figure 4. Visualization of payload Cy3 release from conjugate P-Cy3-Cy5 in cathepsin B over-expressing A2780 human ovarian cancer cells by FRET. The cells were first incubated with P-Cy3-Cy5 at 37°C for 4 h and then were washed. Half of the cells were fixed immediately, while the other half were incubated with fresh medium at 37°C for another 20 h and fixed. The fixed cells were observed under confocal microscope using the standard acceptor Cy5 photobleaching method. Bleached areas are indicated by red boxes. Representative images of pre- and post-bleaching are shown.

Evaluation of HPMA copolymer-EPR conjugates

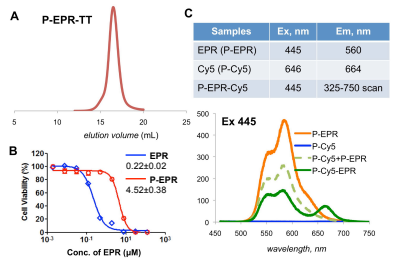

Samples	Ex, nm	Em, nm
EPR (P-EPR)	445	560
Cy5 (P-Cy5)	646	664
P-EPR-Cy5	445	325-750 scan

Figure 5. Conjugate P-epirubicin (P-EPR) had cytotoxic potency and its Cy5-labeled derivative showed FRET effect. (A). SEC profile of P-EPR-TT. (B). *In vitro* cytotoxicity of free drug epirubicin (EPR) and its HPMA copolymer conjugate (P-EPR) toward A2780 human ovarian carcinoma cells. (C). Fluorescence spectra of conjugates (P-EPR-Cy5, P-EPR, P-Cy5, P-EPR+P-Cy5).

Validation of reversible attachment of miRNA and pH-dependent destabilization of cell membranes

Table 1. Characterization of polymer precursors

	Mn, Da	PDI Mw/Mn	Yield %	Composition of polymer		
				BuMA	*NH_2*	*PDTEMA*
P-NH_2	63700	1.12	86		3.8% (17 NH_2/chain)	
P-BuMA-NH_2-PDTEMA	48800	1.27	70	~ 30% (molar ratio)	18 NH_2/chain	16 S-S/chain
ST-PHPMA	4800	1.12	98			

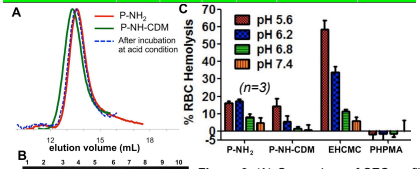

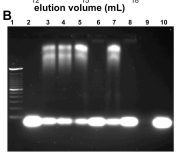

Figure 6. (A) Comparison of SEC profiles of P-NH_2 before and after amino-masking (P-NH-CDM), and after incubation of P-NH-CDM at acidic condition. (B) Gel retardation assay of HPMA copolymer-miR34a conjugates containing a reducible disulfide bond: free miRNA (lanes 2,10); HPMA copolymer-miRNA conjugate (lanes 3,4 with 5x excess, and lanes 5,7 with 10x excess). The bottom shows unbound fraction of miRNA; after addition of 0.1 M DTT to the polymer-miRNA conjugates at 37°C for 30 min (lanes 6,8); polymer only (lane 9) and Mw ladder (lane 1). C). Red blood cell hemolysis assay [3]. Human erythrocytes were incubated with endosomolytic copolymers in a series of buffers simulating the pH range from endosomes (5.6) to physiologic (7.4).

Design & synthesis of FRET-trackable biodegradable HPMA copolymer-based conjugates

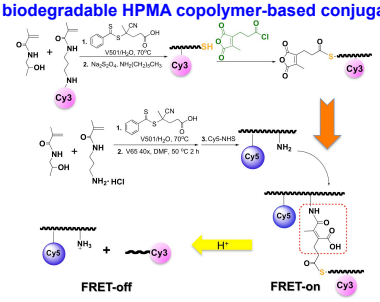

CONCLUSIONS

- We successfully developed dual-labeled conjugates that permit using FRET to monitor drug release and backbone degradation;
- A FRET-trackable dynamic endosomolytic polymer carrier was designed and synthesized. The structure optimization aided by FRET technique is in process.

REFERENCES

1. J. Yang, J. Kopeček, J. Controlled Release 190 (2014) 288-303.
2. R. Zhang, J. Yang, M. Sima, Y. Zhou, J. Kopeček, Proc. Natl. Acad. Sci. USA 111 (2014) 12181-12186.
3. B.B. Lundy, A. Convertine, M. Miteva, P.S. Stayton, Bioconjugate Chem. 24 (2013) 398-407.

ACKNOWLEDGEMENTS

The research was supported in part by US Department of Defense grant W81XWH-13-1-0160. We also acknowledge support in conjunction with grant P30 CA042014 awarded to the Huntsman Cancer Institute, University of Utah.

Postdoctoral position available!

Please visit our website: www.pharmacy.utah.edu/pharmaceutics/groups/kopecek

FRET-TRACKABLE BIODEGRADABLE HPMA COPOLYMER-EPIRUBICIN CONJUGATES FOR OVARIAN CARCINOMA THERAPY— IN VITRO AND IN VIVO EVALUATION

J. Yang[1], R. Zhang[1], D. C. Radford[2], and J. Kopeček[1,2]

[1]Department of Pharmaceutics and Pharmaceutical Chemistry, [2]Department of Bioengineering, University of Utah, Salt Lake City, Utah 84112, USA

INTRODUCTION

Recently we designed 2nd generation backbone-degradable *N*-(2-hydroxypropyl)methacrylamide (HPMA) copolymer carriers.[1] The combination therapy of A2780 human ovarian carcinoma xenografts with long-circulating HPMA copolymer-paclitaxel/gemcitabine conjugates showed distinct advantages over 1st generation conjugates.[2] Herein we used fluorescence resonance energy transfer (FRET) as a tool to track chain scission of the conjugates and to elucidate separately the fate of the polymer backbone and the drug. The conjugates were double-labeled with a pair of fluorophores: the polymer backbone was labeled with Cy5, whereas Cy3 or epirubicin (EPI), the 4'-epimer of the anthracycline doxorubicin (DOX), was attached to HPMA polymer backbone via enzyme-cleavable linker (Fig. 1). The cell uptake and drug release of the HPMA copolymer-epirubicin conjugates were determined by the changes of FRET signal. The in vitro cytotoxicity, pharmacokinetics (PK), and in vivo antitumor activity of the conjugates were evaluated.

EXPERIMENTAL METHODS

Synthesis Dual-labeled, backbone-degradable HPMA copolymers were synthesized using RAFT polymerization followed by multi-step conjugation as described in Fig. 1.

In vitro evaluation A2780 human ovarian cancer cells (ATCC) were used for drug release, cell uptake and cytotoxicity studies. FRET efficiency was determined using spectrofluorometry and flow cytometry.[3]

Pharmacokinetics (PK). HPMA-copolymer-EPI conjugates containing tyrosinamide in the side chain were radiolabeled with $Na^{125}I$ (Perkin Elmer) and intravenously injected to healthy female nude mice (n=5). Blood samples were taken at predetermined intervals, and the radioactivity of each sample was measured with Gamma Counter (Packard). Data were analyzed using a two-compartmental model with WinNonlin 5.0.1 software (Pharsight).

In vivo antitumor activity. EPI (or EPI equivalent) with dose 5 mg/kg were i.v. injected to female nude mice bearing

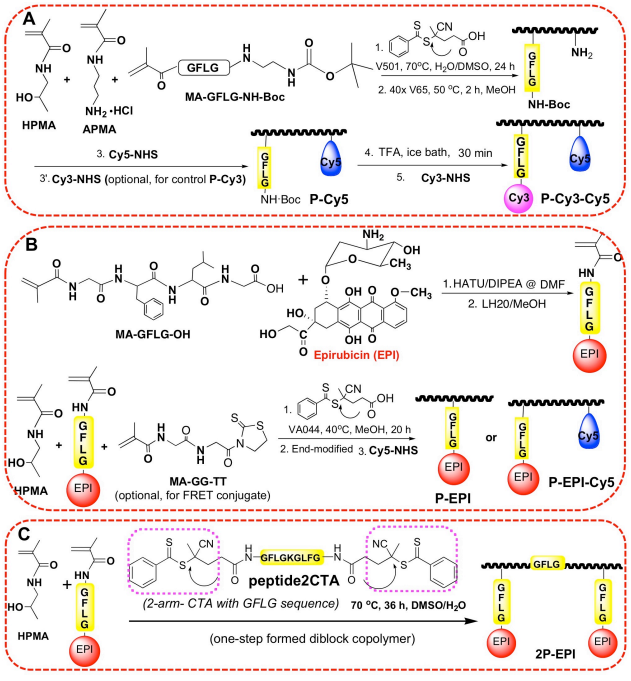

Figure 1. Synthetic schemes of A) Dual-labeled HPMA-copolymer conjugate P-Cy3-Cy5, B) HPMA copolymer-EPI conjugate P-EPI & P-EPI-Cy5, and C) backbone degradable HPMA copolymer-EPI conjugate (2P-EPI).

subcutaneous A2780 ovarian tumors on day 0, 4 and 8 (n=5). Saline treated mice were used as control. Tumor size and body weight were closely monitored. Conjugates used for treatment P-EPI (6.5% wt. EPI, Mn 43.4 kDa, Mw/Mn 1.06), and 2P-EPI (5.8% wt. EPI, Mn 110 kDa, Mw/Mn 1.39).

RESULTS AND DISCUSSION

In vitro the reduction of FRET ratio against time (Fig. 2) indicated that EPI molecules could be released from the conjugate inside A2780 cancer cells (high cathepsin B expression). PK study showed 2P-EPI had a 10-fold higher systemic exposure than P-EPI, which may explain the enhanced treatment efficacy (Fig. 3).

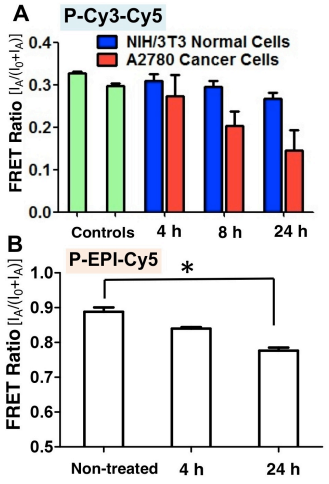

Figure 2. A) FRET ratios of copolymer P-Cy3-Cy5 changes when cultured in NIH3T3 cells (low cathepsin B expression) and A2780 ovarian cancer cells (high cathepsin B expression) at different time intervals. B) A2780 cells were incubated with P-EPI-Cy5 at 37°C for 4 h or 24 h. FRET ratios were compared with that of non-treated cells.

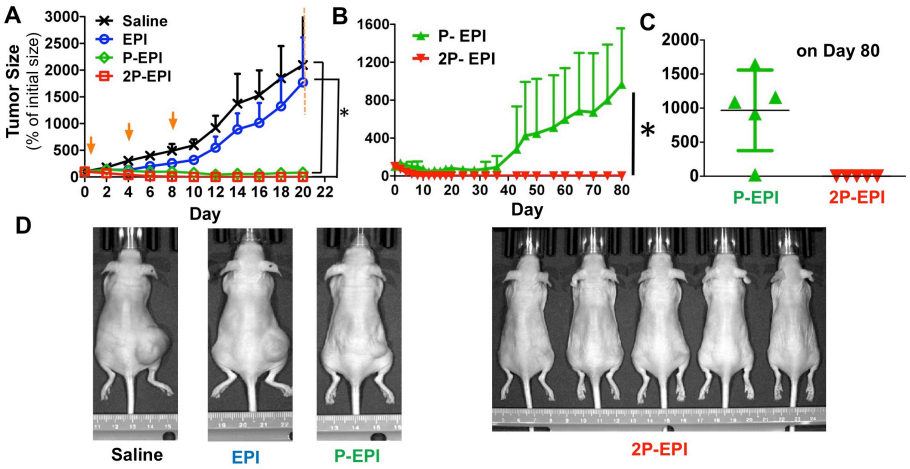

Figure 3. Comparison of i*n vivo* anti-tumor activity on female nude mice bearing A2780 human ovarian carcinoma xenografts. A) The mice were intravenously injected with 3 doses of EPI or HPMA copolymer-EPI conjugates (P-EPI and 2P-EPI). Free drug and untreated groups were stopped on day 20 due to large size of tumors. B) Long-term monitoring of tumor growth in conjugate treatments. C) The tumor size on day 80 of the polymer conjugates, and D) End point photographs of tumor-bearing mice from variable treatments.

CONCLUSION

- We successfully developed dual-labeled conjugates that permit using FRET to monitor drug release and backbone degradation.
- 2nd generation long-circulating HPMA copolymer-epirubicin conjugate led to long-term cancer regression/eradication, which suggests an efficient strategy in cancer treatment.

REFERENCES

1. J. Yang, J. Kopeček, J. Control. Release 190 (2014) 288-303.
2. R. Zhang, J. Yang, M. Sima, Y. Zhou, J. Kopeček, Proc. Natl. Acad. Sci. USA 111 (2014) 12181-12186.
3. J. Yang, R. Zhang, D.C. Radford, J. Kopeček, *J. Controlled Release*, to be submitted

Acknowledgements. This research was supported by Department of Defense Grant W81XWH-13-1-0160.